ARTI Air-Conditioning and Refrigeration Technology Institute

ARTI Report No. 10110-01

RECOVERY OF THROTTLING LOSSES BY A TWO-PHASE EJECTOR IN A VAPOR COMPRESSION CYCLE

Final Report

May 2008

Author(s) Fang Liu and Eckhard A. Groll

HERRICK LABORATORIES
PURDUE UNIVERSITY

PURDUE UNIVERSITY
Ray W. Herrick Laboratories, 140 S. Martin Jischke Drive, West Lafayette, IN 47907

Prepared for

AIR-CONDITIONING AND REFRIGERATION TECHNOLOGY INSTITUTE, INC
4100 N. Fairfax Drive, Suite 200, Arlington, Virginia 22203-1678

DISCLAIMER

This report was prepared as an account of work sponsored by the Air-Conditioning and Refrigeration Technology Institute, Inc. (ARTI). Neither ARTI, its research program financial supporters, or any agency thereof, nor any of their employees, contractors, subcontractors or employees thereof - makes any warranty, expressed or implied; assumes any legal liability or responsibility for the accuracy, completeness, any third party's use of, or the results of such use of any information, apparatus, product, or process disclosed in this report; or represents that its use would not infringe privately owned rights. Reference herein to any specific commercial product, process, or service by trade name, trademark, manufacturer, or otherwise, does not necessarily constitute nor imply its endorsement, recommendation, or favoring by ARTI, its sponsors, or any agency thereof or their contractors or subcontractors. The views and opinions of authors expressed herein do not necessarily state or reflect those of ARTI, its program sponsors, or any agency thereof.

Funding for this project was provided by (listed alphabetically):
- Air-Conditioning & Refrigeration Institute (ARI)
- Copper Development Association (CDA)
- Heating, Refrigeration and Air Conditioning Institute of Canada (HRAI)
- New York State Energy Research and Development Authority (NYSERDA)

TABLE OF CONTENTS

LIST OF FIGURES

LIST OF TABLES

NOMENCLATURE

Symbols

A	area, m^2
Bo	boiling number
Co	convection number
COP	coefficient of performance
c	specific heat, kJ/kg·K; correlation parameter
c_p	specific heat at constant pressure, kJ/kg·K
D	diameter, m
d	diameter, m
F	two-phase correction factor for heat transfer and pressure drop correlations
Fr	Froude number
f	friction factor; function
G	mass flux, $kg/m^2 \cdot s$
Gr	Grashof number
H	height, m
h	specific enthalpy, kJ/kg; heat transfer coefficient, $kW/m^2 \cdot K$, height, m
j_H	Colburn j-factor
K	pressure loss coefficient
k	thermal conductivity, kW/m·K
L	length, m or mm
l	length, m or mm
L_p	louver pitch, m
M	molecular weight, kg/kmol
m	correlation parameter; fin parameter; mass flow rate, kg/s
NTU	number of transfer units
Nu	Nusselt number
N	number of channels/extruded tube
n	correlation parameter; compressor speed, rpm
P	pressure, MPa
p	pressure, MPa; fin pitch, fins/m; tube pitch, tubes/m
Pr	Prandtl number
Q	heat transfer rate, cooling capacity, kW
q	specific heat transfer rate, kW/kg
r	radius, m
Re	Reynolds number
RH	Relative humidity
T	temperature, K
t	thickness, m or mm
UA	heat conductance
V	velocity, m/s, volume, m^3
W	power, kW
Δp	pressure drop, MPa
ΔW	length of single finite element, m

Γ	perimeter, m
ε	effectiveness; fining factor ($A_{finned}/A_{unfinned}$)
η	efficiency
ρ	density, kg/m^3
φ	ejection ratio
σ	free flow area ratio
μ	viscosity, Pa·s
v	specific volume, m^3/kg
χ	quality

Superscripts

-	average
·	time derivative

Subscripts

air	air side quantity
b	basic cycle; inlet of mixing section; bulk
c	critical, minimum area flow velocity
comp	compressor
diff	diffuser
d	ejector diffuser
dis	compressor displacement; discharge port
e	ejector
evap	evaporator
f	fluid
g	vapor
gc	gas cooler
h	heated
i	inner; internal
id	indoor
in	inlet
isen	isentropic
Lp	louver pitch
l	liquid; louver; velocity over the louver; longitudinal
m	motive stream
mix	mixing section; mixing stream; mixture
o	outer; single phase
od	outdoor
ow	outer wall
p	pressure

r	refers to aspect ratio of end of a louvered fin
s	suction stream; surface
sat	saturation
suc	suction
sup	superheat
t	nozzle throat
th	theoretical
trip, tr	triple point
vol	volumetric
w	wall

EXECUTIVE SUMMARY

This study presents the theoretical and experimental research of ejector expansion devices used in a transcritical vapor compression system using carbon dioxide (CO_2) as the refrigerant and a conventional vapor compression system using R410A as the refrigerant.

The expansion losses of an isenthalpic throttling process have been identified as one of the largest irreversibilities of transcritical CO_2 refrigeration cycles, which contribute to the low efficiency of such cycles. An ejector expansion device is proposed here to recover the expansion losses and increase the cycle efficiency. The ejector was chosen over other expansion work recovery devices because of its unique advantage such as simple construction and robust operation. Understanding the effects of the geometric parameters and operation conditions on the performance of two-phase flow ejectors is considered the main criteria to reach an optimum design and integrate the ejector into an ejector expansion transcritical refrigeration system.

A laboratory transcritical CO_2 environmental control unit (ECU) was tested at various operating conditions using a single-stage semi-hermetic reciprocating compressor and microchannel heat exchangers as the gas cooler and evaporator. The test results were used to validate an existing simulation model for transcritical CO_2 air conditioning systems. After modifications, the simulation model was able to predict the cooling coefficient of performance (COP) and cooling capacity with standard deviation of ±3.91% and ±3.71% of the measured results, respectively. At "standard" indoor air conditions of 26.7 °C (80 °F), 50% relative humidity, and an outdoor air temperature of 35 °C (95 °F), the measured COP of the basic CO_2 system is 1.105 with compressor discharge pressure 121.26 bar.

A new two-phase flow ejector simulation model was developed to investigate the effects of design parameters and operation conditions on the performance of the ejector expansion device. This ejector model was incorporated into the transcritical CO_2 air conditioning system simulation model to predict the performance of ejector expansion transcritical CO_2 air conditioners. A controllable ejector expansion device was designed, fabricated, and installed in the ECU to test the performance of an ejector expansion transcritical CO_2 refrigeration system. Experimental results were used to validate the two-phase flow ejector model and the ejector expansion transcritical CO_2 air conditioning system simulation model. At "standard" indoor air conditions of 26.7 °C (80 °F), 50% relative humidity, and an outdoor air temperature of 35 °C (95 °F), the measured COP of the ejector CO_2 system is 1.422 with compressor discharge pressure 129.1 bar. The ejector expansion transcritical CO_2 air conditioning system model predicts the cooling COP with a standard deviation of ±3.14% and cooling capacity with a standard deviation of ±3.97% with the experimentally determined motive nozzle isentropic efficiency, suction nozzle isentropic efficiency and mixing section efficiency.

A comparison of the cooling COP and cooling capacity between the ejector cycle and the basic cycle showed that the ejector expansion device increases the performance of the CO_2 system more significantly as the outdoor temperature increases. The highest predicted improvements in cooling COP and cooling capacity were found to be 38.3% (COP_b = 1.185, COP_e = 1.639) and 40.8% (Q_b = 11.42 kW, Q_e = 16.08 kW), respectively, at an outdoor temperature of 37.8 °C (100.0 °F), an indoor temperature of 26.7 °C (80.0 °F), and an indoor relative humidity of 50%.

Empirical equations of the ejector efficiencies as functions of pressure ratio, mass flow rate ratio, and throat diameter ratio were developed using the experimental data. The ejector expansion system simulation model was modified using the empirical equations for the ejector efficiencies and exercised to perform parametric studies of the ejector expansion transcritical CO_2 air conditioning system. It was found that the COP and cooling capacity of the CO_2 system increase as the throat area increases with the same mixing section diameter and that they reach maxima at a certain mixing section diameter for a constant throat diameter at the assumed operation conditions.

This study also presents the theoretical research of using an ejector expansion device in a conventional vapor compression system with R410A as the refrigerant. The two-phase flow ejector model was modified for subcritical operation and incorporated into an existing system simulation model, called ACMODEL. The ejector expansion ACMODEL was exercised to perform parametric studies of the ejector expansion subcritical R410A air conditioning system. At “standard” indoor air conditions of 26.7 °C (80 °F), 50% relative humidity, and an outdoor air temperature of 35 °C (95 °F), the calculated COP and cooling capacity of the ejector R410A system are 4.786 and 23.222 kW, respectively, which is an increase of 11.1% and 19.8% compared to the values of the basic R410A system. The ejector expansion device increases the COP and the cooling capacity of the subcritical R410A air conditioning system from 13.1% to 16.0% and from 10.9% to 20.8%, respectively, at outdoor temperatures varying from 27.9 °C (82.2 °F) to 50.9 °C (105.6 °F), an indoor temperature of 26.9 °C (80.4 °F), and an indoor relative humidity of 50.8%.

1. INTRODUCTION

1.1. Motivation

Research studies on transcritical carbon dioxide refrigeration systems have drastically increased in recent years because carbon dioxide is being advocated as one of the natural refrigerants to replace CFCs and HCFCs in vapor compression systems. This is mainly due to the high latent heat of vaporization, good transport properties, and other environmentally friendly characteristics of carbon dioxide. However, the low coefficient of performance (COP) of the basic transcritical carbon dioxide refrigeration cycle that is shown in Figure 1.1 compared to the COP of the vapor compression cycle using CFCs, HCFCs and HFCs is a major hindrance for the technology to make progress towards practical applications. To improve the efficiency of transcritical carbon dioxide refrigeration systems, various innovative ideas and techniques have been proposed, including the use of micro-channel heat exchanger, optimal control of high side pressure, and the use of expansion work recovery machines. The thermodynamic analysis of the transcritical carbon dioxide refrigeration cycle indicates that recovery of the expansion losses that occur during the isenthalpic expansion process can be one of the key issues to improve the system efficiency. Among various expansion work recovery schemes, an ejector expansion device has the advantages of simplicity, reliability and availability compared to other devices.

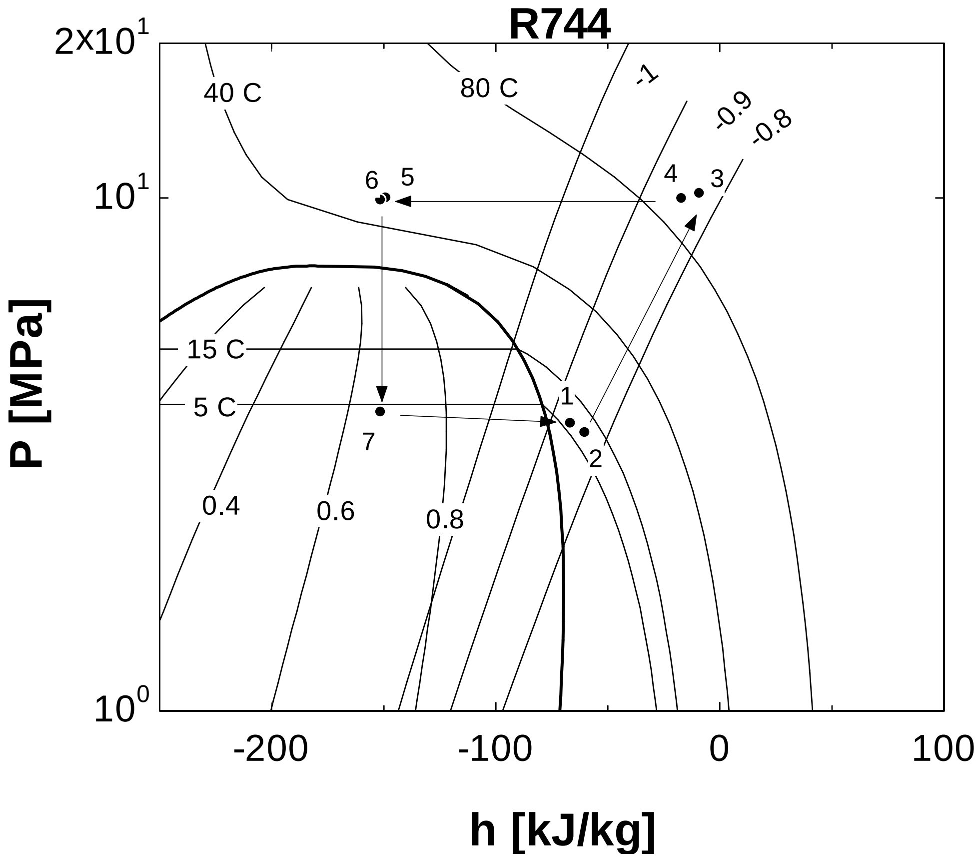

Figure 1.1: Transcritical cycle in a CO_2 pressure-enthalpy diagram

Although ejectors have been widely used in the refrigeration and other industries for many years, most ejector applications use single-phase working fluids. In comparison, only few studies can be found in the literature on two-phase flow ejectors, as used in ejector expansion refrigeration cycles. However, the design parameters and the operation conditions of a transcritical two-phase flow ejector are significantly different than the ones for a single-phase application. In addition, the interaction of the ejector expansion device with other system components such as compressor, gas cooler and evaporator is not well understood.

1.2. Objectives

Thus, the current study was carried out to conduct a detailed theoretical investigation of using an ejector expansion device in a transcritical carbon dioxide cycle and a conventional R410A vapor compression cycle. The main objectives of this study are:

- Develop a two-phase flow ejector simulation model to investigate the effects of the geometry parameters and operation conditions on the performance of a two-phase flow ejector used in ejector expansion transcritical CO_2 systems.
- Develop a detailed ejector expansion transcritical CO_2 system simulation model to investigate the impact of the ejector expansion device on the performance of the overall system and the other system components such as compressor, gas cooler and evaporator.
- Validate the two-phase flow ejector simulation model and the simulation model of the ejector expansion transcritical CO_2 system with experimental results,
- Repeat the two-phase flow ejector model and system model development for R410A vapor compression systems.
- Perform parametric studies with the ejector expansion transcritical CO_2 system and R410A vapor compression system simulation models to investigate the potential performance improvements over the basic systems for various applications.

1.3. Approach

In a first step, an extensive literature review was conducted. The results of this literature review are summarized in the second chapter of this document. In particular, the recent advancements in ejector research and design, the availability and usage of ejectors in applications in and beyond the field of refrigeration, technologies and solutions found in other application fields that can be applied to ejectors used in refrigeration systems, and the COP improvements of using ejector expansion devices in refrigeration systems, are documented.

Secondly, by combining the one-dimensional global conservation equations of mass, momentum, and energy balances and the two-phase flow characteristics such as critical flow conditions in the nozzle and pressure recovery degradation in the diffuser, a two-phase flow ejector model was established (Chapter 3). The ejector model includes sub-models for the motive nozzle, suction nozzle, mixing section and diffuser. The irreversibilities of certain processes in the two-phase flow ejector were accounted for by using efficiency values determined by experimental results or taken from available literature studies. The ejector model was used to predict the effects of design parameters and operation conditions on the ejector performance.

Thirdly, a detailed ejector expansion transcritical refrigeration system simulation model was developed to predict the performance of air-to-air unitary air conditioners and heat pumps with CO_2 as the refrigerant (Chapter 4). The model was based on the previous work by Robinson (2000) and Ortiz (2002). The gas cooler and the evaporator were modeled based on microchannel heat exchanger geometries. The compressor was modeled based on map-based compressor performance data (Hubacher and Groll 2002). In addition, the two-phase flow ejector was incorporated into the overall system simulation model.

Within a previous study (Li 2005), a transcritical CO_2 refrigeration system has been designed and constructed (Chapters 5 and 6). The system is based on a military standard 10.3 kW (3 ton) environmental control unit (ECU). Experiments were performed by operating the fully instrumented system as a basic transcritical CO_2 air conditioner and by using an ejector expansion device with otherwise, the same compressor and heat exchangers. The experimental results were compared to simulation results of the two-phase flow ejector model and the system simulation model in order to validate the models. The models were modified to provide reasonable predictions of the component and system performance.

Next, the two-phase flow ejector and system model development were repeated for the refrigerant R410A (Chapter 7). The two-phase flow ejector model for CO_2 was updated to predict the performance of R410A ejector expansion devices. Then, the R410A ejector model was incorporated into an existing vapor compression system simulation model, called ACMODEL, to predict the performance of air-to-air unitary air conditioners and heat pumps.

Finally, the ejector expansion transcritical CO_2 system simulation model and the ejector expansion R410A vapor compression system simulation model were exercised to conduct parametric studies (Chapter 8). These studies investigated the feasibility, the potential improvement in cycle performance, and the required design of ejector expansion devices for transcritical CO_2 cycles and R410A vapor compression cycles for various refrigeration, air conditioning and heat pumping applications and operation conditions.

2. LITERATURE REVIEW

2.1. Transcritical CO_2 refrigeration cycle research

Kim et al. (2004) published an overview of the fundamental processes and system design issues of CO_2 vapor compression systems. The authors presented recent developments and the state of the art of the transcritical CO_2 cycle technology for various refrigeration, air-conditioning and heat pump applications. Their review included discussions of properties and characteristics of CO_2, cycle fundamentals, method of high-side pressure control, thermodynamic losses, cycle modifications, component/system design, safety factors, and promising application areas. Thus, the overview presented here is focused more specifically on the throttling losses associated with the transcritical CO_2 refrigeration cycle and various approaches to reduce these losses in order to improve the energy efficiency of the overall system.

Robinson and Groll (1998) first applied a second law thermodynamic analysis on the transcritical CO_2 refrigeration cycles with and without an expansion turbine. It was found that the expansion valve is the component with the largest percentage of total irreversibility of the expansion valve carbon dioxide cycle. Replacing the expansion valve with an expansion work recovery turbine with an isentropic efficiency of 60% reduces the process's contribution to total cycle irreversibility by 35%. It was also found that the use of an internal heat exchanger in conjunction with the use of a work recovery device tends to reduce the COP of the transcritical carbon dioxide cycle by up to 8%.

Brown et al. (2002) presented the evaluation of carbon dioxide as an R-22 substitute for residential air conditioning applications. The performance of CO_2 and R-22 in residential air-conditioning applications was compared using semi-theoretical vapor compression and transcritical cycle models. It was found that the R-22 system had a significantly better COP than the CO_2 system when equivalent heat exchangers were used in the CO_2 and R-22 systems. An entropy generation analysis showed that the highest level of irreversibility was realized in the CO_2 expansion device, and together with the irreversibility in the gas cooler, were mainly responsible for the low COP of the CO_2 system.

Based on these studies it can be concluded that the reduction of the throttling losses is one of the key issues to improve the efficiency of transcritical CO_2 refrigeration cycles. Various ideas on novel expansion work recovery devices to improve the efficiency of the basic transcritical CO_2 refrigeration cycle have been introduced during the last decade. The major of these ideas focused on the development of expansion work recovery machines.

A free piston expander-compressor unit was proposed by Heyl et al. (1998) to recover the expansion losses. The machine has two double-acting pistons, which were connected by a piston rod. The cylinder was divided by each piston into a compression chamber and an expansion chamber. However, implementation of the concept requires a two-stage refrigeration cycle as the machine was intended to be used as a second-stage compressor (from intermediate to high pressure), driven by the expansion work from high to low pressure.

Maurer and Zinn (1999) performed a theoretical and experimental study of expanders for CO_2. They detailed the practical challenges for expansion work recovery devices from a hardware standpoint. As cooling systems experience a wide range of mass flow rates, a robust design is required. Both axial piston machines and gear machines were studied. Axial piston machines reached 40-50% energy efficiency and gear machines reached 55% energy efficiency.

Hesse and Tiedemann (1999) applied for a patent for the possible use of a pressure wave machine to compress a part of vapor from the evaporator outlet by using the expansion energy.

Adachi et al. (1999) also applied for a patent in which a combined axial-piston compressor/expander unit with expansion ratio control was used to keep the high-side pressure at the optimum for a transcritical CO_2 refrigeration cycle.

Li et al. (2000) performed a thermodynamic analysis of different expansion devices for the transcritical CO_2 cycle. A vortex tube expansion device and an expansion work output device were proposed to recover the expansion losses. The maximum increase in COP using a vortex tube or expansion work output device, assuming ideal expansion processes, was approximately 37% compared to the one using an isenthalpic expansion process. The increase in COP reduced to about 20% when the efficiency for the expansion work output device was 0.5. In order to achieve the same improvement in COP using a vortex tube expansion device, the efficiency of the vortex tube had to be above 0.38.

Heidelck and Kruse (2000) proposed a CO_2 expander design based on a modified axial piston machine. They suggested the use of a rotating control disc and slots similar to what is used in hydraulic machines for the mechanically controlled valves needed by the expander. They also discussed the design for a combined compressor-expander machine in one axial-piston unit. However, only moderate efficiencies were reached during the experiments of a modified hydraulic machine due to internal leakage in the control disc sealing surfaces.

Hesse (2000) studied the use of a gear machine with helical gears as an expander in CO_2 vehicle air conditioning systems. Adiabatic efficiencies of up to 50% were predicted for such a machine.

Nickl et al. (2002) proposed a second generation expander-compressor with a simpler design and a 10% increase in COP compared to the first generation machine proposed by Heyl et al. (1998). They estimated that it might provide a 50% improvement in COP over the throttle valve system.

Baek et al. (2002) discussed the development of a piston-cylinder expansion device for the transcritical carbon dioxide cycle. A prototype piston-cylinder work output expansion device was designed based on a highly modified small four-cycle, two-piston engine that is commercially available. Fast-acting solenoid valves were used as intake and exhaust valves to control the expansion process. A 10% increase of COP was measured by replacing the expansion valve with the work output expansion device in an experimental transcritical CO_2 system.

Stosic et al. (2002) discussed using a twin screw combined compressor and expander for CO_2 refrigeration systems. They proposed a balanced rotor concept that can partially balance the rotor forces created by the compression and expansion processes in order to eliminate the axial forces and reduce the radial bearing forces. Design problems associated with high bearing loads in screw compressors for CO_2 systems are thereby reduced.

Westphalen and Dieckmann (2004) developed a scroll expander design for use in carbon dioxide air-conditioning cycles operating at high ambient conditions. The expander efficiency is projected to be 70%. A 20% reduction in system power input when using a 60% efficient expander was estimated by cycle analysis. It was suggested that the most attractive approach to utilize the expander shaft power is to offset the compressor shaft power in an integrated compressor/expander unit.

2.2. Ejector expansion transcritical CO_2 cycles and the COP improvements of using ejector expansion devices in refrigeration systems

Only limited work can be found with respect to transcritical ejector expansion devices although the COP can be improved by using them in refrigeration systems.

Liu et al. (2002) performed a thermodynamic analysis of a transcritical CO_2 vapor-compression/ejection hybrid refrigeration cycle. In this cycle, an ejector is used instead of a throttling valve to recover some of the kinetic energy of the expansion process. Through the action of the ejector the compressor suction pressure is higher than it would be in a standard cycle, resulting in less compression work and improved system efficiency.

Elbel and Hrnjak (2004) studied the effect of an internal heat exchanger on the performance of a transcritical CO_2 system with an ejector. Instead of using a simplified thermodynamic cycle analysis, their approach was based on a more elaborated and experimentally validated system model for a real mobile air-conditioning system for a typical mid-sized car. The modeling of the ejector within the system model was based on several idealized assumptions. Their results indicated that the use of an ejector significantly increases the performance compared to systems without ejector and without internal heat exchanger. In comparison to a conventional system with internal heat exchanger, the utilization of an internal heat exchanger in the ejector system yields less performance increase than the ejector system without an internal heat exchanger.

Jeong et al. (2004) constructed a simulation model of a two-phase flow ejector and a vapor compression cycle with an ejector. They investigated the characteristics of the ejector and the performance of the cycle using the ejector by simulation. The working fluids were ammonia and CO_2. Based on the simulation result, an optimum mixing section inlet pressure exists which maximizes the performance of the ejector. In case of an ejector efficiency of 90%, the COP of the vapor compression cycle using ammonia with the ejector is 5% higher than that of the conventional cycle and the COP of the cycle using CO_2 with the ejector is 22% higher than that without an ejector.

Ozaki et al. (2004) studied the regeneration of expansion energy by using an ejector in a CO_2 cycle. The COP improvement by employing an ejector cycle was compared with that for an expander cycle for ideal and realistic cases. An experiment was carried out in order to verify the potential of COP improvement. When the COP improvement of the ejector cycle was compared to that of the expander cycle under the condition that the recovered expansion power was used ideally, the ejector cycle provides the COP improvement of less than half of that the expander cycle due to the unavoidable losses caused by the irreversible mixing in the mixing section of the ejector. However, if the efficiencies of the ejector and the expander were taken into consideration, the COP improvement of the ejector cycle was equal to, or better than that of the expander cycle. It was determined that the refrigerant flow in the nozzle reaches supersonic flow conditions. The critical flow rate of the CO_2 coincided with the value calculated by the IHE (Isentropic Homogeneous Equilibrium) model. The gas cooling pressure of the CO_2 cycle could be controlled by changing the throat area of the nozzle. Finally, the experiment using the ejector in a car air-conditioner verified the COP improvement of approximately 20 %.

Li and Groll (2005) proposed an ejector expansion transcritical CO_2 refrigeration cycle to improve the COP of the basic transcritical CO_2 cycle by reducing the expansion losses. A constant pressure mixing model for the ejector was established to perform the thermodynamic analysis of the ejector expansion transcritical CO_2 cycle. The effect of the entrainment ratio and the pressure drop in the receiving section of the ejector on the relative performance of the ejector expansion transcritical CO_2 cycle was investigated for a typical air conditioning operation condition. The effect of the different operation parameters on the relative performance of the ejector expansion transcritical CO_2 cycle was also investigated using an assumed value for the entrainment ratio and pressure drop in the receiving section of the ejector. It was found that the COP of the ejector expansion transcritical CO_2 cycle can be improved by more than 16% over the basic transcritical CO_2 cycle for typical air conditioning operation conditions.

Ksayer and Clodic (2006) used a constant pressure-mixing-zone model for the ejector and found that the COP of the ejector expansion transcritical CO_2 can be improved by more than 15% compared to the conventional transcritical cycle for typical air conditioning operating conditions.

Deng et al. (2007) conducted a theoretical analysis of a transcritical CO_2 ejector expansion refrigeration cycle which uses an ejector as the main expansion device instead of an expansion valve. It was found that the maximum cooling COP of the ejector expansion cycle is up to 22% better than the cooling COP of a conventional vapor compression refrigeration cycle and the ejector expansion cycle cooling capacity is 11.5% better than the conventional refrigeration cycle cooling capacity. In addition, the ejector expansion cycle performance was found to be very sensitive to operating conditions.

The following conclusions can be drawn from the literature review presented in Sections 2.1 and 2.2:

- The expansion losses by an isenthalpic throttling process are a major irreversibility that contributes to the low energy efficiency of transcritical CO_2 refrigeration cycles.
- The expander-compressor approach to reduce the throttling losses in a transcritical CO_2 refrigeration cycle involves complex mechanical construction, difficulty in control, restricted system integration and other issues that make it immature for practical applications.
- Using an ejector expansion device in a transcritical CO_2 refrigeration cycle is attractive because the ejector is simple to construct and provides robust operation without moving parts.

2.3. Ejector expansion refrigeration cycle

A typical ejector consists of a motive nozzle, a suction nozzle or receiving chamber, a mixing section and a diffuser. High pressure motive stream expands in the motive nozzle and its internal energy converts to kinetic energy. The high speed motive stream entrains low pressure suction stream into the mixing section. Both streams exchange momentum, kinetic and internal energies in the mixing section and become one stream with almost uniform pressure and speed. The stream converts its kinetic energy into internal energy in the diffuser to reach a pressure higher than the suction stream inlet pressure. When an ejector is used to replace the expansion valve in a transcritical CO_2 cycle, the expansion work lost during isenthalpic expansion process will be recovered by the ejector to increase the evaporator outlet pressure to a higher compressor suction pressure. The compression work may be reduced due to the lower pressure ratio, which increases the COP of the system.

The working processes of an ejector are shown in detail in Figures 2.1 and 2.2. The motive stream expands in the motive nozzle from the high pressure P_1 to the receiving chamber pressure P_b. The enthalpy reduces from h_1 to h_{mb} and the velocity increases to u_{mb}. The suction stream expands in the suction nozzle from pressure P_2 to P_b. The enthalpy reduces from h_2 to h_{sb} and the velocity increases to u_{sb}. The two streams mix in the mixing section and become one stream with pressure P_m and velocity u_{mix}. This stream further increases its pressure to P_3 in the diffuser by converting its kinetic energy into internal energy.

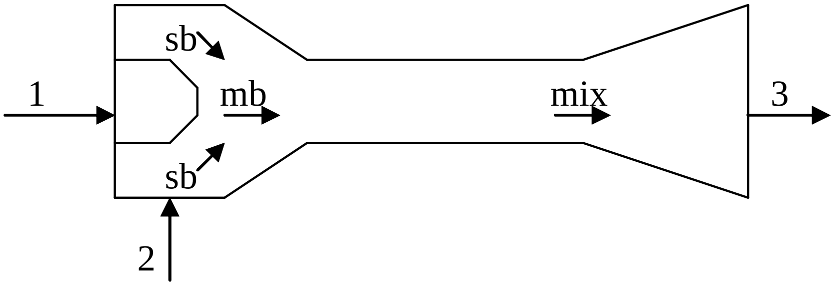

Figure 2.1: Schematic of the ejector working processes

The ejector is the key component in jet refrigeration cycles. Chunnanond et al. (2004) presented a literature review on ejectors and their applications in refrigeration. A number of studies are grouped and discussed based on several topics, i.e. background and theory of ejectors and jet refrigeration cycles, performance characteristics, working fluids and improvements of jet refrigerators. Moreover, other applications of an ejector in other type of refrigeration systems are also described. Thus, the literature review presented here is only focused on ejector expansion refrigeration cycle research with conventional refrigerants as working fluids.

Ejector expansion refrigeration cycles are shown in Figures 2.3 and 2.4. Gay (1931) invented the ejector expansion refrigeration cycle and received a patent for it. Modifications were proposed by Kemper et al. (1966) and Newton (1972a, 1972b). Kornhauser (1990) first presented an analysis of the cycle and predicted that improvements of up to 21% over the standard cycle are possible. Menegay (1991) performed an experimental investigation of an ejector as a refrigerant expansion device and showed a more modest improvement of 3.7%. The inefficiency of the ejector was attributed to the discrepancy between these numbers.

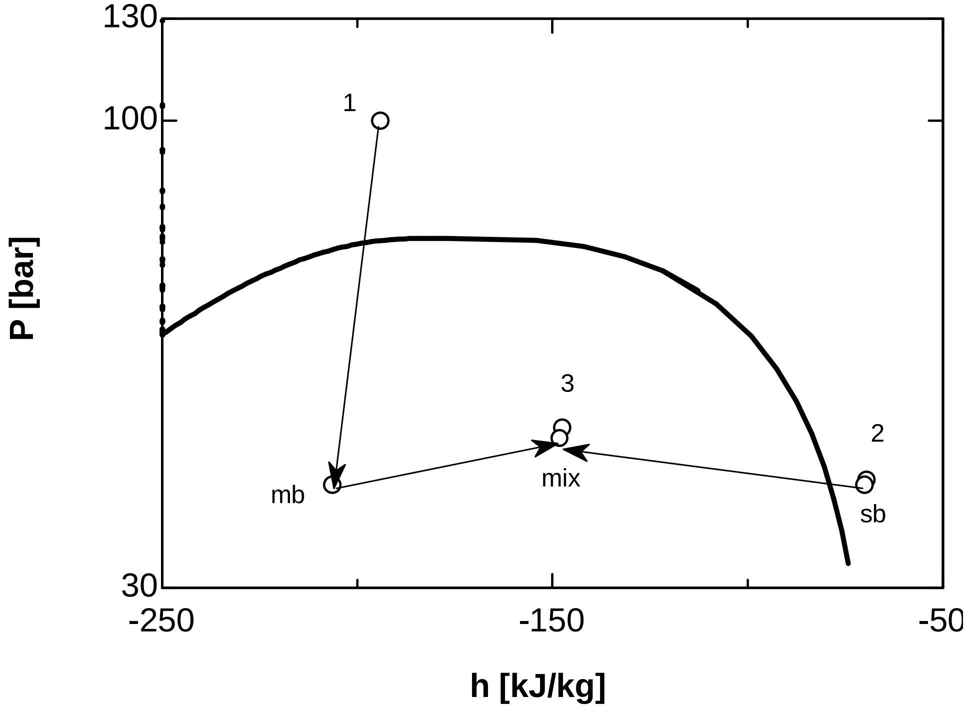

Figure 2.2: Ejector working processes in a CO_2 pressure-enthalpy diagram

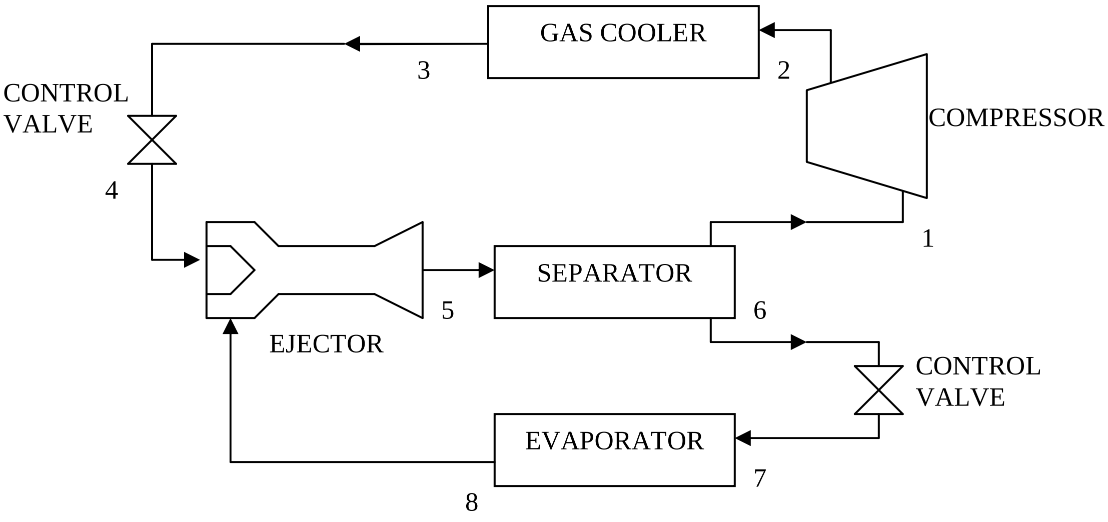

Figure 2.3: Schematic of ejector expansion transcritical cycle

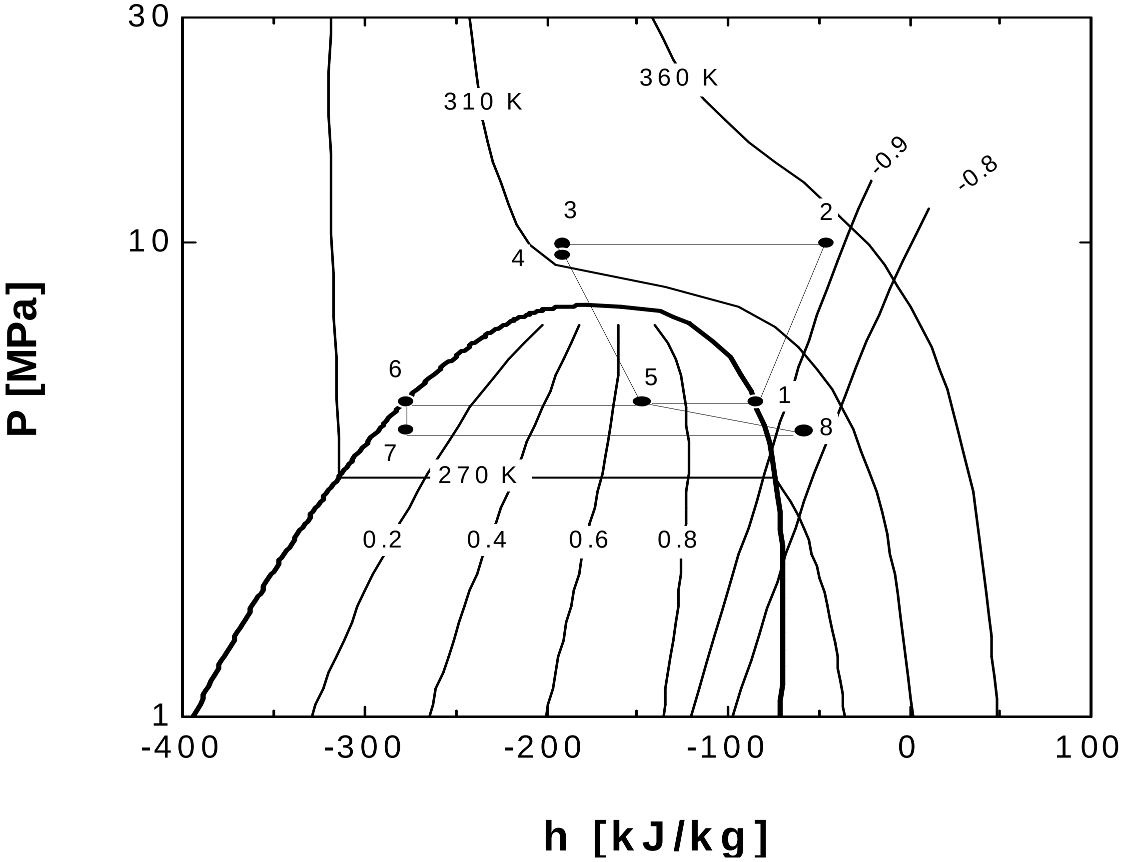

Figure 2.4: Ejector expansion refrigeration cycle in a CO_2 pressure-enthalpy diagram

Menegay and Kornhauser (1994) proposed an improved design method for ejectors used as refrigerant expansion devices in vapor compression cycles. They showed that the assumption that the motive and suction nozzles should have the same outlet pressures for the ejector to reach optimal efficiency is only valid when both the motive and suction nozzles have efficiencies equal to one. Under all other circumstances, the motive nozzle discharge pressure is, optimally, greater than that of the suction nozzle. A one-dimensional, homogeneous equilibrium model with constant area mixing assumption was used for the ejector design. Refrigerant R-134a was used in their analysis.

Harrell and Kornhauser (1995) reported on performance tests of a two-phase flow ejector for ejector expansion refrigeration applications. Theoretically, a cooling COP improvement of approximately 23% is achievable for a typical refrigerating cycle and an ideal ejector. If the ejector has the same performance of typical single-phase ejectors, an improvement of 12% could be achieved. However, their preliminary data only showed an ejector performance corresponding to refrigeration cycle COP improvements ranging from 3.9% to 7.6%. They suggested that a more through understanding of the flow occurring within the ejector must be developed to achieve the operating potential of the ejector expansion refrigeration cycle.

Menegay and Kornhauser (1996) proposed improvements to the ejector expansion refrigeration cycle. They realized that unlike single-phase ejectors, upstream throttling is beneficial for flashing flow nozzles. By adding a throttle valve and a bubbly flow tube before the motive nozzle, the measured COP improvements reached 3.2% to 3.8%. The test apparatus was a 3.5 kW air-to-air R-12 air conditioning system designed for typical AC operating temperatures.

Domanski (1995) analyzed the performance of pure-component refrigerants in the basic vapor compression refrigeration cycle and in three modified cycles in which the throttling-process irreversibilities are minimized. One of these cycles was the ejector expansion vapor compression cycle. He found that the COP of the ejector cycle is very sensitive to the ejector efficiency. Thus, he noted that it is unclear what performance level the ejector cycle can achieve due to the limited knowledge of the efficiency of two-phase ejectors. The economizer cycle had a marginally better COP than the ejector cycle when the single-phase component efficiencies (0.85 for the nozzle, 0.7 for the diffuser) were used in simulations for R-134a at some operating conditions.

Based on the summaries given in this section, it can be seen that the ejector expansion refrigeration cycle with conventional refrigerants as working fluids only attracted limited researcher’s interests because the expansion losses in vapor compression refrigeration cycles with CFC, HCFC or HFC refrigerants are relatively small and the liquid/vapor two-phase ejectors are considered to have lower efficiencies than typical single-phase ejectors (Harrell and Kornhauser 1995). However, the experiences gained from the ejector expansion refrigeration cycles with conventional refrigerants prove that it is feasible to implement an ejector expansion transcritical refrigeration cycle with CO_2 as the working fluid. A better understanding of two-phase flow ejectors is necessary to realize the potential of the ejector expansion transcritical refrigeration cycle.

2.4. Recent advancements in ejector research and design: the availability and usage of ejectors in applications in and beyond the field of refrigeration

For single-phase ejectors, there are well established models to conduct performance analysis and design calculations (Keenan et al., 1950, Munday and Bagster, 1977, Huang et al., 1999). Keenan *et al.* (1950) made an investigation of ejector designs by analysis and experiment. Their experimental observations indicated that the length required between motive nozzle exit and mixing section exit depends upon both the mixing process and the shock process. Even when using optimum geometries for the ejector, the performance of the ejector varied drastically based on the position of the motive nozzle relative to the suction nozzle and mixing chamber entrance. The variations in maximum ejection ratio with different position of motive nozzle for four different types of secondary inlet were depicted. When the mixed flow is subsonic, the requirement of mixing dominates; when the mixed flow is supersonic, the requirement of the shock dominates. The length required for the mixing process was indicated to be 7 to 8 times of the mixing section diameter in Keenan and Neumann (1942), where the mixed stream was always subsonic. When the mixed stream is supersonic, the total length from motive nozzle exit to mixing section exit is nearly constant with the increase of Pi/Po as shown in Figure 2.5 (state “i” is the initial stagnation state of the motive stream and state “o” is the initial stagnation state of the suction stream). This is much the same as that for a shock in a tube carrying a single stream.

No empirical function has been found to determine the optimum length of the ejector mixing section.

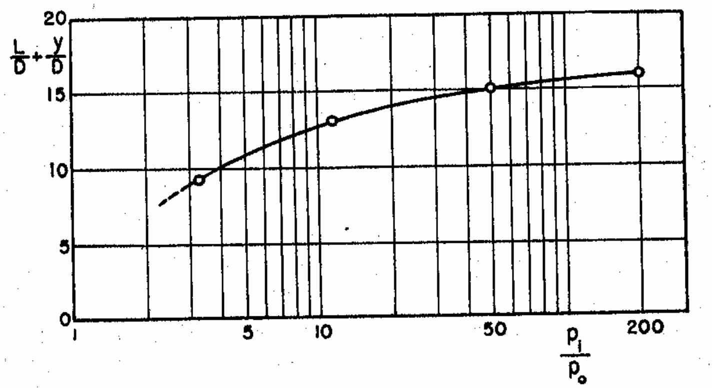

Figure 2. 5: Optimum length from motive nozzle exit to diffuser entrance as a function of pressure ratio (Keenan *et al.* 1950)

Sun (1995) gave a review of the design theories and applications of ejectors with single-phase working fluids. However, for two-phase flow ejectors, there are no established models to perform an analysis or design a device because of the complexity of the two-phase flow. A review on the two-phase flow ejector models is presented below to demonstrate the issues involved in two-phase flow ejector modeling.

Cunningham (1974) proposed a one dimensional model including frictional losses to describe the isothermal compression of a gas by a liquid jet in a mixing throat followed by secondary compression in a diffuser. Mixing throat and diffuser energy analyses are presented. The efficiency of a liquid-jet gas pump is concluded to be dependent primarily on the mixing losses. The mixing loss function, the throat compression ratio and the Mach number are developed as functions of the throat inlet velocity ratio between liquid jet and suction gas and the jet pump number, a dimensionless parameter defined by the author.

Neve (1988) developed a computer simulation model based on the simplification of the model proposed by Cunningham (1974) to predict the performance of liquid jet gas pumps. By incorporating the empirical relations developed from the experimental results into the simplified model of Cunningham (1974), a computer simulation model was developed to predict the performance of a liquid jet gas pump when the geometric parameters are given, or to calculate the geometric parameters when the performance specifications are given.

Cunningham (1995) extended his model on liquid jet gas pumps to liquid jet gas liquid pumps that have a suction stream of a two-phase mixture. Friction-loss coefficients used in the model should be determined experimentally. Throat-entry choking of the secondary flow can be predicted. However, no phase changing is allowed in the model, i.e. no vapor evaporation from or condensation to the liquid.

Rao and Kremer (1993) developed a general method of designing gas and gas-liquid injectors based on the equation for entrainment of a turbulent free jet. They claim that compared to the conventional design of injectors, starting from macroscopic mass and momentum balances, their method is much simpler, easily applicable and involves only one empirical entrainment coefficient. The motive stream is gas and the suction stream is liquid, and no phase change is allowed in the process.

Menegay and Kornhauser (1995) presented a plan to develop a semi-parabolic two-fluid model for two-phase flow ejectors. The applicable two-phase flow conservation equations are presented. The model was also supposed to include the interfacial interaction terms which are important in modeling the non-equilibrium effects and the compressibility effects for the gaseous phase. However, no further literature was published on the progress of this model.

Deberne et al. (1999) developed a model to calculate the performance of steam injector. General conservation relationships were presented from the nozzle exit to the steam injector outlet. It was shown that the flow contains a condensation shock. To achieve modeling of the mixing zone, an empirical correlation giving an equivalent pressure for the value of the condensation rate was found using experimental results. A parametric study was then made to determine the significant parameters and the operating range of the steam injector. Calculated results from the model agreed well with the experimental results.

Lear et al. (2000) presented a design-oriented model for two-phase flow ejectors for refrigeration and thermal management applications. The motive stream is a two-phase one component fluid and the suction stream is a subcooled liquid of the same substance. The analysis accounts for the possibility of supersonic flow entering the diffuser and inducing the formation of a shock wave. The change in properties across such shocks was computed using the Rankine-Hugoniot relations developed for two-phase flow. A constant pressure mixing chamber is assumed for the analysis. The results of the model show optimal geometric area ratio as well as system state point information as a function of the inlet states and entrainment ratio. However, the speed of sound of the two-phase fluid is simply calculated with the single-phase speed of sound formula.

Rogdakis and Alexis (2000) discussed the design and parametric investigation of an ejector in an air-conditioning system with R-717 as the working fluid. They developed a computer simulation model based on the theory developed by Munday and Bagster (1977). A thermodynamic shock and mixing was assumed to occur at the very end of the converging cone of the mixing chamber. The subsonic velocity of the mixed stream after shock was found by the intersection of the Fanno and Rayleigh lines. They later published a verification study of their steam ejector refrigeration model with experimental results (Alexis and Rogdakis, 2003).

Parker and Lear (2001) reported on a mathematical analysis of a two-phase flow ejector to determine the optimum area ratio for ejector performance. Inlet conditions were specified and nozzle outlet areas were varied to determine the effect on the compression ratio. The mixing chamber was assumed to have a constant cross-sectional area. At the diffuser inlet, the Mach number was checked to determine if a shock wave occurred.

Lear et al. (2002) further extended their model on two-phase flow ejectors to handle the Fabri limit on the secondary mass flow rate. A constant area mixing chamber is assumed. To simplify the model, no frictional loss or thermal loss were considered and the two-phase flow was treated as homogeneous equilibrium flow. However, the calculation of the speed of sound of the two-phase flow remains the same as that of Lear et al. (2000).

Bergander (2006) developed a novel two-phase ejector model for refrigerant R-22 with a condensing ejector as a second-stage compressor. The condensing ejector is a two-phase jet device in which a sub-cooled working fluid in a liquid state is mixed with its vapor phase, producing a liquid stream with a pressure that is higher than the pressure of either of the two inlet streams. The amount of mechanical energy required by a compressor is reduced and the efficiency is increased. A possible 38% theoretical efficiency improvement can be achieved compared to the traditional vapor compression cycle. Practical demonstrations of 16% energy savings were achieved using a prototype.

Yu and Li (2006) carried out a theoretical analysis of the performance characteristics of a novel cycle with the refrigerant R-141b. An auxiliary jet pump (liquid-vapor type ejector) and a conventional regenerator were used to enhance the performance of the novel cycle. In this case, a single-phase ejector is used to enhance the cycle performance. The COP improvement of the novel cycle reached 17.8% compared to the one of an ejector expansion refrigeration cycle. The performance characteristics of the novel cycle showed its promise by using low grade thermal energy for the ejector refrigeration system.

Chaiwongsa and Wongwises (2007) studied experimentally the effect of throat diameters of the ejector on the performance of the refrigeration cycle using three two-phase ejectors as an expansion device. These ejectors consist of convergent-divergent motive nozzles with various throat diameters of 0.8 mm, 0.9 mm and 1.0 mm, a constant pressure mixing chamber having a constant diameter of 10.0 mm, and a constant diffuser exit diameter of 22.0 mm. The test runs were carried out at heat source temperatures of 8 °C (46.4 °F), 12 °C (53.6 °F) and 16 °C (60.8 °F). The variation of the system's COP was obtained from using the various throat diameters at the heat sink temperature of 26.5 °C (79.7 °F), 29.5 °C (85.1 °F), 32.5 °C (90.5 °F), 35.5 °C (95.9 °F) and 38.5 °C (101.3 °F). It was found that in the R-134a system, the motive nozzle having a throat diameter of 0.8 mm yielded the highest COP, while the motive nozzle having a throat diameter of 1.0 mm yielded the lowest COP.

The experimental data in Elbel and Hrnjak (2008) showed that the ejector simultaneously improved the COP and cooling capacity by up to 7% and 8%, respectively, in the CO_2 system. Values of 0.8 were assumed for the individual ejector component efficiencies in the ejector calculation routine to get the results that served as the basis for the design of the experimental prototype ejector. An overall ejector efficiency based on standard pressure, temperature, and mass flow rate measurements was defined. Experiments showed that the ejector performed with a higher efficiency when the high-side pressure was relatively low. However, it was also found experimentally that despite lower ejector efficiencies, the COP increased as the high-side pressure increased as a result of using the integrated needle to reduce the motive nozzle throat area in the ejector.

Elias (2007) assumed that the efficiencies of the motive nozzle, suction nozzle and diffuser were all equal to 1, and calculated a newly defined mixing section efficiency to meet the measured ejector outlet pressure. The empirical equation expressing the mixing section efficiency as a function of the flow and ejector parameters was obtained.

Table 2.1 provides a summary of the theoretical and experimental studies related to ejectors, indicating the efficiencies of the suction and motive nozzles or of the ejector, if they were available.

Table 2.1: Summary of ejector studies found in the literature

Authors	Fluid	Type of studies and value of ejector efficiencies
Keenan and Neumann (1942)	Air	Modeling study: isentropic flow through the throat motive nozzle; the secondary fluid expands reversibly and adiabatically in the suction nozzle; The frictional forces applied by the stream on the walls of the mixing section are negligible; $A_m + A_s = A_{mix}$. Experimental study: converging nozzles; converging-diverging nozzles; $(L_{mix}/D_{mix})_{opt} = 7$. For the largest measured pressure rise across the suction stream, the experimental flow rate is approximately 87% of the calculated flow rate using a converging primary nozzle. The measured pressure rise of the flow from suction nozzle exit to the mixing section exit is 90% of the calculated value for converging nozzles.
Keenan et al. (1950)	Air	Modeling study: $\eta_m = \eta_s = 1$, reversible subsonic diffuser. Mixing is complete. Experimental study: one dimensional analysis of converging-diverging nozzle; $A_{mix}/A_t = 4\text{-}100$; $y/D_{mix} = 6\text{-}8$; $L_{mix}/D_{mix} = 7\text{-}8$ (mixing stream subsonic). The measured values of the static pressures at the mixing section exit are between 93 to 99% of the corresponding computed values for a broad range of operating conditions. Coefficients to account for irreversibilities in the subsonic diffuser and the accelerating nozzles, and for friction along the mixing-tube walls could be added to the design procedure, should a more precise prediction be desired, but were not given in the study. The ejector measurements yielded values of $P_{diffuser\text{-}exit} / P_{suction\text{-}nozzle\text{-}inlet}$ equal to 86% of the computed values at measured flow rates of 85% of the computed values.
Emanuel (1976)	Gas	Modeling study: supersonic motive nozzle; η_n not given. The flow is fully mixed at the entrance to the diffuser, and heat transfer and drag losses to the walls are negligible in gaseous flow.
Domanski (1995)	R134a	Modeling study: single phase, $\eta_m = \eta_s = 0.85\text{-}0.9$, $\eta_d = 0.7$ (assumed)
Takeuchi et al. (2002)	CO_2	Invention disclosure: Supersonic nozzle; $L_{mix} / D_{mix} \leq 120$; $D_{mix} / D_m = 1.05 – 4.5$; η_m, η_s and η_d not given.

Alexis and Rogdakis (2003)	Water	Modeling study: $\eta_m = 0.7$, $\eta_d = 0.8$ (assumed).
Elbel and Hrnjak (2004)	CO_2	Modeling study (EES): $\eta_m = \eta_s = \eta_d = 0.9$ (assumed)
Disawas and Wongwises (2004)	R134a	Experimental study: converging-diverging motive nozzle; mixing section; $L_{mix} / D_{mix} = 11$; (based on ASHRAE Handbook); η_m and η_s not given.
Yapici and Ersoy (2005)	R123	Modeling study: supersonic motive nozzle; constant area mixing section; $\eta_m = \eta_s = \eta_d = 0.85$ (assumed); one dimensional adiabatic flow; motive and suction flows are fully mixed at the exit of mixing section.
Li and Groll (2005)	CO_2	Theoretical model (EES): the flow in the ejector is considered a one-dimensional homogeneous equilibrium flow; assumed: $\eta_m = \eta_s = 0.9$, $\eta_d = 0.8$.
Rusly (2005)	R141b	CFD study: Converging-diverging nozzle; constant area mixing section; $(L+ y)/D_m=10$; $y/D_m = 1.5D_m$; $\alpha_d = 3.5°$; $\alpha_{rc} = 10$; η_n not given.
Ksayer and Clodic (2006)	CO_2	Modeling study (supersonic motive nozzle): Assumed: $\eta_m = \eta_s = 0.85$, $\eta_d = 0.75$.
Kim and Kwon (2006)		Experimental study (supersonic ejector): L/D = 6, 8, 10; $\alpha_{rc} = 4, 7, 10$; η_m and η_s not given.
Yu and Li (2006)	R141b	Modeling study: homogenous two-phase flow in mixing chamber; isentropic flows in the nozzles and the diffuser are affected by an isentropic efficiency coefficient accounting for friction losses; mixing losses are accounted for by a coefficient equivalent to friction; Assumed: $\eta_m = 0.90$, $\eta_d = 0.85$, $\eta_{mix} = 0.85$.
Deng et al. (2007)	CO_2	Modeling study: $\eta_m = 0.7$, $\eta_s = 0.8$ (assumed)

Based on the literature review presented in this section, it can be seen that most models on two-phase flow ejectors are established by applying one-dimensional conservation equations to different component sections such as motive nozzle, suction nozzle, mixing section and diffuser. Often two-phase flow is treated as homogeneous equilibrium flow to simplify the model. In addition, the speed of sound of the two-phase flow is often calculated based on the single-phase fluid formula. It seems that without a better understanding of the two-phase flow characteristics during the process in each component of the ejector, it is very difficult to set up a two-phase flow ejector model that is predictive enough to serve as a design tool. A review of the research studies of the different processes involved in a two-phase flow ejector is presented below to illustrate the two-phase flow characteristics in a two-phase flow ejector.

2.5. Technologies and solutions found in other applications that can be applied to ejectors used in refrigeration system

Henry and Fauske (1971) investigated the two-phase critical flow of one-component mixtures in nozzles, orifices, and short tubes. Their two-phase critical flow model for convergent nozzle, orifices and short tubes included considerations of the interphase heat, mass, and momentum transfer rates. Based on the experimental results available at that time, they made credible assumptions to approximate these interphase processes and generated a transcendental expression for the critical pressure ratio as a function of the stagnation pressure and quality. A solution to this expression also yielded a prediction for the critical flow rate. The predictions showed good agreement with the experimental data.

Elliott (1985) discussed the computation of two-phase nozzle flow through a prescribed shape. Gas and liquid are assumed to travel at different velocities. The liquid phase is assumed to be uniformly dispersed as spherical drops with the same diameter. The phases interact through drop drag, drop heat transfer, drop evaporation, and gas solubility. A critical value of the Weber number determines the drop breakup and the diameter of drops after breakup. Frictional loss is calculated by multiplying the wall shear for the liquid by the liquid volume fraction. It was found that the flow rate in a two-phase nozzle may be determined by choking at the exit rather than at the throat. In over-expanded two-phase flow nozzles, the pressure drops below the external pressure in the diverging section and then rises to match the external pressure at the exit.

Romstedt and Werner (1986) performed a numerical analysis of critical two-phase flow in a convergent-divergent nozzle. The critical state is identified by its mathematical properties, i.e., characteristics and solvability of linear systems with a singular matrix. The critical state is calculated numerically as the asymptotic steady-state solution of the time- and space-dependent two-phase flow equations. The two-phase flow is described by a model with equal phase velocities and thermodynamic nonequilibrium. A “model consistent” two-phase sonic velocity was identified as a component of the eigenvalues of the two-phase flow equation set.

Ochi et al. (1996) discussed the application of a three-layer model analysis to single-component two-phase critical flow through a converging nozzle. By assuming a mixing layer between the gas and liquid phase layers, the model accounts for the complicated two-phase mixture near the interface due to the entrainment of droplets and bubbles caused by the velocity difference between the gas and liquid phase during the acceleration in a converging nozzle. The homogeneous model or a complete separation model provides the limiting case of this three layer model. Katto’s principle for two-phase critical flow (Katto, 1968, 1969) is applied to determine the critical conditions from the two-phase flow equations set. The calculation results are compared to the experimental results obtained with steam-water mixtures and carbon dioxide and show good agreement with experimental data over a wide range of quality.

Attou and Seynhaeve (1999) investigated steady-state critical two-phase flashing flow with possible multiple choking phenomena. They gave a clear demonstration of how to derive critical flow conditions and a formula for the speed of sound for two-phase flow. Given the system of non-linear ordinary first order differential equations established from the local mass, momentum and energy balances of the two-phase flow, the necessary and sufficient conditions of choking can be defined mathematically by setting the determinant of either the coefficient matrix or the expanded coefficient matrix equal to zero (Bouré et al., 1976). The same practice is adopted in this thesis.

Witte (1969) discussed mixing shocks in two-phase flow. A sudden change of jet flow to froth flow accompanied by static pressure rise and energy dissipation for certain two-phase flow configurations was named by the author a mixing shock. The jet flow is characterized by a core of fast-moving liquid droplets surrounded by gas. Froth flow consists of liquid in which the gas is dispersed in the form of bubbles. A one-dimensional macroscopic model was established by the laws of conservation of mass, momentum and energy to obtain the expressions for the pressure and entropy change across the mixing process. A theory that explains the gas entrainment mechanism in the mixing shock was also proposed. A water-air ejector with the water as motive stream was experimentally tested. The experiments confirmed the proposed macroscopic and microscopic theories.

Cunningham and Dopkin (1974) investigated the jet breakup and mixing throat lengths of liquid jet gas pumps. The effects of throat length, nozzle contour and spacing, nozzle-throat area ratio, jet velocity and suction pressure were investigated. Two jet breakup flow regimes were identified: impact and jet disintegration. For the impact flow regime, the jet breakup length depends on inlet velocity ratio, jet Reynolds number and nozzle-throat area ratio. The optimum throat lengths were found to be an empirical function of nozzle-throat area ratio and ranged from 12 to 32 throat diameters.

Young and Guha (1991) studied the normal shock-wave structure in two-phase vapor-droplet flows. Three types of fully dispersed waves are identified. Type I waves are dominated by thermal relaxation and an approximate analytical solution provides results in close agreement with the accurate numerical solution of the governing equations. An approximate analysis is also presented for Type II waves, which are dominated by both velocity and thermal relaxation. Type III waves are only briefly discussed as they are of little practical significance. Four reference velocities corresponding to the speed of sound in two-phase flow under different thermal and mechanical constraints are introduced.

Wadle (1988) presented a theoretical and numerical examination of two-phase flow in a diverging nozzle. Stationary experiments with strongly accelerated steam-water and air-water mixtures were performed in a well-instrumented horizontal diffuser for a broad variation of inflow conditions. Experimental results were compared to calculations with a one-dimensional computer model. Both homogeneous and drift-flux two-phase flow models as well as empirical parameters in constitutive correlations of different computer models were tested systematically. It was found that the pressure rise in the diffuser could only be adequately calculated using the drift-flux correlation taken from the SOLA-DF code. The velocity data for choked flow conditions were compared to four different two-phase speed of sound models.

Neve (1991) investigated diffuser performance in two-phase jet pumps. Experimental results are presented from tests of a two-phase variable geometry jet pump to assess how well the included diffuser handles inlet flows with considerable non-uniformities of both velocity and density. It was found that the pressure recovering abilities of the diffuser are significantly influenced by increasing non-uniformities at the entry and by those potentially developing in the diffuser itself. The author suggested that in two-phase jet pumps, short mixing tubes and thin primary jets should generally be avoided.

Owen et al. (1992) performed an experimental study in which the pressure recovery from a homogenized two-phase flow in a conical diffuser was measured. The flow was an air/water mixture with volumetric void fractions of up to 35%. It was found that although the pressure recovery was reduced for a two-phase mixture, the use of a diffuser is still beneficial. The optimum angle of the diffuser in two-phase flow was found to be the same as that in single-phase flow, i.e. 7°. The pressure recovery coefficient can be defined using the homogeneous density and the velocity of the mixtures at the inlet to the diffuser. An expression was proposed for predicting the pressure recovery coefficient of a diffuser operating in two-phase flow and was adopted to build a two-phase flow ejector model.

Rusly et al. (2005) performed a one-dimensional CFD analysis of an ejector in a combined ejector cooling system for R-141b. The CFD results were validated with available experimental data. It was found that the maximum entrainment ratio happens in the ejector just before a shock occurs and that the position of the convergent-divergent nozzle (its exit distance from the constant area mixing section entry) is an important ejector design parameter.

Cizungu et al. (2005) formulated a one-dimensional compressible flow model to optimize single- and two-phase flow ejectors in steady-state operation with particular reference to their deployment in a jet cooling system. It was found that the dimension of the ejector configuration has a dominant influence in deciding the operating range.

Selvaraju and Mani (2006) conducted an experimental investigation of an R-134a vapor ejector refrigeration system, which consists of a vapor generator, an ejector, evaporator, condenser, liquid receiver, capillary tube, liquid pump and measuring devices. The authors found that the entrainment ratio, refrigerating effect and coefficient of performance depend on the ejector configuration and operating temperatures of generator, evaporator and condenser. For a given ejector configuration, there exists an optimum temperature of primary vapor at a particular condenser and evaporating temperatures, which yields maximum entrainment ratio and COP.

2.6. Summary of literature review

The preceding literature review has shown that the expansion losses associate with the isenthalpic throttling process are one of the most important factors that contribute to the low efficiency of the transcritical CO_2 refrigeration cycle. Using an ejector as the expansion device to recover the expansion losses has the advantages of simple construction, robust operation, and easy control in comparison to more complex work recovery expanders. However, limited knowledge of the design and flow characteristics of two-phase flow ejectors restricts ejector expansion refrigeration cycles to realize their potential performance. Understanding the effects of the geometric parameters and operation conditions on the performance of two-phase flow ejectors is the key to reach an optimum design and integrate the ejector into an ejector expansion transcritical refrigeration system. To obtain such knowledge, a simulation model that takes two-phase flow characteristics into account has to be developed for the two-phase flow ejector. To explore the potential of the ejector expansion transcritical refrigeration system for air-conditioning and other applications, a system simulation model has to be developed by incorporating the two-phase flow ejector with other detailed components models such as gas cooler, evaporator and compressor models. These tasks, i.e., development of a two-phase flow ejector model and development of an ejector expansion transcritical refrigeration system model, were performed in this project.

3. THEORETICAL MODEL OF TWO-PHASE FLOW EJECTOR

The ejector that is used in an ejector-expansion transcritical cycle is a two-phase flow ejector and transcritical expansion occurs in the motive nozzle. A theoretical model that can predict the performance of such an ejector is needed to properly design the ejector and to predict the performance of the ejector expansion transcritical carbon dioxide refrigeration system.

3.1. Critical flow model of two-phase flow

In the motive nozzle of the ejector, carbon dioxide initially at supercritical pressure and temperature expands into the sub-critical two-phase region. At the nozzle throat, the flow will become critical for typical operating conditions of an ejector-expansion transcritical refrigeration cycle. A critical flow model of the two-phase flow must be established first to predict the performance of the motive nozzle. The critical flow model introduced here is established by applying Katto's principle (Katto, 1968, 1969) for two-phase critical flow to one-dimensional one-component homogeneous equilibrium two-phase pipe flow.

A one-dimensional one-component homogeneous equilibrium two-phase pipe flow is depicted in Figure 3.1. The following assumptions are made to analyze this flow:

- The flow is a steady one-dimensional flow.
- The flow is homogeneous.
- The two phases are at thermodynamic equilibrium.
- The effect of the thermal diffusion is neglected.

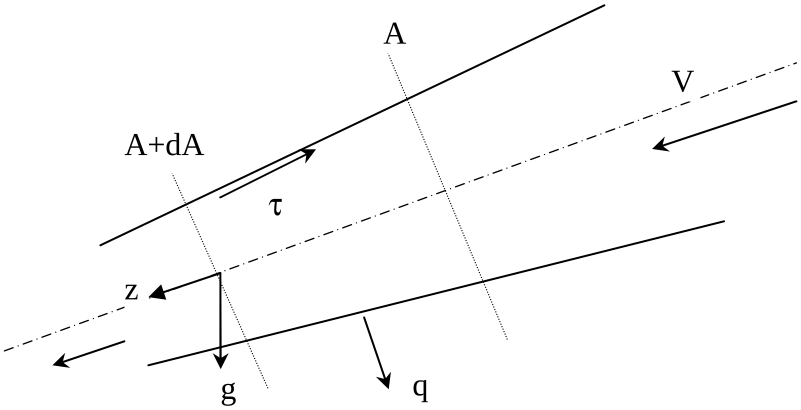

Figure 3.1: One-dimensional Two-Phase Flow

Based on the given assumptions, the mass, momentum and energy conservation equations of the flow lead to the following system of ordinary differential equations:

$$\begin{aligned}
&\frac{d}{dz}(A\rho_{mix}V)=0\\
&\frac{d}{dz}(A\rho_{mix}V^2)+A\frac{dp}{dz}=-\Gamma_w\tau_w+A\rho_{mix}g_z\\
&\frac{d}{dz}\left(A\rho_{mix}V\left(h_{mix}+\frac{V^2}{2}\right)\right)=\Gamma_h q_w+A\rho_{mix}Vg_z
\end{aligned}\tag{3.1}$$

where A is the cross section area, V is the flow velocity, p is the static pressure, Γ_w and Γ_h are the wetted and heated perimeters respectively, τ_w is the wall shear stress and q_w is the wall heat transfer density. Because of the homogeneous equilibrium assumption, the specific volume and enthalpy of the mixture are then given by the following constitutive relations, respectively:

$$v_{mix}=\frac{1}{\rho_{mix}}=xv_g+(1-x)v_f \tag{3.2}$$

$$h_{mix}=xh_g+(1-x)h_f \tag{3.3}$$

By choosing p,V and x as the dependent variables of the flow and considering Equations (3.1) can be rewritten as:

$$\begin{pmatrix} (xv_g'+(1-x)v_f') & -\frac{v_{mix}}{V} & (v_g-v_f) \\ 1 & \frac{V}{v_{mix}} & 0 \\ (xh_g'+(1-x)h_f') & V & (h_g-h_f) \end{pmatrix}\begin{pmatrix} \frac{dp}{dz} \\ \frac{dV}{dz} \\ \frac{dx}{dz} \end{pmatrix}=\begin{pmatrix} \frac{v_{mix}}{A}\frac{dA}{dz} \\ -\frac{\Gamma_w}{A}\tau_w+\frac{g_z}{v_{mix}} \\ g_z \end{pmatrix} \tag{3.4}$$

where the derivatives of specific volume of saturated liquid and vapor are defined as follows:

$$v_g'=\left(\frac{\partial v_g}{\partial p}\right)_{sat},\ v_f'=\left(\frac{\partial v_f}{\partial p}\right)_{sat},\ h_g'=\left(\frac{\partial h_g}{\partial p}\right)_{sat},\ h_f'=\left(\frac{\partial h_f}{\partial p}\right)_{sat} \tag{3.5}$$

According to Katto's principle (Katto, 1968, 1969) for two-phase critical flow, the critical flow occurs when the determinant of the coefficient matrix on the left side of Equation (3.4) equals zero as the system represented by Equation (3.4) reaches a local mathematical singularity.

The critical flow condition can then be expressed as:

$$\begin{vmatrix} v_{mix}' & -\frac{v_{mix}}{V} & (v_g-v_f) \\ 1 & \frac{V}{v_{mix}} & 0 \\ h_{mix}' & V & (h_g-h_f) \end{vmatrix}=0 \tag{3.6}$$

where:

$$v_{mix}'=xv_g'+(1-x)v_f',\ h_{mix}'=xh_g'+(1-x)h_f' \tag{3.7}$$

From Equation (3.6), the expression of the speed of sound can be obtained as (Attou and Seynhaeve (1999)):

$$V_c = \left(\frac{v_{mix}^2 (h_g - h_f)}{(v_g - v_f)(h_{mix}' - v_{mix}) - v_{mix}'(h_g - h_f)} \right)^{\frac{1}{2}} \qquad (3.8)$$

It can be seen that the speed of sound given in Equation (3.8) depends only on pressure and quality.

3.2. Model of motive nozzle flow

The schematic of the ejector working processes has been updated as shown in Figure 3.2. Based on the critical flow model introduced in the previous section, a model for the motive nozzle of the ejector can be setup using the following assumptions:

- The flow inside the motive nozzle is a steady, one dimensional flow.
- The nozzle is a converging nozzle and its throat is at its exit.
- At the nozzle throat, the flow reaches the critical flow condition.
- The isentropic efficiency of the nozzle, η_m, is given
- The inlet flow velocity is neglected.
- The heat transfer between the fluid and nozzle wall is neglected.
- The gravitational force effect on the flow is neglected.

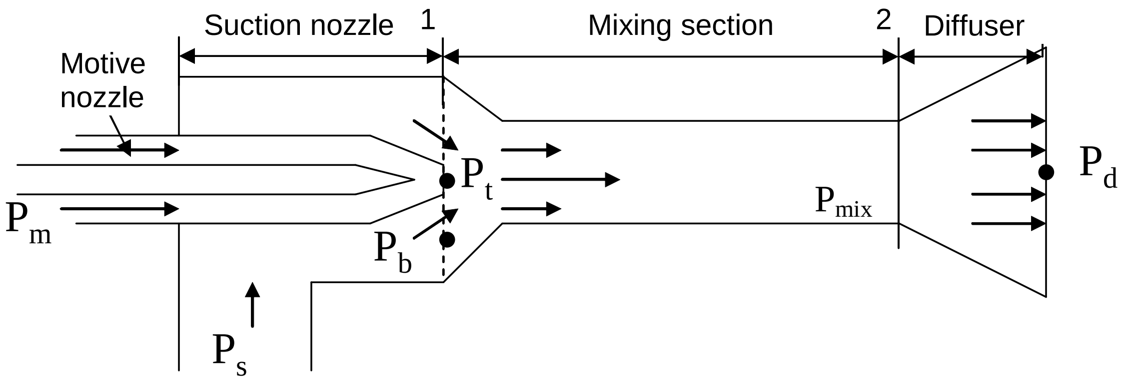

Figure 3.2: Schematic of the ejector working processes

Considering that the fluid enters the motive nozzle at a pressure p_m and temperature T_m, the following model will predict the pressure p_t and velocity V_t at nozzle exit, which is also its throat.

The isentropic efficiency of the nozzle is defined by:

$$\eta_m = \frac{h_m - h_t}{h_m - h_{t,is}} \qquad (3.9)$$

where h_m is the enthalpy of inlet flow, h_t is the enthalpy of exit flow and $h_{t,is}$ is the enthalpy assuming an isentropic expansion from p_m to p_t.

By assuming a value for the exit pressure p_t, $h_{t,is}$ can be determined from the inlet entropy s_i and pressure p_t . Thus, the enthalpy h_t can be calculated for a given nozzle efficiency η_m.

The energy conservation between the inlet and exit of the motive nozzle can be expressed as shown in Equation (3.10) in order to calculate the exit velocity, V_t:

$$h_i = h_t + \frac{V_t^2}{2} \tag{3.10}$$

For the assumed exit pressure p_t and the calculated h_t, the quality x_t can be determined. The speed of sound V_c can then be calculated based on Equation (3.8). In the next step, the speed of sound, V_c, is compared to the exit velocity, V_t, and the pressure p_t is updated until the iteration provides reasonable agreement. For a given throat area A_t, the mass flow rate through the motive nozzle can be determined by:

$$\dot{m}_m = \rho_t A_t V_t \tag{3.11}$$

where the flow density at the nozzle throat is calculated as follows:

$$\rho_t = \frac{1}{\dfrac{x_t}{\rho_{g,t}} + \dfrac{1-x_t}{\rho_{f,t}}} \tag{3.12}$$

In summary, the exit pressure and velocity of the motive nozzle is determined by the given inlet flow conditions and its isentropic efficiency. Using a specified throat area, the mass flow rate is determined as well.

When the mass flow rate through the motive nozzle is less than the critical mass flow rate as determined with the above model, the motive nozzle is operated under non-critical mode. With the mass flow rate as a given parameter, Equations (3.9) to (3.12) can be used to determine the exit pressure and velocity.

3.3. Model of suction nozzle flow

In a real ejector, the suction nozzle is typically replaced by a suction chamber. However, to simplify the analysis, the expansion process from the suction inlet to the mixing section inlet is treated in the same way as the expansion process of a converging nozzle using the following assumptions:

- The flow is steady one-dimensional flow.
- The isentropic efficiency of the nozzle is given.
- The inlet flow velocity is neglected.
- The heat transfer between the fluid and nozzle wall is neglected.
- The gravitational force effect on the flow is neglected.

Once the mass flow rate through the motive nozzle has been determined, the mass flow rate through the suction nozzle can be determined using the ejection ratio φ as shown in Equation (3.13).

$$\dot{m}_s = \varphi \dot{m}_m \tag{3.13}$$

For a given inlet pressure p_s and enthalpy h_s of the suction nozzle, the exit pressure p_b and velocity V_b can be predicted for a specified isentropic efficiency η_s and an exit area A_b using the following procedure.

The isentropic efficiency of the nozzle is defined as:

$$\eta_s = \frac{h_s - h_b}{h_s - h_{b,is}} \tag{3.14}$$

where h_s is the enthalpy of inlet flow, h_b is the enthalpy of exit flow and $h_{b,is}$ is the enthalpy for an isentropic expansion process from p_s to p_b.

Assuming an exit pressure p_b, $h_{b,is}$ can be determined based on the inlet entropy s_s and exit pressure p_b . Using Equation (3.14), the actual exit enthalpy h_b can be calculated for a given isentropic efficiency η_s.

The energy conservation equation between the inlet and exit of the suction nozzle can be expressed as:

$$h_s = h_b + \frac{V_b^2}{2} \tag{3.15}$$

With the assumed exit pressure p_b and the calculated exit enthalpy h_b, the density ρ_b can be determined. The exit velocity V_b can be calculated based on mass conservation equation:

$$\dot{m}_s = \rho_b A_b V_b \tag{3.16}$$

In the next step, the exit velocity V_b calculated from Equation (3.15) is compared to the exit velocity calculated from Equation (3.16) and the exit pressure p_b is updated until the iteration provides reasonable agreement. For typical operating conditions, the critical flow condition will not be reached in suction nozzle because of the small pressure difference between p_s and p_b.

3.4. Model of mixing section flow

The mixing section of the ejector starts from the exits of the motive nozzle and the suction nozzle to the exit of the mixing section as shown in Figure 3.2. To simplify the model of the mixing section, the following assumptions are made:

- At the inlet plane 1, the motive stream has a velocity of V_t, a pressure of p_t, and occupies the area A_t.
- At the inlet plane 1, the suction stream has a velocity of V_b, a pressure of p_b, and occupies the area A_b.
- At the outlet plane 2, the flow becomes uniform and has a velocity of V_{mix} and a pressure of p_m.
- The motive stream pressure and suction stream pressure keep unchanged from the nozzle exits until the inlet of the constant area mixing section. There is no mixing between the motive stream and suction stream before the inlet of the constant area mixing section.
- The heat transfer between the fluid and the mixing section wall is neglected.

- The friction between the fluid and the mixing section wall is neglected.
- The gravitational force effect is neglected.

Using the above assumptions, the model to predict the mixing stream velocity V_m and pressure p_m based on the motive stream velocity V_t and pressure p_t, and the suction stream velocity V_b and pressure p_b can be established as follows.

The mass conservation equation between the inlet plane and outlet plane reduces to:

$$\rho_t A_t V_t + \rho_b A_b V_b = \rho_{mix} A_{mix} V_{mix} \qquad (3.17)$$

where ρ_m is the density of the mixing stream at the outlet plane.

The mixing efficiency η_{mix} was used to account for the frictional losses of the whole mixing chamber (Huang et al, 1999, cited by Elias, 2007). With the assumed η_{mix} of the mixing section, the momentum conservation equation between the inlet plane and outlet plane reduces to:

$$p_t A_t + \eta_{mix} \rho_t A_t V_t^2 + p_b \left(A_{mix} - A_t\right) + \eta_{mix} \rho_b \left(A_{mix} - A_t\right) V_b^2 = p_{mix} A_{mix} + \rho_{mix} A_{mix} V_{mix}^2 \qquad (3.18)$$

The energy conservation equation between the inlet plane and outlet plane reduces to:

$$\dot{m}_m (h_t + \frac{V_t^2}{2}) + \dot{m}_s (h_b + \frac{V_b^2}{2}) = (\dot{m}_m + \dot{m}_s)(h_{mix} + \frac{V_{mix}^2}{2}) \qquad (3.19)$$

Based on the thermophysical property relationships of the fluid, the density ρ_m can be determined from the pressure p_{mix} and enthalpy h_{mix}. Thus, the pressure p_{mix}, velocity V_{mix} and enthalpy h_{mix} can be calculated from Equations (3.17), (3.18) and (3.19).

At the exit plane of the mixing section, the fluid will be in the two-phase region for typical operating conditions of the ejector-expansion transcritical carbon dioxide cycle. The quality of the mixing stream can be determined from its pressure and enthalpy. The speed of sound of the two-phase mixing stream can then be calculated using Equation (3.8) to see if the critical flow condition is reached.

3.5. Model of diffuser flow

In the diffuser, the kinetic energy of the mixing stream will be converted to a static pressure increase. By assuming that the mixing stream at the outlet of the mixing section is a homogeneous equilibrium flow, a pressure recovery coefficient, *Ct* can be defined as:

$$Ct = \frac{p_d - p_{mix}}{\frac{1}{2} \rho_{mix} V_{mix}^2} \qquad (3.20)$$

where p_d is the pressure at the exit of the diffuser.

A correlation proposed by Owen et al. (1992) is used here to calculate the pressure recovery coefficient from the area ratio of the diffuser as follows:

$$Ct = 0.85\rho_{mix}\left[1-\left(\frac{A_{mix}}{A_d}\right)^2\right]\left[\frac{x_{mix}^2}{\rho_{g,mix}}+\frac{\left(1-x_{mix}\right)^2}{\rho_{f,mix}}\right] \qquad (3.21)$$

where x_{mix} is the quality of mixing stream at the diffuser inlet, and $\rho_{g,mix}$ and $\rho_{f,mix}$ are the saturated vapor and liquid densities at pressure p_{mix}, respectively. A_d is the exit area of the diffuser.

By neglecting the heat loss from the ejector to the environment, the enthalpy at the diffuser outlet h_d can be determined from the energy conservation equation of the whole ejector as follows:

$$\dot{m}_m h_i + \dot{m}_s h_s = (\dot{m}_m + \dot{m}_s) h_d \qquad (3.22)$$

The quality at the diffuser outlet x_d can then be determined from the exit pressure p_d and exit enthalpy h_d using the thermophysical property relationships of the fluid.

3.6. Discussion of the ejector model

By combining the models of the motive nozzle flow, suction nozzle flow, mixing section flow and diffuser flow, a simulation model of a two-phase flow ejector has been developed. The model uses a specified motive nozzle throat area and efficiency, suction nozzle efficiency, cross sectional area of the mixing section, and exit area of the diffuser. The model predicts the pressure, quality and mass flow rate of the outlet stream for given inlet conditions of the motive stream and suction stream, and a given ratio of the mass flow rates between these two streams. The ejector simulation model is used to investigate the effects of the design parameters of the ejector and the operating conditions on the performance of the ejector. In the following sections, a discussion of the ejector model will be presented.

3.6.1. Discussion of the motive nozzle model

In the motive nozzle model, which is presented in Section 3.2, it is implicitly assumed that the exit stream will be in the two-phase region. It is also assumed that the flow becomes critical at the exit. During the simulation, these two assumptions are not always being satisfied and have to be checked. Therefore, a certain iteration procedure for the simulation of motive nozzle had to be adopted, which is depicted in the flow chart in Figure 3.3. It can be seen from Figure 3.3 that the model searches for a throat pressure p_t at pressures below the critical pressure p_{cr} as well as at pressures above the critical pressure to match the throat velocity with the speed of sound for the given input parameters. If the model is not able to solve for a pressure p_t, the flow can not expand with the specified isentropic efficiency to reach critical flow at the nozzle throat for the given input pressure and temperature. Either the isentropic efficiency has to be adjusted or the inlet conditions must be changed, e.g., by using a upstream throttle, to successfully simulate the motive nozzle flow.

3.6.2. Discussion of the geometric parameters of the ejector

It can be seen from Section 3.6.1 that the mass flux through the motive nozzle is only determined by the inlet flow conditions. Thus, the throat area of the motive nozzle is determined by the desired mass flow rate through the motive nozzle. Assuming an ejection ratio, the mass flow rate of the suction stream can be calculated. By assuming a pressure drop across the suction nozzle, the suction nozzle exit area can be determined from the suction nozzle model. Then, the cross sectional area of the mixing section can be calculated by adding the motive nozzle exit area and the suction nozzle exit area. In the next step, the pressure at the exit of the mixing section can be calculated from the mixing section model. By choosing a desired pressure elevation from the ejector suction inlet to the ejector exit, the pressure increase across the diffuser can be determined and the exit area of the diffuser can be calculated from the diffuser model. This procedure can be used to find some geometric parameters of the ejector to meet the desired operating performance. To better understand the characteristics of the ejector, an investigation of the geometric parameters on the performance of the ejector is presented next.

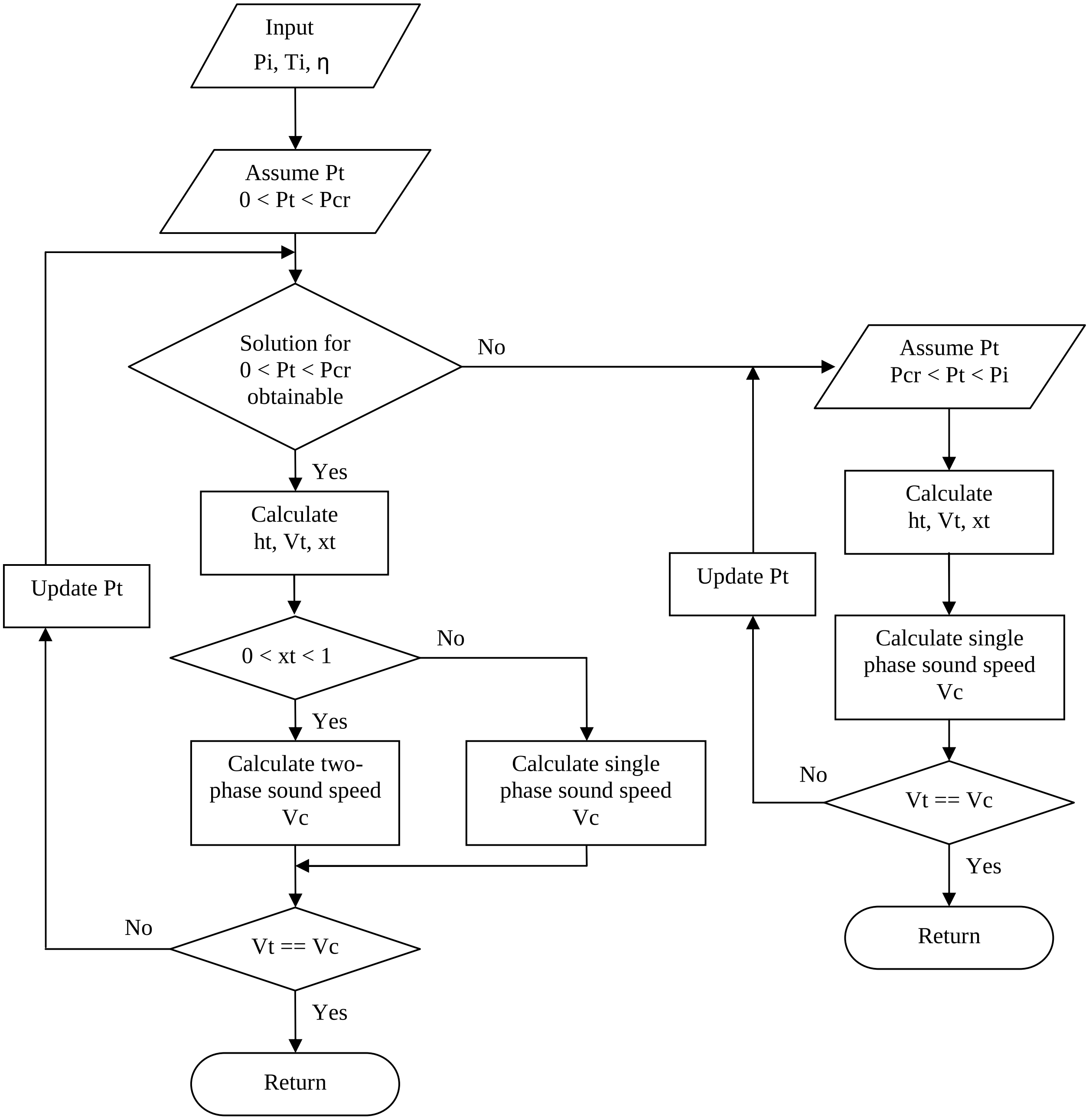

Figure 3.3: Flow chart of motive nozzle simulation

A higher diffuser exit pressure is desired in an ejector expansion refrigeration cycle as it means a higher compressor inlet pressure. A higher quality at the diffuser exit means that less liquid refrigerant enters the evaporator and that leads to a smaller refrigeration capacity. Therefore, a high diffuser exit pressure and a low diffuser exit quality are desirable in an ejector expansion refrigeration cycle. The analysis of the ejector performance was repeated with motive and suction nozzle efficiencies of 0.9, 0.8 and 0.7, and ejection ratios of 0.3 to 0.6 as shown in the following figures. Based on these results, it is found that a higher isentropic nozzle efficiency and lower ejection ratio are desirable for the ejector performance. However, the ejection ratio can only be reduced to a certain value since it determines the mass flow rate of the suction stream that flows through the evaporator for an ejector expansion refrigeration cycle.

Figure 3.4 presents the ejector exit pressure and quality as functions of the diffuser diameter ratio for an inlet motive stream at P_i = 9.5 MPa, T_i = 313.15 K (40 °C), an inlet suction stream at P_s = 3.969 MPa, T_{sup} = 5 K, and an ejection ratio φ = 0.3, while η_m and η_s vary from 0.7 to 0.9. It can be seen that the diffuser exit pressure increases quickly at low diffuser diameter ratios and then increases slowly at high diffuser diameter ratios for a given ejection ratio; the diffuser exit quality decreases quickly at low diffuser diameter ratios and then slowly at high diffuser diameter ratios. Thus, a diffuser diameter ratio of approximately 3.0 is desired for the given operating conditions as it means a higher compressor inlet pressure and lower refrigerant quality.

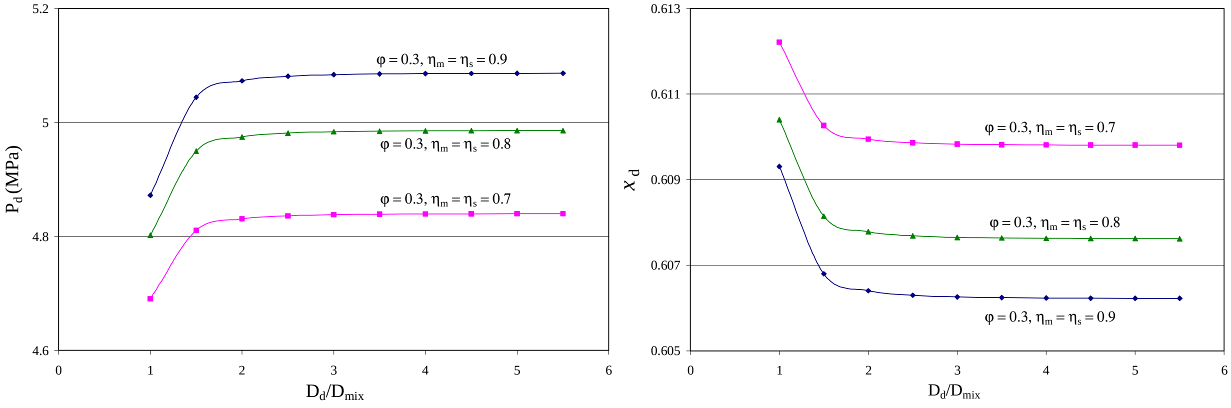

Figure 3.4: Ejector discharge pressure and quality versus diffuser diameter ratio (P_i = 9.5MPa, T_i = 313.15 K, P_s = 3.969MPa, φ = 0.3, D_t =2mm, D_m = 4mm)

Figure 3.5 presents the ejector exit pressure and quality as functions of the throat diameter D_t of the motive nozzle for an inlet motive stream at P_i = 9.5 MPa, T_i = 313.15 K (40 °C), an inlet suction stream at P_s = 3.969 MPa, T_{sup} = 5 K, and ejection ratio φ = 0.3, with η_m and η_s varying from 0.7 to 0.9. It can be seen that as D_t increases, the diffuser exit pressure increases and then decreases, while the diffuser exit quality decreases and then increases. The quality does not vary too much as D_t increases. The diffuser exit pressure reaches a maximum and the diffuser exit quality reaches a minimum at a value for D_t of approximately 2.3 mm. It can also be seen that higher nozzle efficiencies are desirable in an ejector expansion refrigeration cycle.

Figure 3.6 presents the ejector exit pressure and quality as functions of the throat diameter D_t of the motive nozzle for an inlet motive stream at P_i = 9.5 MPa, T_i = 313.15 K (40 °C), an inlet suction stream at P_s = 3.969 MPa, T_{sup} = 5 K, and $\eta_m = \eta_s = 0.9$, with the ejection ratio φ varying from 0.3 to 0.6. It can be seen that as D_t increases, the diffuser exit pressure increases and then decreases, while the diffuser exit quality decreases and then increases. The quality does not vary too much as D_t increases. As the ejection ratio increases from the 0.3 to 0.4 to 0.6, the diffuser exit pressure reaches maxima at values for D_t of 2.3 mm, 2.1 mm and 1.8 mm, respectively. It can be seen that a low ejection ratio is desirable in an ejector expansion refrigeration cycle.

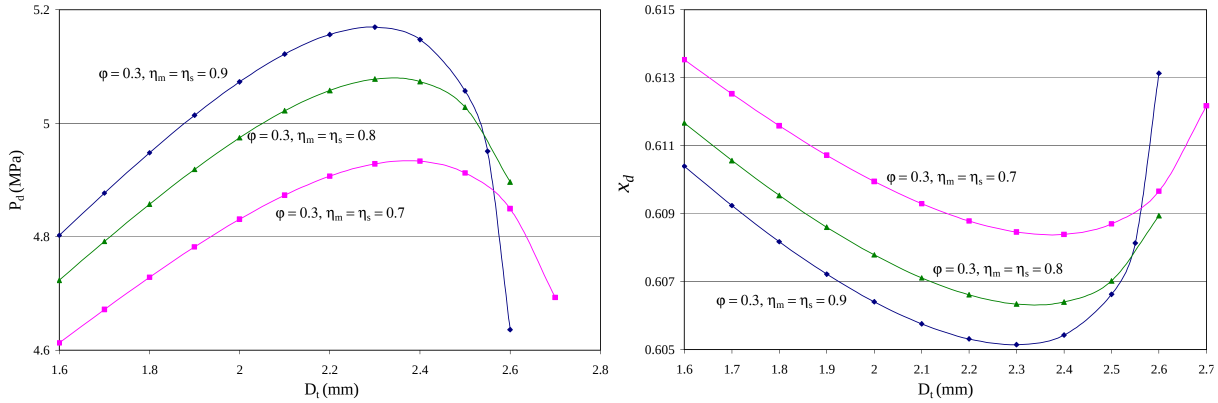

Figure 3.5: Ejector discharge pressure and quality versus motive nozzle exit diameter with φ = 0.3 (P_i = 9.5 MPa, T_i = 313.15 K, P_s = 3.969 MPa, D_{mix} = 4 mm, D_d = 8 mm)

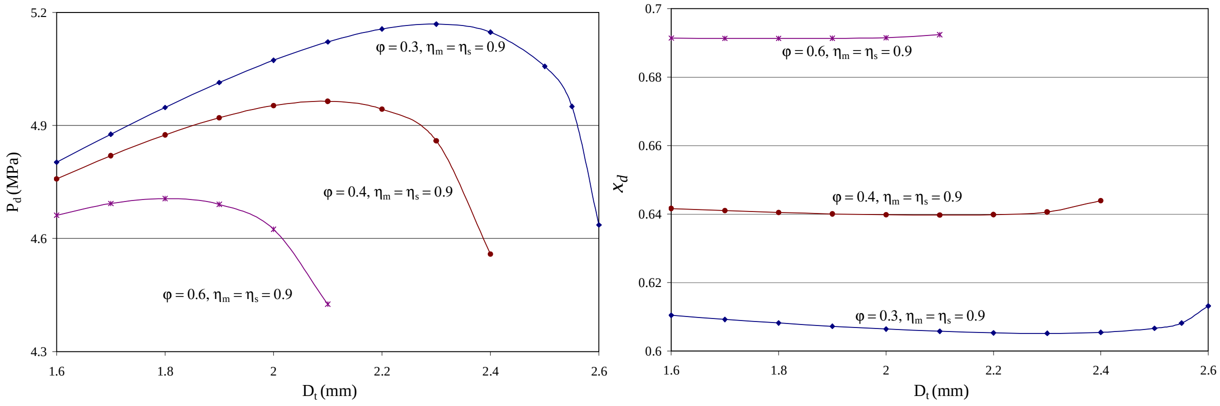

Figure 3.6: Ejector discharge pressure and quality versus motive nozzle exit diameter with $\eta_m = \eta_s = 0.9$ (P_i = 9.5 MPa, T_i = 313.15 K, P_s = 3.969 MPa, D_{mix} = 4 mm, D_d = 8 mm)

Figure 3.7 presents the ejector exit pressure and quality as functions of the mixing section diameter D_{mix} for an inlet motive stream at P_i = 9.5 MPa, T_i = 313.15 K (40 °C), an inlet suction stream at P_s = 3.969 MPa, T_{sup} = 5 K, and $\eta_m = \eta_s = 0.9$, with the ejection ratio φ varying from 0.3 to 0.6. It can be seen that as D_{mix} increases, the diffuser exit pressure increases and then decreases, while the diffuser exit quality decreases and then increases. As the ejection ratio φ increases from 0.3, to 0.4, and to 0.6, the diffuser exit pressures reaches maxima at D_{mix} of 3.5 mm, 4 mm and 4.5 mm, respectively. The quality does not vary too much as D_{mix} increases. It can also be seen that a low ejection ratio is desirable in an ejector expansion refrigeration cycle.

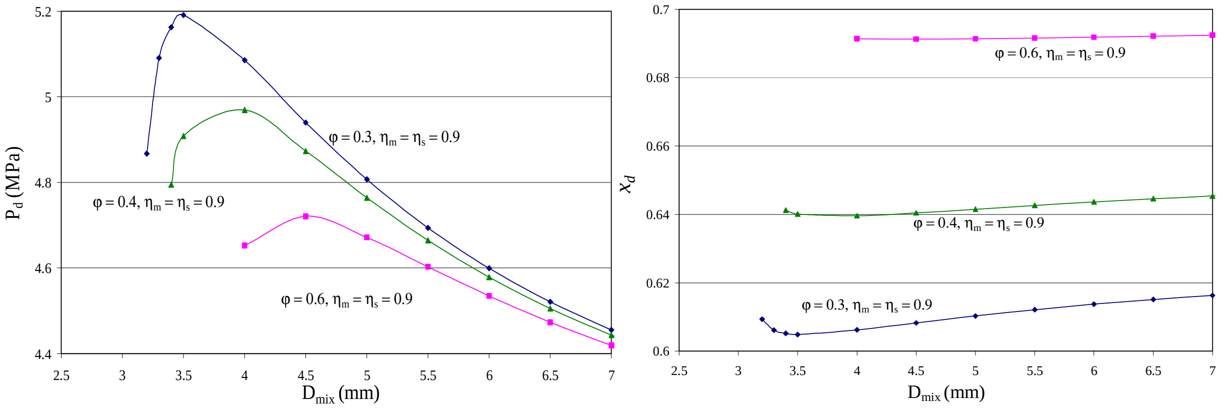

Figure 3.7: Ejector discharge pressure and quality versus mixing section diameter with $\eta_m = \eta_s = 0.9$ (P_i = 9.5 MPa, T_i = 313.15 K, P_s = 3.969 MPa, D_t = 2 mm, D_d = 16 mm)

Figure 3.8 presents the ejector exit pressure and quality as functions of the mixing section diameter D_{mix} for an inlet motive stream at P_i = 9.5 MPa, T_i = 313.15 K (40 °C), an inlet suction stream at P_s = 3.969 MPa, T_{sup} = 5 K, and an ejection ratio 0.3, with η_m and η_s varying from 0.7 to 0.9. It can be seen that as D_{mix} increases, the diffuser exit pressure increases and then decreases, while the diffuser exit quality decreases and then increases. The diffuser exit pressure reaches a maximum at a value for D_{mix} of approximately 3.5 mm. The quality does not vary too much as D_{mix} increases. It can be seen that higher ejector nozzle efficiencies are desirable in an ejector expansion refrigeration cycle.

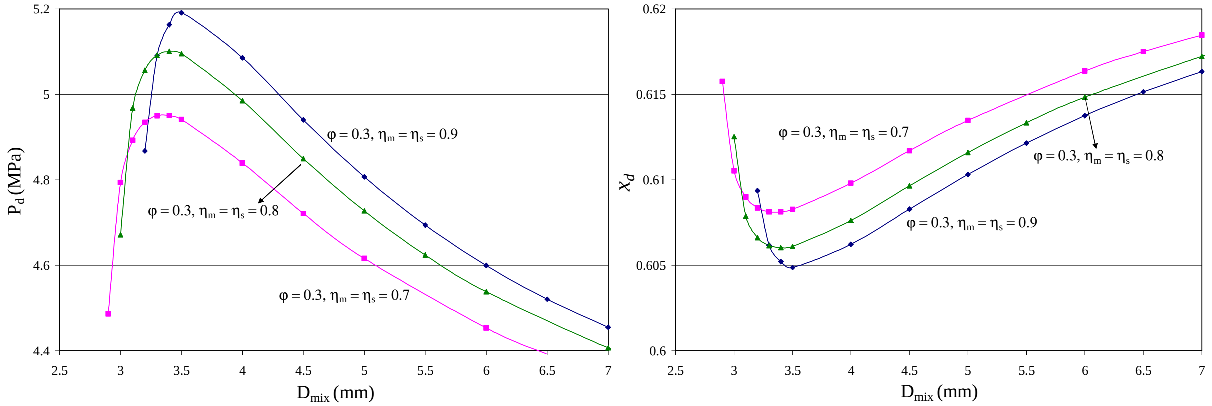

Figure 3.8: Ejector discharge pressure and quality versus mixing section diameter with φ = 0.3 (P_i = 9.5 MPa, T_i = 313.15 K, P_s = 3.969 MPa, D_t = 2 mm, D_d = 16 mm)

3.6.3. Discussion of the operation conditions of the ejector

In addition to the design parameters, the operating conditions also affect the performance of an ejector. The inlet conditions of both the motive and the suction streams and the ejection ratio determine the pressure and quality of the exit stream when the design parameters of the ejector are specified.

Figure 3.9 presents the ejector discharge pressure and quality as functions of the motive nozzle inlet pressure for the operating conditions of T_i = 313.15 K (40 °C), P_s = 3.969 MPa, T_{sup} = 5 K and ejection ratio of 0.3, with η_m and η_s varying from 0.7 to 0.9. The diffuser exit pressure increases while the discharge exit quality decreases as the motive stream inlet pressure increases. The ejector efficiencies do not affect the diffuser exit quality much. It can be seen that higher ejector nozzle efficiencies are desirable in an ejector expansion refrigeration cycle.

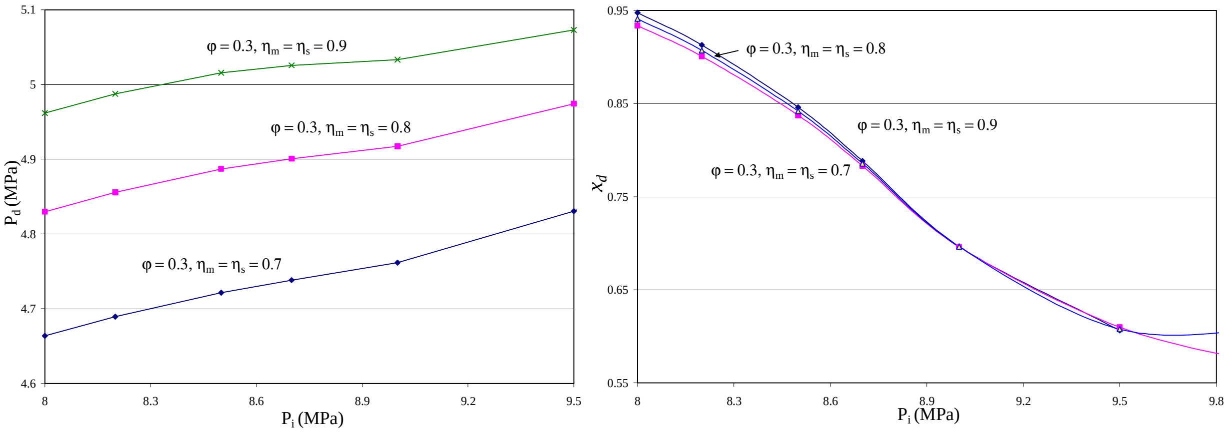

Figure 3.9: Ejector discharge pressure and quality versus motive stream inlet pressure with φ = 0.3 (T_i = 313.15 K, P_s = 3.969 MPa, D_t = 2 mm, D_{mix} = 4 mm, D_d = 8 mm)

Figure 3.10 presents the ejector discharge pressure and quality as functions of the motive nozzle inlet pressure for the operating conditions of T_i = 313.15 K (40 °C), P_s = 3.969 MPa, T_{sup} = 5 K, and $\eta_m = \eta_s = 0.9$ with the ejection ratio varying from 0.3 to 0.6. It can be seen from Figure 3.10 that for high ejection ratios, the diffuser exit pressure increases firstly and then decreases as the motive stream inlet pressure P_i increases. However, for a low ejection ratio of 0.3, the diffuser exit pressure further increases as P_i increases. The discharge quality decreases as the motive stream inlet pressure increases. The diffuser exit pressure decreases and the diffuser exit quality increases with an increase of the ejection ratio.

Figure 3.11 presents the ejector discharge pressure and quality as functions of the suction stream inlet superheat for the operating conditions of T_i = 313.15 K (40 °C), P_s = 3.969 MPa, D_t = 2 mm, D_{mix} = 4 mm, D_d = 12 mm and $\eta_m = \eta_s = 0.9$, with the ejection ratio φ varying from 0.3 to 0.6. It can be seen that the diffuser exit pressure does not change much while the diffuser exit quality increases as the suction stream inlet superheat increases. Thus, low superheat of the suction stream (less than 5 K) is desirable for the ejector expansion refrigeration cycle.

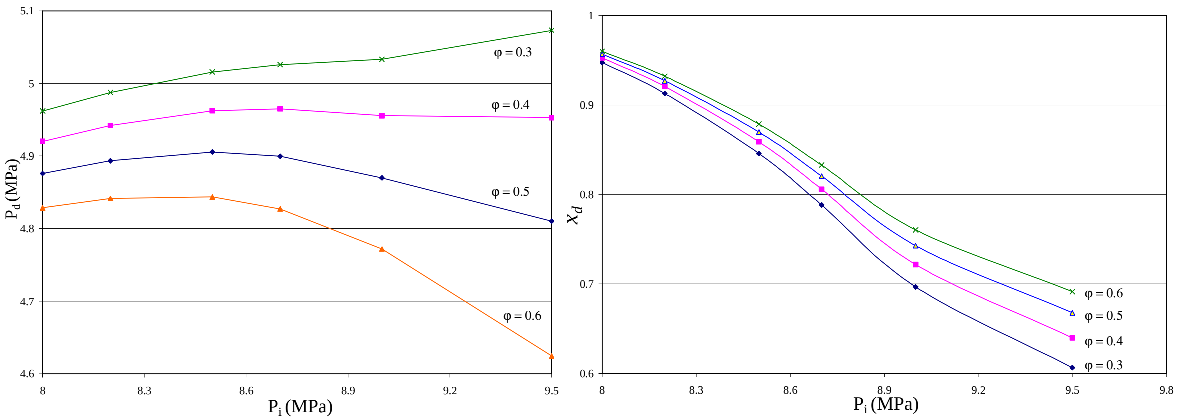

Figure 3.10: Ejector discharge pressure and quality versus motive nozzle inlet pressure with $\eta_m = \eta_s = 0.9$ ($T_i = 313.15$ K, $P_s = 3.969$ MPa, $T_{sup} = 5$ K,)

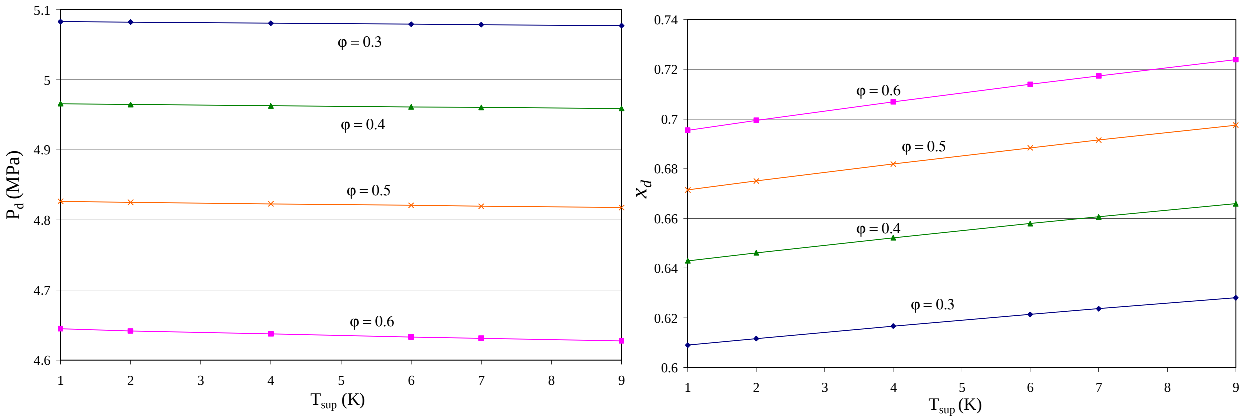

Figure 3.11: Ejector discharge pressure and quality versus suction stream inlet superheat with $\eta_m = \eta_s = 0.9$ ($P_i = 9.5$ MPa, $T_i = 313.15$ K, $P_s = 3.969$ MPa, $D_t = 2$ mm, $D_{mix} = 4$ mm, $D_d = 12$ mm)

Figure 3.12 presents the ejector discharge pressure and quality as functions of the suction stream inlet superheat for the operating conditions of $T_i = 313.15$ K (40 °C), $P_s = 3.969$ MPa, $D_t = 2$ mm, $D_{mix} = 4$ mm, $D_d = 12$ mm and $\varphi = 0.3$ with ejector nozzle efficiencies $\eta_m = \eta_s = 0.7$, 0.8 and 0.9. It can be seen that the diffuser exit pressure decreases little by little while the diffuser exit quality increases as the inlet superheat of the suction stream increases. High ejector efficiencies cause high diffuser exit pressure, while the ejector efficiencies do not affect the diffuser exit quality much. Thus, high ejector efficiencies and low superheat of the suction stream (less than 5 K) are desirable for the ejector expansion refrigeration cycle.

Figure 3.13 presents the ejector discharge pressure and quality as functions of the motive stream inlet temperature for the operating conditions of $P_i = 9.5$ MPa, $P_s = 3.969$ MPa, $T_{sup} = 4$ K, $D_t = 2$ mm, $D_{mix} = 4$ mm, $D_d = 10$ mm and $\eta_m = \eta_s = 0.9$ with $\varphi = 0.3$ to 0.6. It can be seen that both the diffuser exit pressure and quality consistently increase as the motive stream inlet temperature increases. The ejection ratio does not affect the diffuser exit quality at high motive nozzle inlet temperature.

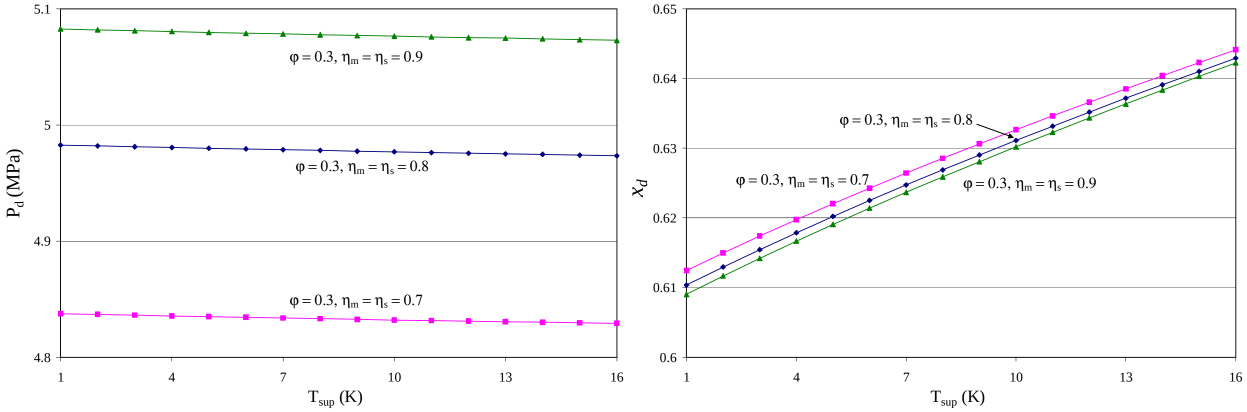

Figure 3.12: Ejector discharge pressure and quality versus suction stream inlet superheat with $\varphi = 0.3$ ($P_i = 9.5$ MPa, $T_i = 313.15$ K, $P_s = 3.969$ MPa, $D_t = 2$ mm, $D_{mix} = 4$ mm, $D_d = 12$ mm)

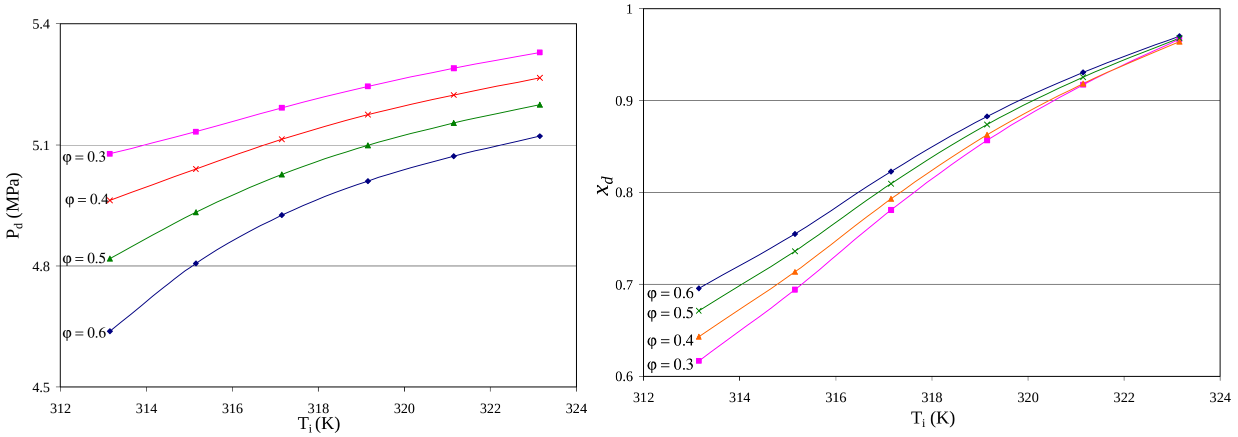

Figure 3.13: Ejector discharge pressure and quality versus motive stream inlet temperature with $\eta_m = \eta_s = 0.9$ ($P_i = 9.5$ MPa, $P_s = 3.969$ MPa, $T_{sup} = 4$ K, $D_t = 2$ mm, $D_{mix} = 4$ mm, $D_d = 10$ mm)

Figure 3.14 presents the ejector discharge pressure and quality as functions of the motive stream inlet temperature for the operating conditions of $P_i = 9.5$ MPa, $P_s = 3.969$ MPa, $T_{sup} = 4$ K, $D_t = 2$ mm, $D_{mix} = 4$ mm, $D_d = 10$ mm and $\varphi = 0.3$ with $\eta_m = \eta_s = 0.7$ to 0.9. It can be seen that both the diffuser exit pressure and quality consistently increase as the motive stream inlet temperature increases. The ejection efficiencies do not affect the diffuser exit quality.

Figure 3.15 presents the ejector discharge pressure and quality as functions of the suction stream inlet pressure for the operating conditions of $P_i = 9.5$ MPa, $T_i = 313.15$ K (40 °C), $T_{sup} = 4$ K, $D_t = 2$ mm, $D_{mix} = 4$ mm, $D_d = 10$ mm and $\eta_m = \eta_s = 0.9$ with $\varphi = 0.3$ to 0.6. It can be seen that the diffuser exit pressure increases while the diffuser exit quality decreases as the inlet pressure of the suction stream increases. Therefore, a higher evaporation temperature is desirable for the ejector expansion refrigeration cycle.

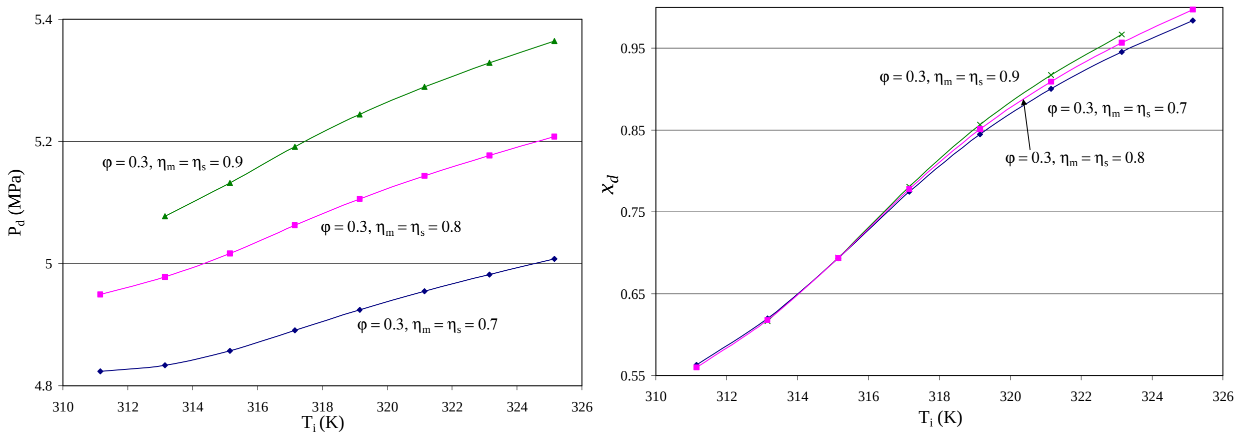

Figure 3.14: Ejector discharge pressure and quality versus motive stream inlet temperature with φ = 0.3 (P_i = 9.5 MPa, P_s = 3.969 MPa, T_{sup} = 4 K, D_t = 2 mm, D_{mix} = 4 mm, D_d = 10 mm)

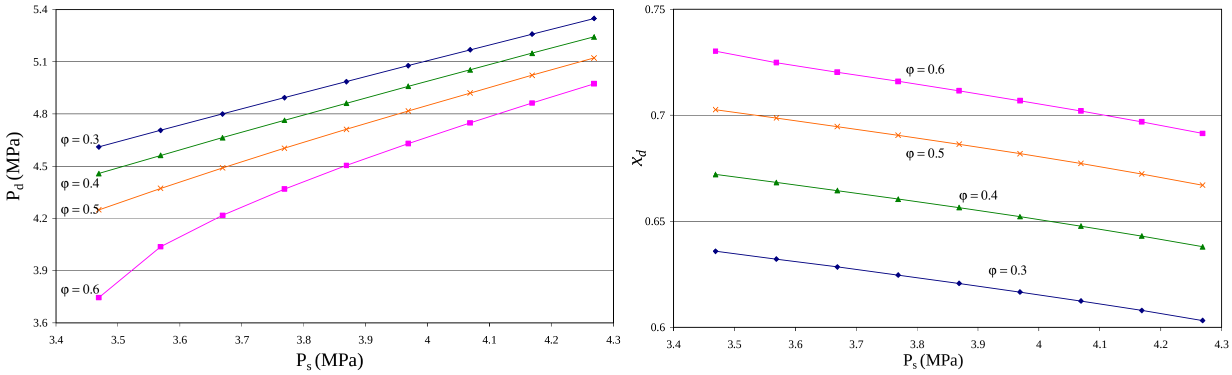

Figure 3.15: Ejector discharge pressure and quality versus suction stream inlet pressure with $\eta_m = \eta_s$ = 0.9 (P_i = 9.5 MPa, T_i = 313.15 K, T_s = 282.15 K, D_t = 2 mm, D_{mix} = 4 mm, D_d = 10 mm)

Figure 3.16 presents the ejector discharge pressure and quality as functions of the suction stream inlet pressure for the operating conditions of P_i = 9.5 MPa, T_i = 313.15 K (40 °C), T_{sup} = 4 K, D_t = 2 mm, D_{mix} = 4 mm, D_d = 10 mm and φ = 0.3 with $\eta_m = \eta_s$ = 0.7, 0.8, 0.9. It can be seen that the diffuser exit pressure increases while the diffuser exit quality decreases as the inlet pressure of the suction stream increases for a given area ratio and ejection ratio. Therefore, a higher evaporation temperature is desirable for the ejector expansion refrigeration cycle.

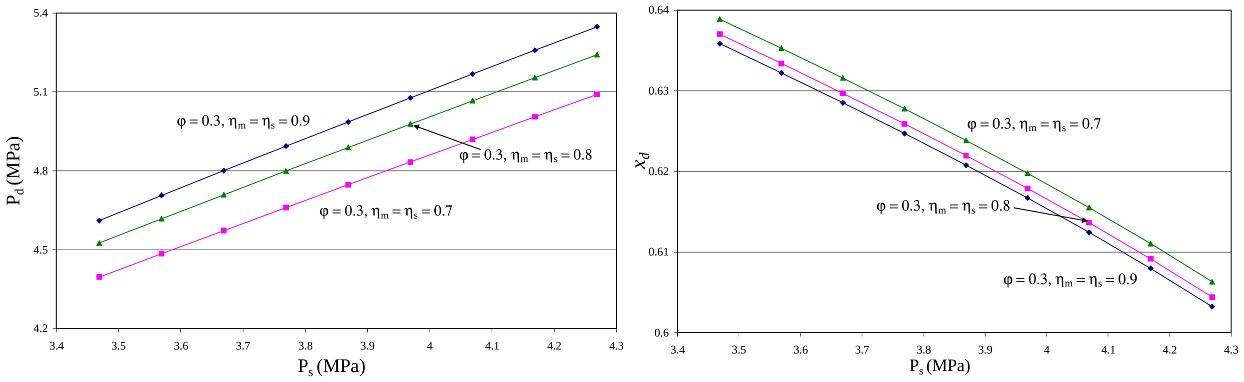

Figure 3.16: Ejector discharge pressure and quality versus suction stream inlet pressure with $\varphi = 0.3$ ($P_i = 9.5$ MPa, $T_i = 313.15$ K, $T_s = 282.15$ K, $D_t = 2$ mm, $D_{mix} = 4$ mm, $D_d = 10$ mm)

3.7. Summary of the two-phase flow ejector modeling

In summary, the two-phase flow ejector model was utilized to determine the ejector performance characteristics as a function of the design parameters and the operating conditions. The model presented in this report is able to predict the performance of the ejector as a stand-alone device. The effects of the ejector geometries and operation conditions on the performance of the ejector were studied. It is found that high ejector efficiencies and low ejection ratio are desirable to increase the ejector exit pressure and decrease the ejector exit quality. It is also found that the optimum mixing section diameter is approximately 4 mm and the optimum diffuser diameter ratio is 3 for the given operating conditions. Furthermore, the optimum motive nozzle throat diameter changes with the ejection ratio and the ejector efficiencies. However, the motive nozzle efficiency, the suction nozzle efficiency and the mixing section efficiency are three parameters that need to be determined experimentally. The two-phase flow ejector model also needs to be validated with experimental results before it can be used to build a detailed simulation model of an ejector expansion transcritical refrigeration system.

4. CO_2 EJECTOR EXPANSION TRANSCRITICAL SYSTEM MODEL

A detailed ejector expansion transcritical refrigeration system simulation model has been developed to predict the performance of air to air unitary air conditioners and heat pumps with CO_2 as the refrigerant. The model is based on the previous work by Robinson (2000) and Ortiz (2002). The gas cooler and the evaporator are modeled based on micro-channel heat exchanger geometries. The compressor is modeled based on map-based compressor performance data (Hubacher and Groll 2002). The two phase flow ejector model is incorporated into the overall system simulation model. A schematic of an ejector expansion transcritical air conditioning system is shown in Figure 4.1. Descriptions of the component models for the compressor, the gas cooler, the evaporator and the separator are given in the following sections.

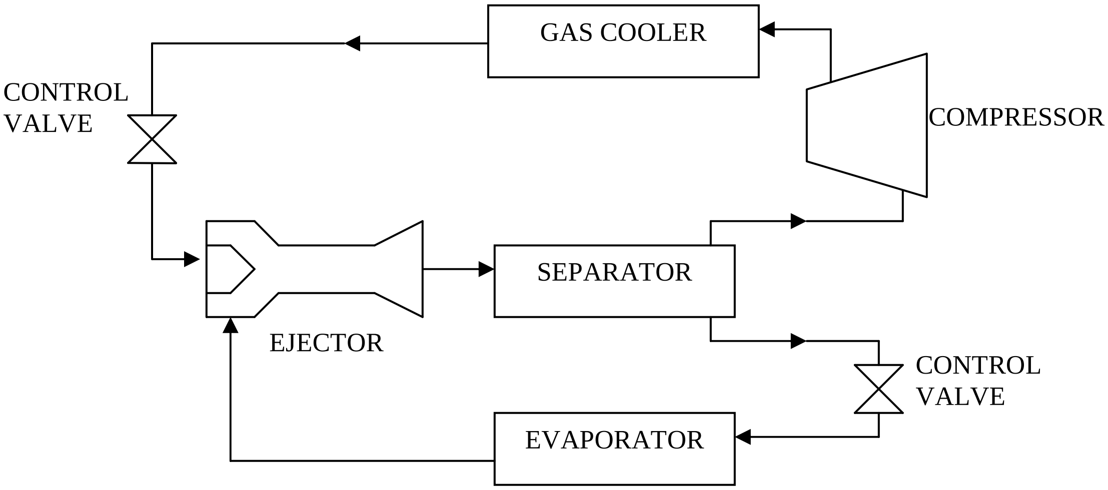

Figure 4.1: Schematic of ejector expansion transcritical air conditioning system

4.1. Compressor model

Since the simulation model will be used to predict the performance of a packaged air conditioning system, only a hermetic compressor model is considered here. The hermetic compressor modeling approach is similar to that of Fischer and Rice (1983). A detailed description of the compressor model that is based on the work by Ortiz et al. (2003) can be found in Appendix A. The compressor performance maps obtained by Hubacher and Groll (2002) at a superheat of 10.7 K are used to calculate the compressor efficiencies at different operation conditions. A superheat correction was made. The mass flow rate was corrected according to an approach shown by Dabiri and Rice (1981) using the following equations:

$$\dot{m} = \dot{m}_{map} \cdot \left[1 + 0.75 \cdot \left(\frac{\rho_{new}}{\rho_{map}} - 1 \right) \right], \rho_{new} = f\left(P_{suc}, h_{suc}\right), \rho_{map} = f\left(P_{suc}, T_{suc\_map}\right) \tag{4.1}$$

$$\dot{W}_{comp} = \dot{W}_{comp\_map} \cdot \frac{\dot{m}}{\dot{m}_{map}} \cdot \left[\frac{h_{dis,is} - h_{suc}}{h_{dis,is\_map} - h_{suc\_map}} \right], h_{dis,is} = f\left(P_{dis}, s_{suc}\right), s_{suc} = f\left(P_{suc}, h_{suc}\right) \tag{4.2}$$

4.2. Gas cooler model

The gas cooler to be modeled here consists of multiple microchannel heat exchanger slabs. Each slab has a refrigerant distribution header on one side of the heat exchanger and a refrigerant collection header on the other side. In between the headers are multi-port-extruded (MPE) tubes and in between the MPE tubes are accordion-style fins as shown in Figure 4.2.

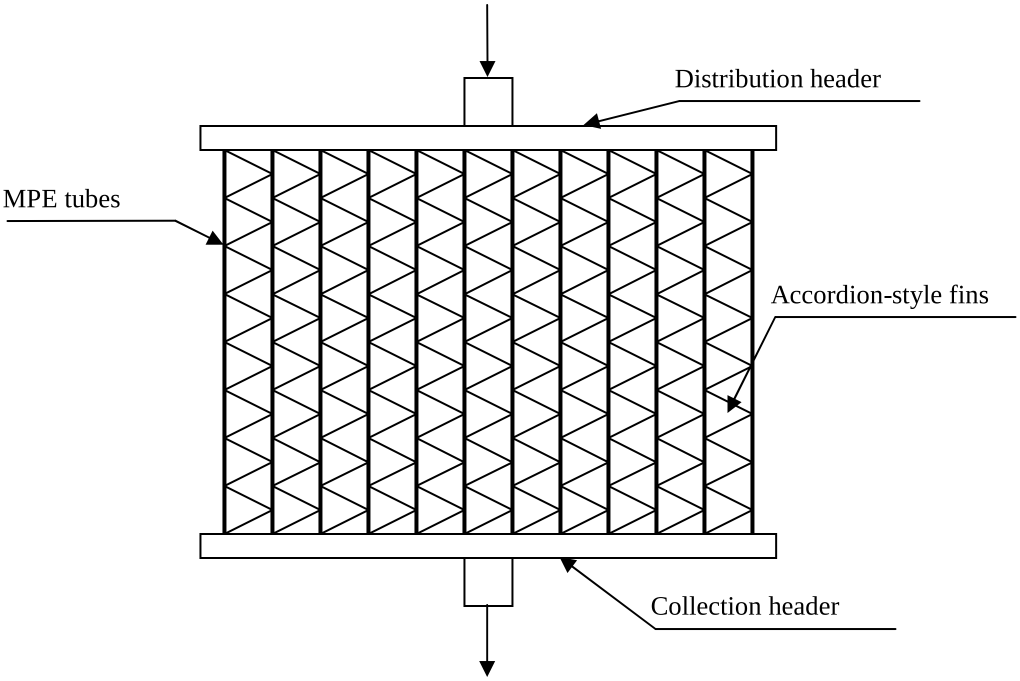

Figure 4.2 : Micro-channel heat exchanger slab

A schematic of the cross section of a multi-port-extruded tube is shown in Figure 4.3 to illustrate the microchannel placement inside an extruded tube.

While the CO_2 flows through the MPE tubes of the gas cooler, it is cooled by air, which flows in cross-flow to the MPE tubes and in parallel to the fin surfaces. The CO_2 is cooled from the compressor outlet temperature to a temperature just above the air temperature at a pressure that is higher than the supercritical pressure. There will be no phase change of the CO_2 inside the gas cooler. Nevertheless, the thermophysical properties of the CO_2 vary dramatically when the refrigerant passes through the pseudo-critical region as it is being cooled down. To account for the property changes of CO_2, each multi-port-extruded tube is divided into small segments along the refrigerant flow direction for the simulation of the gas cooler. A detailed description of the gas cooler model that is based on the work by Ortiz et al. (2003) can be found in Appendix B.

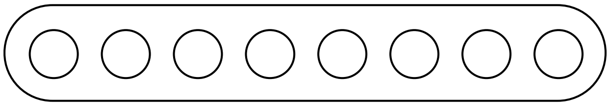

Figure 4.3: Cross section of a multi-port-extruded tube

4.3. Evaporator model

The evaporator to be modeled here consists of the same micro-channel heat exchanger slab configuration as the one of the gas cooler that was described in the previous section.

While the CO_2 flows through the MPE tubes of the evaporator, it is heated by air, which flows in cross-flow to the MPE tubes and in parallel to the fin surfaces. The CO_2 evaporates from a state of two-phase mixture to a superheated vapor just below the air inlet temperature at the given evaporation pressure. To account for the property changes of CO_2 during the evaporation and superheating process, the multi-port-extruded tube is divided into several small segments along the refrigerant flow direction to conduct the simulation of the evaporator. A detailed description of the evaporator model that is based on the work by Ortiz et al. (2003) can be found in Appendix C.

4.4. Basic CO_2 transcritical air conditioning system simulation model

The assumptions for the basic CO_2 transcritical air conditioning system model are as follows:

- The system operates at steady state.
- The pressure drop and heat transfer in the connecting tubes between different components are neglected.
- The throttling process is isenthalpic.
- The discharge pressure of compressor and the outlet pressure of the evaporator are specified.
- Both indoor and outdoor air temperatures and air flow rates are specified.

The computation sequence for the basic CO_2 transcritical air conditioning system simulation model can be listed as follows:

1) The operation conditions and design parameters of the system are read in.
2) A superheat at evaporator outlet T_{sup} is assumed.
3) Based on the specified compressor discharge pressure P_{gc}, the compressor inlet pressure $P_{comp,in} = P_{evap,out}$, and the compressor inlet T_{sup}, the mass flow rate through the compressor $\dot{m}_{comp}$, the power input to the compressor $\dot{W}_{comp}$ and discharge temperature T_{gc} are determined using the compressor model.

4) The gas cooler capacity $\dot{Q}_{gc}$, CO_2 temperature and pressure at outlet of the gas cooler and air temperature and pressure at outlet of the gas cooler are determined using the gas cooler model.

5) Assuming the refrigerant side pressure drop of the evaporator ΔP_{evap}, the evaporator inlet pressure can be determined from the specified evaporator outlet pressure as: $P_{evap,in} = P_{evap,out} + \Delta P_{evap}$

6) The CO_2 inlet conditions (quality) to the evaporator are determined based on an isenthalpic throttling process from the gas cooler outlet pressure to the evaporator inlet pressure $P_{evap,in}$

7) The evaporator capacity $\dot{Q}_{evap}$, CO_2 temperature and pressure at outlet of the evaporator and air temperature and pressure at outlet of the evaporator are determined using the evaporator model. If the calculated refrigerant side pressure drop of the evaporator is different with the assumed value of ΔP_{evap}, go back to step 5) to iterate until the refrigerant side pressure drop of evaporator converges within specified tolerance.

8) The calculated evaporator outlet superheat $T_{sup,n}$ is compared to the assumed evaporator outlet superheat T_{sup}. If they are not equal, the evaporator outlet superheat T_{sup} is updated and steps 3) to 7) are repeated until the superheat agree with each other within specified tolerance.

4.5. Separator model

The separator serves two functions in an ejector expansion transcritical cycle. It separates the vapor flow, which enters the compressor, from the liquid flow, which enters the evaporator. It also serves as a refrigerant receiver. A detailed description of the separator model can be found in Appendix D.

4.6. Ejector expansion transcritical air conditioning system simulation model

The ejector-expansion transcritical air conditioning system model consists of the compressor model, gas cooler model, evaporator model, and separator model in addition to the motive nozzle model, suction nozzle model, mixing section model, and diffuser model that were developed for the two-phase flow ejector.

The assumptions for the ejector expansion transcritical air conditioning system model are as follows:

- The system operates at steady state.
- The pressure drop and heat transfer in the connecting tubes between different components are neglected.
- All throttling processes are isenthalpic.
- The discharge pressure of the compressor and the superheat at the evaporator exit are specified.
- Both indoor and outdoor air temperatures and air flow rates are specified.

A flowchart of the computation sequence for the ejector expansion transcritical air conditioning system model is shown in Figure 4.4. The computation sequence can be described as follows:

1) The operation conditions and design parameters of the system are read in.

2) A pressure P_{diff} is assumed as the diffuser outlet pressure which is the same as the separator pressure and compressor inlet pressure.
3) Based on the specified compressor discharge pressure P_{gc}, the compressor inlet pressure $P_{comp,in} = P_{diff}$, and the compressor inlet quality $x_{comp} = 1$, the mass flow rate through the compressor $\dot{m}_{comp}$, the power input to the compressor $\dot{W}_{comp}$ and discharge temperature T_{gc} are determined using the compressor model.
4) The gas cooler capacity $\dot{Q}_{gc}$, CO_2 temperature and pressure at outlet of the gas cooler and air temperature and pressure at outlet of the gas cooler are determined using the gas cooler model.
5) The mass flow rate of the motive stream $\dot{m}_{nozzle}$ is determined using the motive nozzle model. If the calculation failed (see step 6), the CO_2 motive nozzle inlet pressure P_n is throttled through a control valve to a lower value until the motive nozzle calculation is successful.
6) If the critical mass flow rate of the motive stream is larger than the mass flow rate predicted by the compressor map ($\dot{m}_{nozzle} > \dot{m}_{comp}$), the motive nozzle is operated at non-critical mode and there is $\dot{m}_{nozzle} = \dot{m}_{comp}$. Non-critical motive nozzle model is used to calculate the nozzle outlet pressure and velocity. If the mass flow rate of the motive stream is smaller than the mass flow rate predicted by the compressor model, the simulation is failed as the nozzle area is too small to operate under given operation conditions
7) The CO_2 mass flow rate through the evaporator is determined from the assumed ejection ratio φ by $\dot{m}_{evap} = \varphi \dot{m}_{nozzle}$.
8) Assuming the refrigerant side pressure drop of the evaporator ΔP_{evap} , the evaporator inlet pressure can be determined from the specified evaporator outlet pressure as: $P_{evap,in} = P_{evap,out} + \Delta P_{evap}$.
9) The CO_2 inlet conditions (quality) to the evaporator are determined based on an isenthalpic throttling process from the separator pressure P_{diff} to the evaporator inlet pressure $P_{evap,in}$
10) The evaporator capacity $\dot{Q}_{evap}$, CO_2 temperature and pressure at outlet of the evaporator and air temperature and pressure at outlet of the evaporator are determined using the evaporator model. If the calculated refrigerant side pressure drop of the evaporator is different with the assumed value of ΔP_{evap} , go back to step 8) to iterate until the refrigerant side pressure drop of evaporator converges within specified tolerance.
11) The suction nozzle model calculations are performed to determine the suction nozzle outlet conditions.
12) The mixing section model calculations are performed to determine mixing section outlet conditions.
13) The diffuser model calculations are performed to determine the CO_2 pressure at diffuser outlet $p_{diff,n}$ and quality at the diffuser outlet x_{diff}.
14) The updated ejection ratio is obtained from Equation (D.4). If the calculated value is different with the assumed value of φ, steps 7) to 14) are repeated until the ejection ratio converges within a given tolerance.
15) The calculated diffuser outlet pressure $P_{diff,n}$ is compared to the assumed diffuser outlet pressure P_{diff}. If the pressures are not equal, the diffuser outlet pressure P_{diff} is updated and steps 3) to 14) are repeated until the pressures agree with each other within a given tolerance.

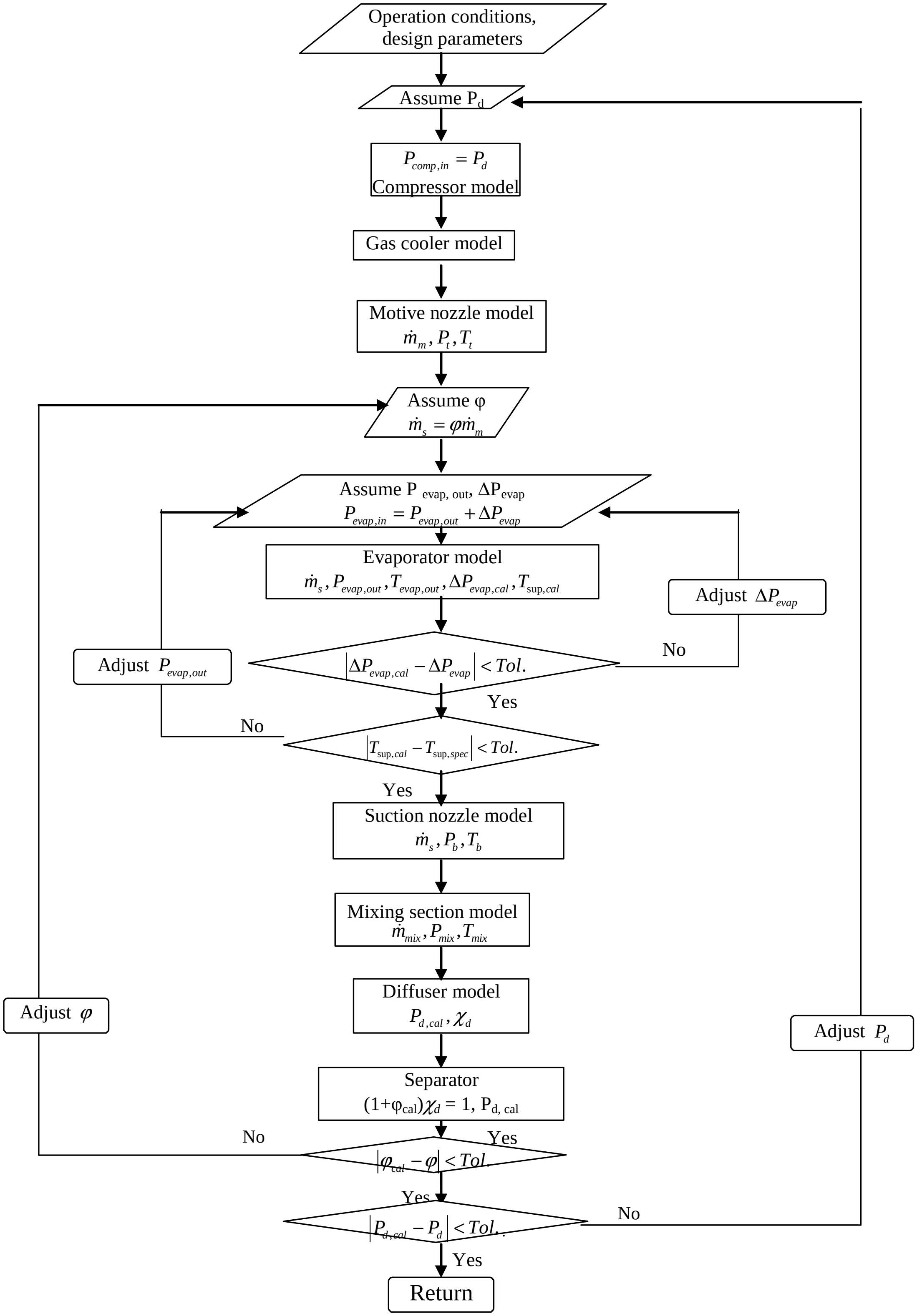

Figure 4.4: Flow chart of computation sequence for ejector expansion transcritical air conditioning system model

4.7. Gas cooler and evaporator dimensions of CO_2 system

Table 4.1 shows the physical dimensions of the gas cooler and the evaporator used in the simulations of the CO_2 system.

Table 4.1: Heat exchanger specifications of CO_2 gas cooler and evaporator models

Simulated CO_2 microchannel heat exchanger (Finned-tube)	gas cooler	evaporator
Face areas (mm^2)	248	48.8
Fin thickness (mm)	0.1524	0.1524
Fin height (mm)	8	8
Tube thickness (mm)	0.5	0.5
Inlet tube diameter (mm)	0.54	0.54
Heat exchanger port diameter (mm)	1	1

To validate the predictions of the ejector expansion transcritical air conditioning system model, an experimental study was conducted as part of the project, which is presented next.

5. EXPERIMENTAL SETUP

5.1. CO_2 based prototype ECU setup

In order to validate the predictions of the simulation model of the transcritical CO_2 air conditioning system that was originally developed by Ortiz et al. (2003) and which is the basis of the ejector expansion transcritical CO_2 air conditioning system simulation model developed in this study, the performance of an existing transcritical CO_2 air conditioning system was tested at various operating conditions. The system design is based on a military standard 10.3 kW (3 ton) Environmental Control Unit (ECU). A detailed description of the CO_2 based bread board ECU is given here.

5.1.1. CO_2 based bread board ECU components

The CO_2 based bread board ECU consists of an indoor unit and an outdoor unit, which are located in the two side-by-side psychrometric chambers. The indoor unit consists of an evaporator, evaporator box, evaporator fan, expansion valve, bypass valve and liquid receiver. The outdoor unit consists of a gas cooler, gas cooler box, gas cooler fan, and compressor and oil separator. A schematic of the system setup is shown in Figure 5.1. The parts that are used in the experimental system and the suppliers or manufacturers of these parts are listed in Table 5.1. The numbers used for the parts in Figure 5.1 correspond to the numbers listed in Table 5.1.

Table 5.1: Parts list of CO_2 based bread board ECU test setup

No.	Description	Supplier or Manufacturer
1	CO_2 Compressor	Dorin
2	Oil Separator	Parker (assembled at HERL)
3	Gas Cooler (Microchannel)	Hydro Aluminum/Livernois (circuited at HERL)
4	Gas Cooler Box	Manufactured at HERL
5	Gas Cooler Fan	Lau Industries
6	Bypass Valve	Swagelok
7	Back Pressure valve	Enpro
8	Liquid Receiver	Parker (assembled at HERL)
9	Evaporator (Microchannel)	Hydro Aluminum/Livernois (circuited at HERL)
10	Evaporator Box	Manufactured at HERL
11	Evaporator Fan	Keco Industries

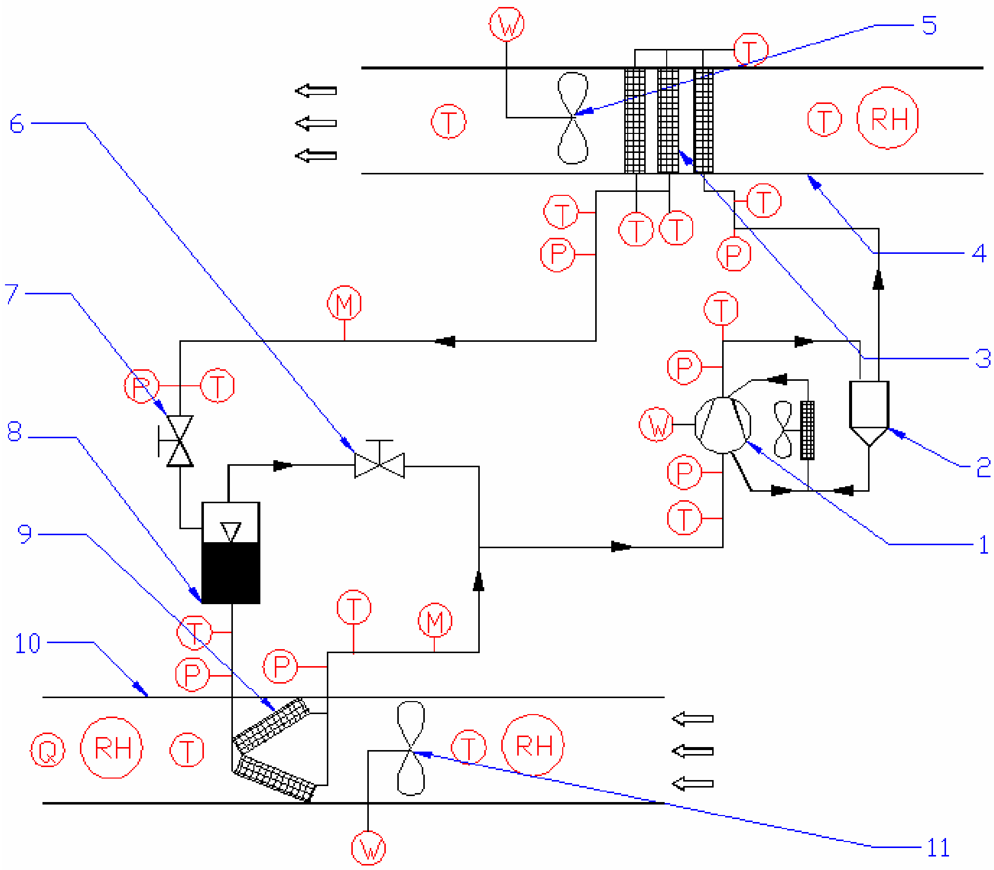

P: Pressure Transducer, T: Temperature Transducer, M: Mass Flow Meter,
W: Power, RH: Dew Point meter

Figure 5.1: Schematic of CO_2 based bread board ECU test setup

The gas cooler and the evaporator are made up of multiple micro-channel heat exchanger slabs. A schematic of one micro-channel heat exchanger slab is shown in Figure 5.2. A gas cooler air flow box and an evaporator air flow box were constructed to make the bread board ECU match the current design of a military standard ECU. The gas cooler and evaporator boxes were built according to the dimensional parameters provided by the Keco Industries, a manufacturer of military standard ECUs. During the selection and circuiting of the micro-channel heat exchanger slabs, every effort was made to fit the slabs into the gas cooler and evaporator boxes without compromising air flow and effectiveness. The schematics of the gas cooler box and the evaporator box are shown in Figures 5.3 and 5.4, respectively.

The gas cooler consists of three micro-channel heat exchanger slabs and the evaporator consists of two micro-channel heat exchanger slabs. The circuiting of the gas cooler slabs and the evaporator slabs can be varied to investigate a variety of refrigerant flow configurations. Currently, the gas cooler micro-channel heat exchanger slabs are piped together and oriented in the air flow as shown in Figure 5.5 and the evaporator micro-channel heat exchanger slabs are piped together and oriented in the air flow as shown in Figure 5.6.

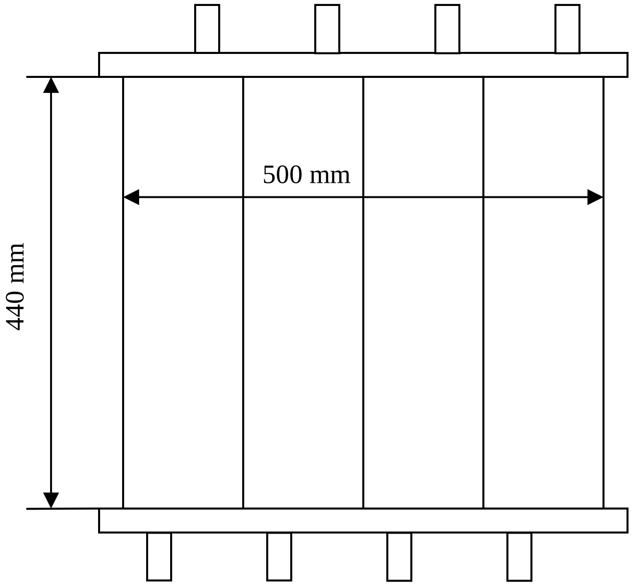

Figure 5.2: Schematic of micro-channel heat exchanger slab

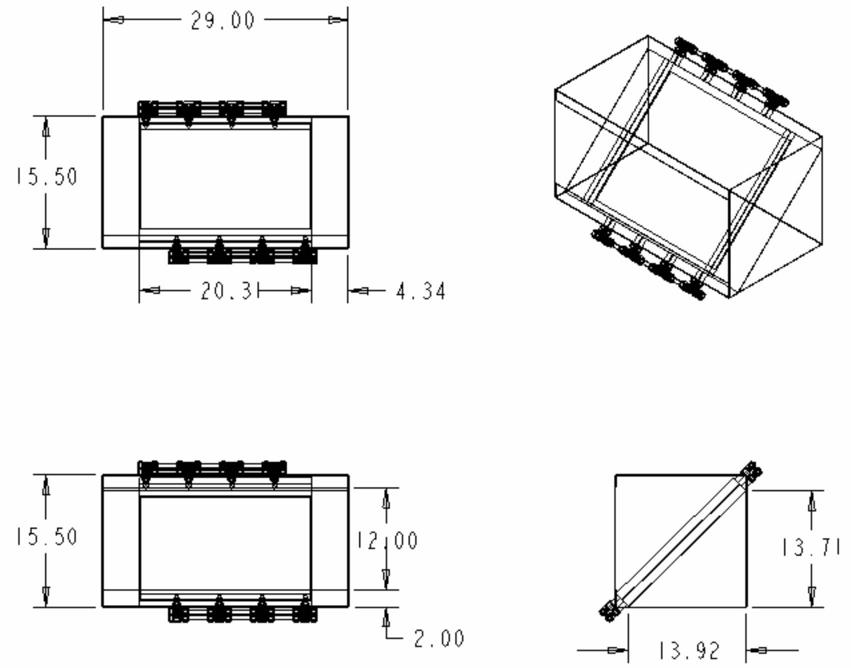

Figure 5.3: Drawing of the evaporator of the CO_2 based bread board ECU

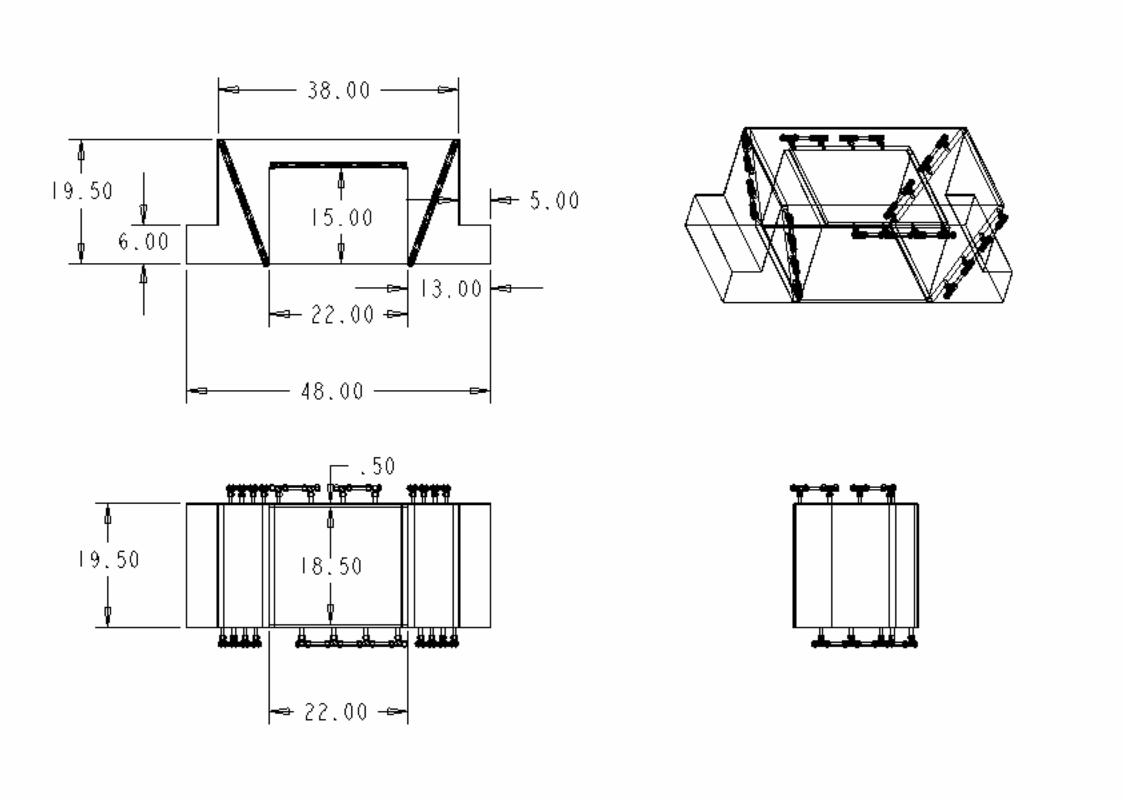

Figure 5.4: Drawing of the gas cooler of the CO_2 based bread board ECU

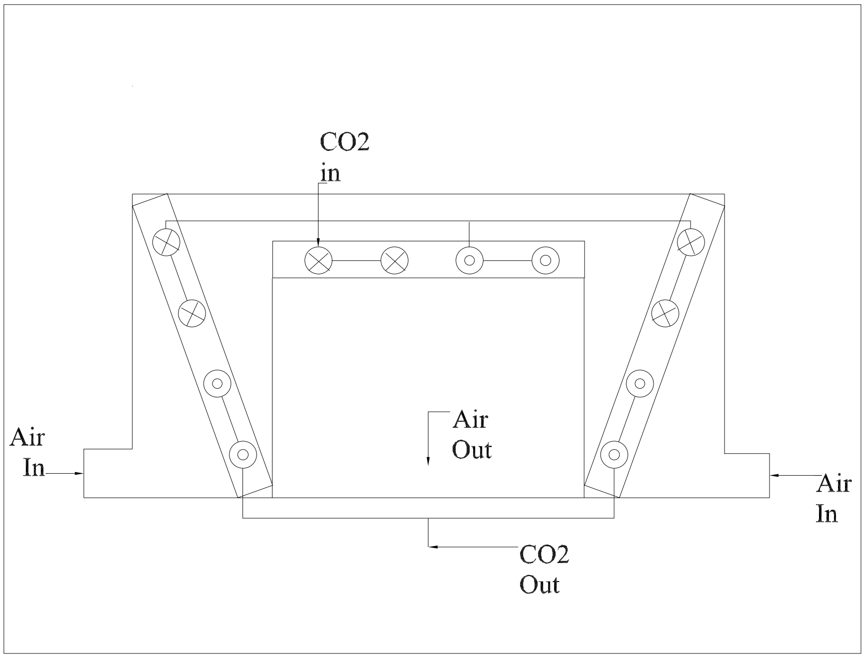

Figure 5.5: Schematic of the gas cooler flow circuits

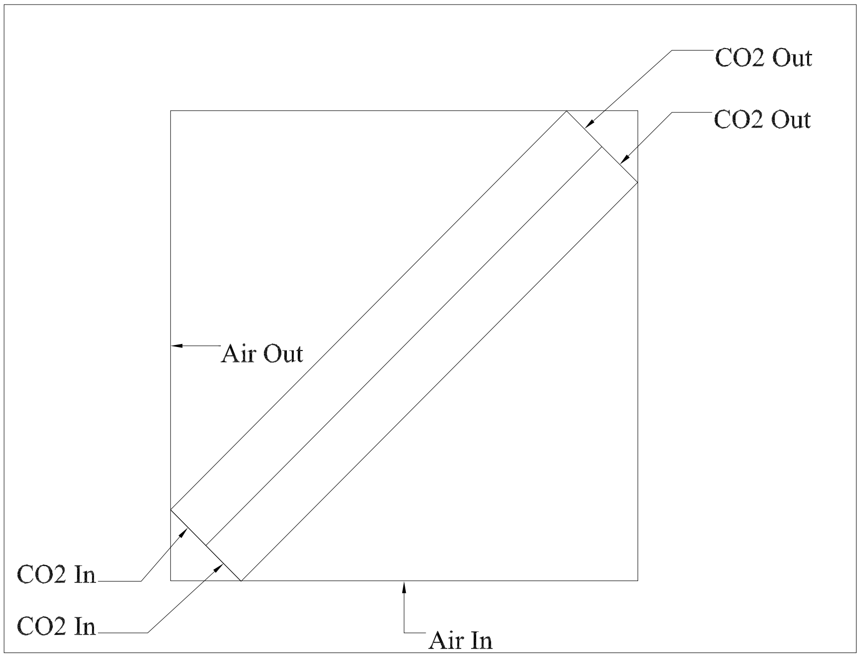

Figure 5.6: Schematic of the evaporator flow circuits

The evaporator fan was provided by Keco Industries and is the same as the one currently used in military standard ECUs with the same design capacity. The gas cooler fan was obtained from the same manufacturer that provides condenser fans to the military standard ECU. However, the fan has a 50 mm smaller diameter than the one installed in the currently used military standard ECU with the same design capacity.

The oil separator is made out of one gallon stainless-steel sample cylinder obtained from Parker. The liquid receiver is made out of one gallon carbon steel accumulator from Accumulators, Inc. High pressure double window sight glasses made by John C. Ernst Company were installed downstream of the oil separator and the liquid receiver to observe the oil flow and the refrigerant flow, respectively.

The expansion valve is a back pressure regulator valve, which was obtained from Enpro and has a maximum operating pressure of 2500 psig.

A photo of the indoor unit is shown in Figure 5.7 and a photo of the outdoor unit is shown in Figure 5.8.

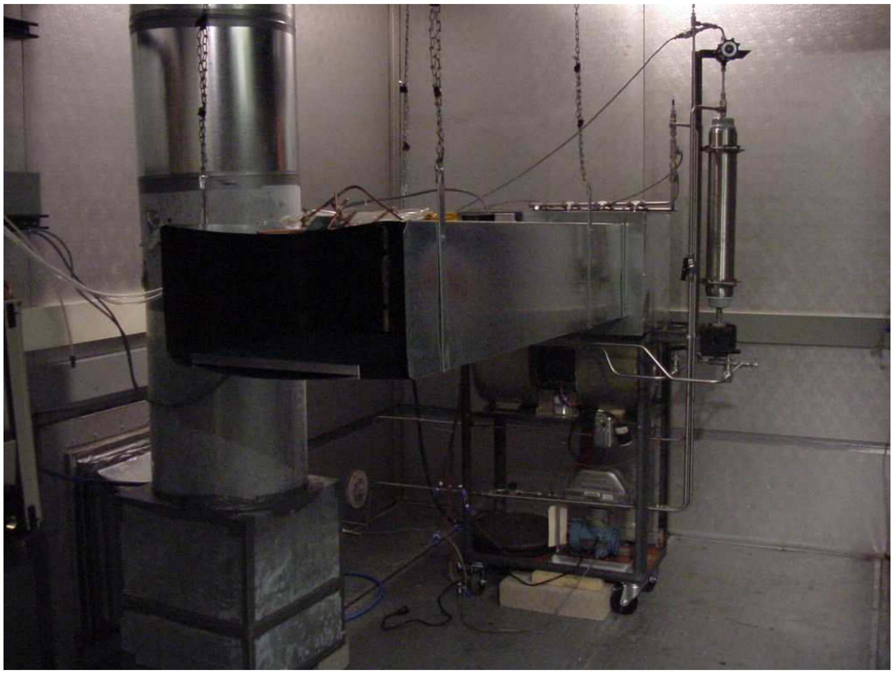

Figure 5.7: Indoor unit of CO_2 based bread board ECU setup

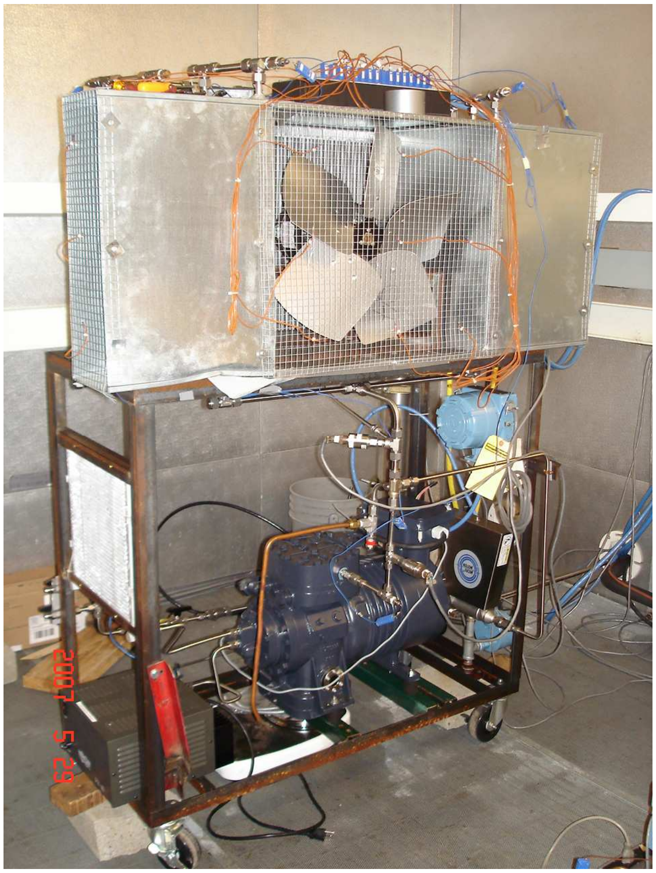

Figure 5.8: Outdoor unit of CO_2 based bread board ECU setup

5.1.2. CO_2 based bread board ECU instrumentation

All measuring instrumentation is indicated in Figure 5.1. All temperatures are measured with T-type thermocouples with ±0.5 ºC accuracy. The refrigerant side pressures are measured with absolute pressure sensor PX32B1-2.5 KAV from Omegadyne, Inc. with a full-scale accuracy of 0.11%. Two micro-motion mass flow meters with an accuracy of ±0.5% of the reading value are installed to measure the refrigerant mass flow rate across the compressor and the mass flow rate across the evaporator, respectively. The relative humidity of the air is measured with a General Eastern Dew Point meter with an accuracy of ±1%. The air volume flow rate across the evaporator is measured with GTx116-PC thermal dispersion air flow sensor from Ebtron Company, which has an accuracy of ±2% of the reading value. The electrical power consumptions of the compressor, the gas cooler fan and the evaporator fan are measured with three separately installed Scientific Columbus power meters with an accuracy of ±0.2% of reading value. An Agilent 13890A and a Hewlett Packard Model 75000 Series B data acquisition system are used to convert the incoming voltages from the measuring instrumentation to digital signals and then to transfer the signals to a personal computer. The computer uses the program LabVIEW for the data analysis.

5.1.3. Data reduction of CO_2 based bread board ECU test

The methodology by which the recorded data was used to calculate the various engineering parameters that characterize the performance of the experimental system for given operating conditions is described in the following section. The main parameters are cooling capacity and COP.

The air and refrigerant enthalpies were calculated using thermodynamic property functions in EES (Klein 2004). The air enthalpies were determined by the measured dry bulb and dew point temperatures and the atmospheric pressure at a corresponding location. The refrigerant enthalpies were determined by the local pressure and temperature measurements. However, the refrigerant enthalpy of a two-phase mixture state cannot be determined with the available measurements. In this case, only the air side measurements and calculations were used.

- Air Enthalpy Method

  During the cooling tests, the sensible, total, and latent cooling capacities based on the air-side evaporator test data will be calculated using Equations (5.1), (5.2) and (5.3):

  - Sensible air-side cooling capacity:

$$\dot{Q}_{c,sen} = \dot{m}_{air} C_{p,air} \left(T_{air,ei} - T_{air,eo} \right) \tag{5.1}$$

  where $C_{p,air}$ is the specific heat of air with the average temperature and average relative humidity between inlet and outlet.

  - Total cooling capacity:

$$\dot{Q}_{c,air} = \dot{m}_{air} \left(h_{air,ei} - h_{air,eo} \right) \tag{5.2}$$

- Latent air-side cooling capacity:

$$\dot{Q}_{c,lat} = \dot{Q}_{c,air} - \dot{Q}_{c,sen} \tag{5.3}$$

- Refrigerant Flow Enthalpy Method

  The total cooling capacity of the evaporator air coil measured on the refrigerant side was calculated by Equation (5.4):

$$\dot{Q}_{c,ref} = \dot{m}_{ref}\left(h_{ref,2} - h_{ref,1}\right) \tag{5.4}$$

  where $h_{ref,1}$ and $h_{ref,2}$ are the refrigerant enthalpies at the inlet of the expansion valve assuming an isenthalpic expansion process and at outlet of the evaporator.

- Energy Balance

  The cooling capacities calculated with the air enthalpy method and the refrigerant enthalpy flow method was compared for each test. Both values had to agree with each other within their measurement uncertainties obtained from the error analysis to consider the test a valid test.

- System Performance

  The refrigerant side cooling coefficient of performance (COP) was determined by Equation (5.5):

$$COP_c = \frac{\dot{Q}_{c,ref}}{\dot{W}_{comp}} \tag{5.5}$$

  where $\dot{W}_{comp}$ is the electrical compressor power consumption.

5.1.4. CO_2 based bread board ECU test uncertainty analysis

Table 5.2 lists the measured parameters that are used to determine the cooling capacity $\dot{Q}_{c,ref}$ and the cooling COP by the refrigerant flow enthalpy method. For each parameter, the measured value and the absolute uncertainty are listed as well. In addition, Table 5.2 presents the calculated capacity and the COP based on the measured values and the uncertainties that are associated with this capacity and the COP based on the uncertainties of the individual measurements. The uncertainties of the capacity and the COP were determined using a standard error analysis in EES (Klein 2004). It can be seen that the refrigerant-side cooling capacity can be measured within ±4.95% (3 σ) and the cooling COP within ±4.98% (3 σ) given the listed accuracy of the various measurement instrumentations. It can also be seen that the uncertainties associated with the expansion valve inlet temperatures of ±0.5 ºC are the most significant contributions to the final uncertainty of the calculated cooling capacity and COP.

Since the refrigerant side results have a higher accuracy than air side results, the measured cooling capacity $\dot{Q}_{c,ref}$ and cooling COP are determined using the refrigerant side data.

Table 5.2: Uncertainty analysis for the refrigerant enthalpy flow method

Measured data	Value	Absolute uncertainty	$\dot{Q}_{c,ref}$ (kW)	COP
			Uncertainty Contributions	
P_{exv} (MPa)	12.69	0.01897	0.31%	0.31%
P_{evap} (MPa)	3.84	0.01897	3.79%	3.74%
T_{exv} (ºC)	45.24	0.5	70.65%	69.63%
T_{evap} (ºC)	9.78	0.5	16.06%	15.83%
$\dot{m}_{ref}$ (kg/s)	0.11	0.00055	9.18%	9.04%
$\dot{W}_{comp}$ (kW)	10.28	0.02056	0.00%	1.45%
Calculated Results			14.23	1.384
Absolute Uncertainty			0.2349	0.02302
Relative Uncertainty (1 σ)			1.65%	1.66%

5.2. CO_2 ejector expansion ECU setup

To validate the prediction of the two-phase flow ejector model and the ejector expansion transcritical CO_2 air conditioning system simulation model, a controllable ejector expansion device was designed, constructed, and installed in the CO_2 based bread board ECU to replace the expansive valve. In addition, a new separator at the outlet of the ejector was obtained and installed. Afterwards, the ejector-expansion ECU was tested at various operating conditions.

5.2.1. Description of the controllable ejector expansion device

The stainless-steel controllable ejector expansion device constructed by the Mechanical Engineering machine shop at Purdue University is presented in Figure 5.9. The section drawing of the ejector expansion device is shown in Figure 5.10. The detailed design of the motive nozzle, suction nozzle-mixing section-diffuser, and needle are shown in Figures 5.11 to 5.14. The motive nozzle, the suction nozzle-mixing section-diffuser, and the needle were assembled using the connectors shown in Figure 5.15. This ejector expansion device was installed in the CO_2 based bread board ECU using Swagelok NPT thread connector.

Figure 5.9: Photograph of controllable ejector expansion device

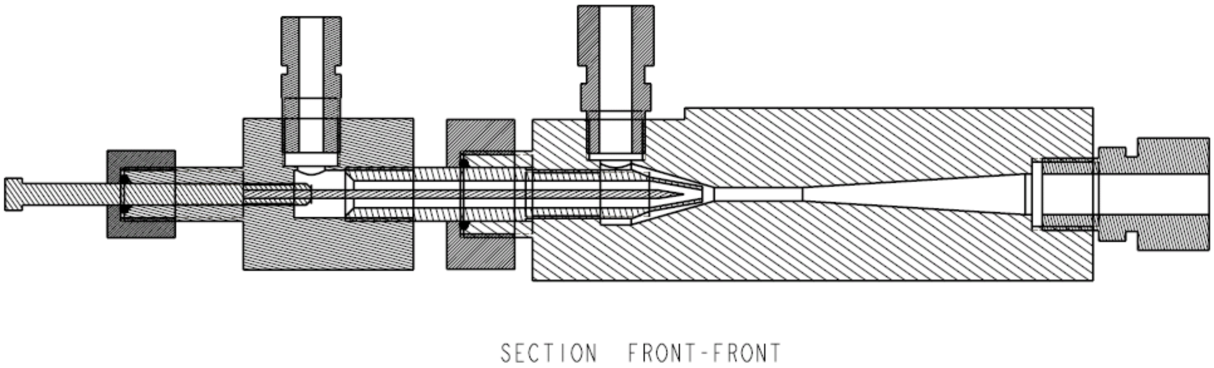

Figure 5.10: Schematic of controllable ejector expansion device

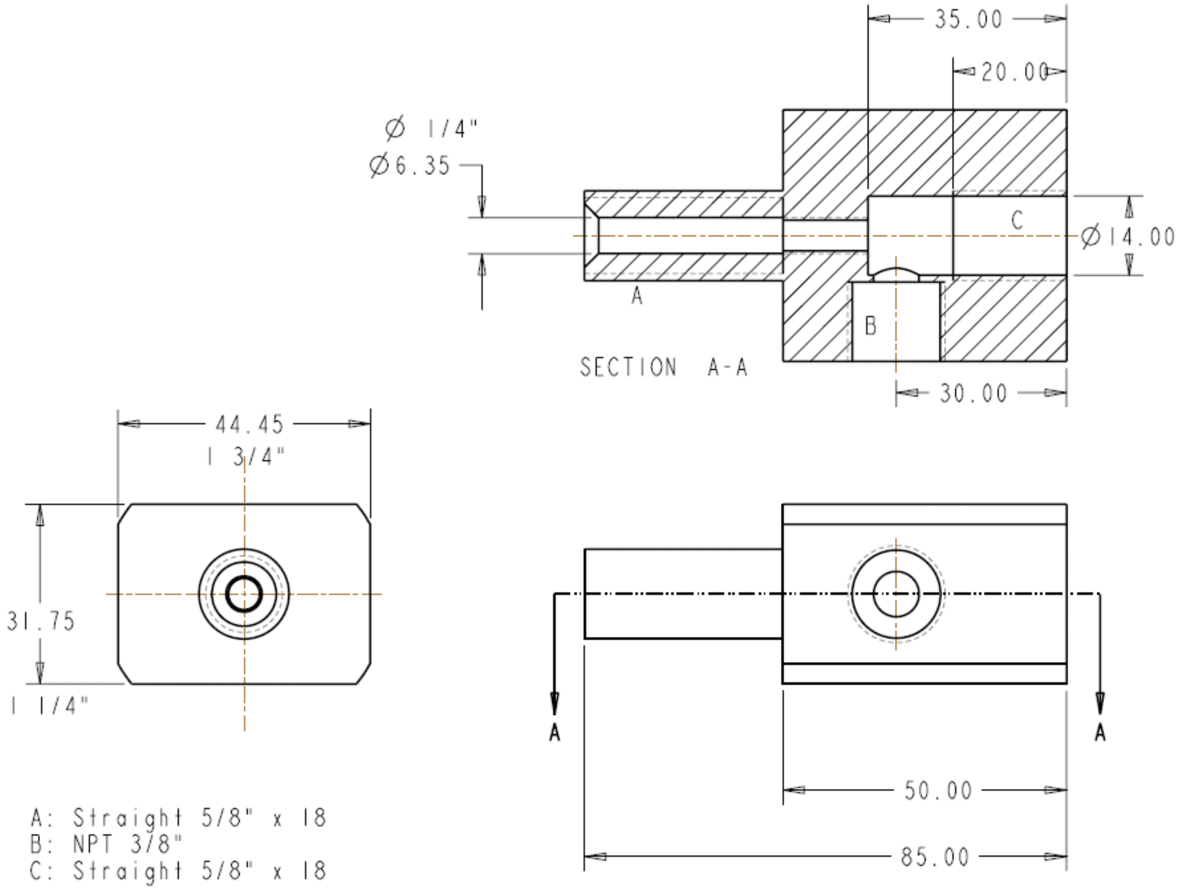

Figure 5.11: Schematic of motive nozzle receiving section

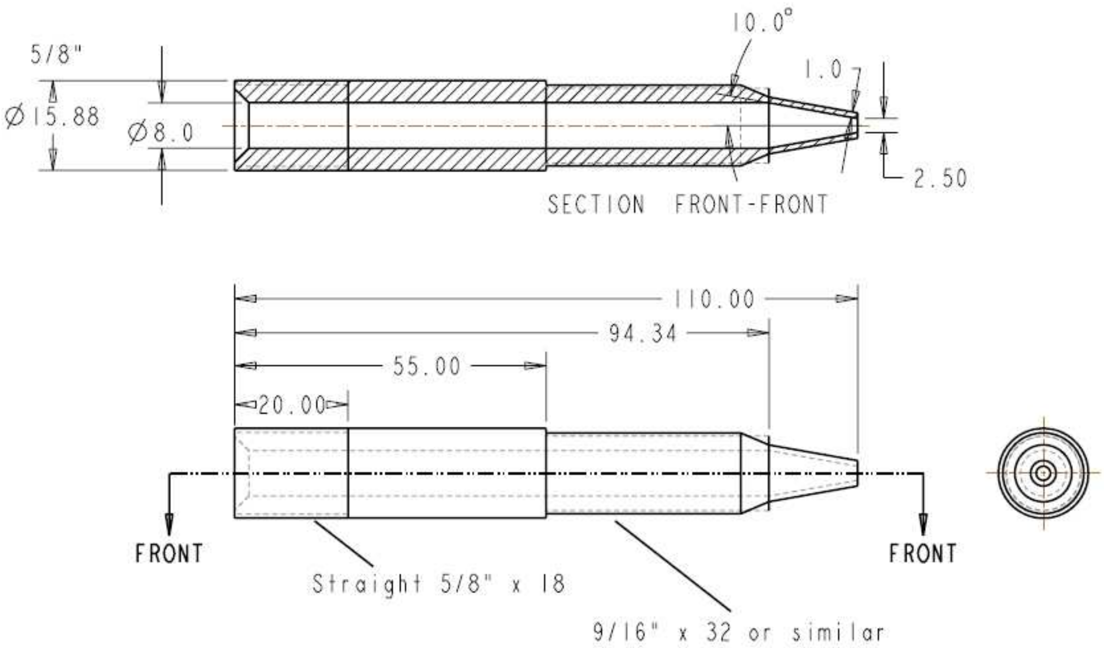

Figure 5.12: Schematic of motive nozzle

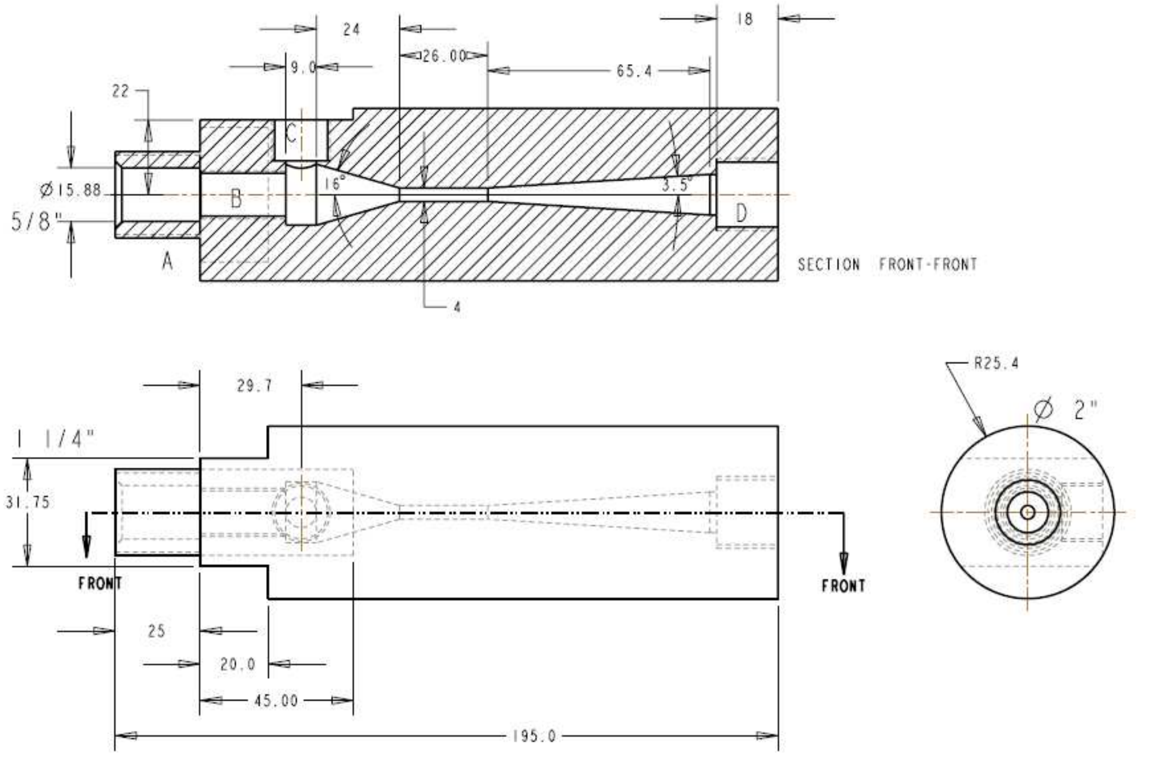

A: Straight 1" x 16 or similar
B: Straight 9/16 x 32 or similar
C: NPT 3/8"
D: NPT 1/2"

Figure 5.13: Schematic of suction nozzle – mixing section – diffuser

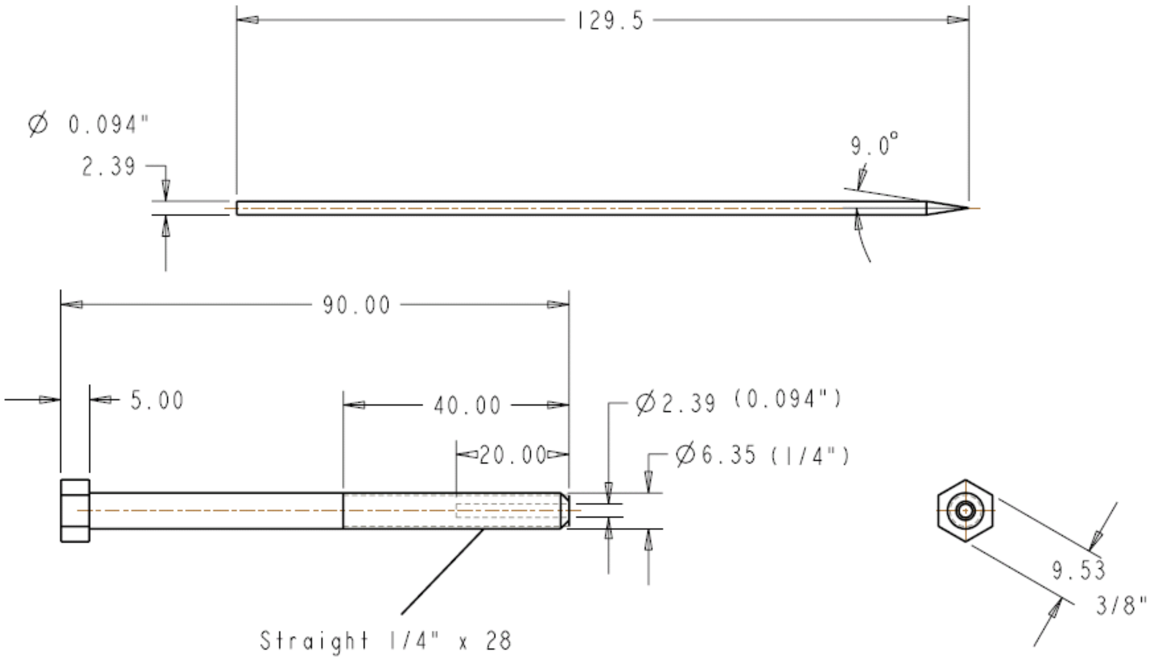

Figure 5.14: Design of needle

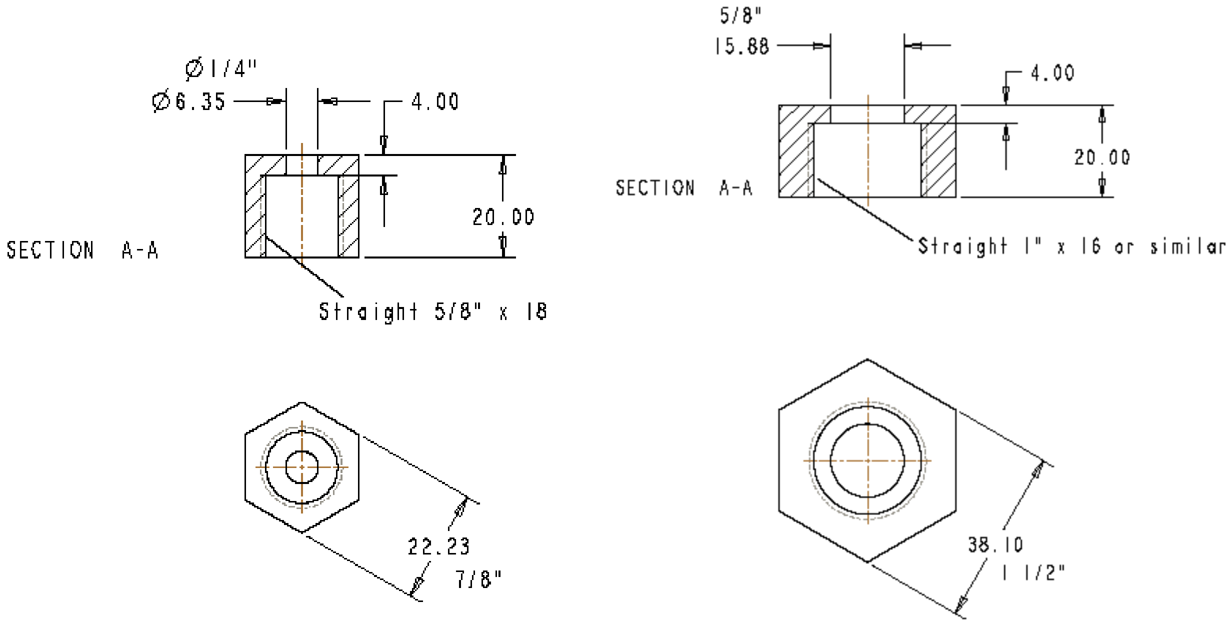

Figure 5.15: Design of straight thread connectors

5.2.2. Description of the ejector expansion CO_2 ECU test setup

To validate the two-phase flow ejector model and the ejector expansion CO_2 system simulation model, the ejector expansion device was installed in the experimental setup of the CO_2 based bread board ECU as shown in Figure 5.16. The back pressure valve in the CO_2 ECU was replaced by the ejector (Part No. 7 in Figure 5.16), which is fabricated by the ME machine shop at Purdue University. In addition, three control valves (Part No. 6 in Figure 5.16) were added to control the mass flow rates of the motive nozzle and suction nozzle.

A photo of the modified indoor unit is shown in Figure 5.17 and a photo of the modified outdoor unit is shown in Figure 5.18.

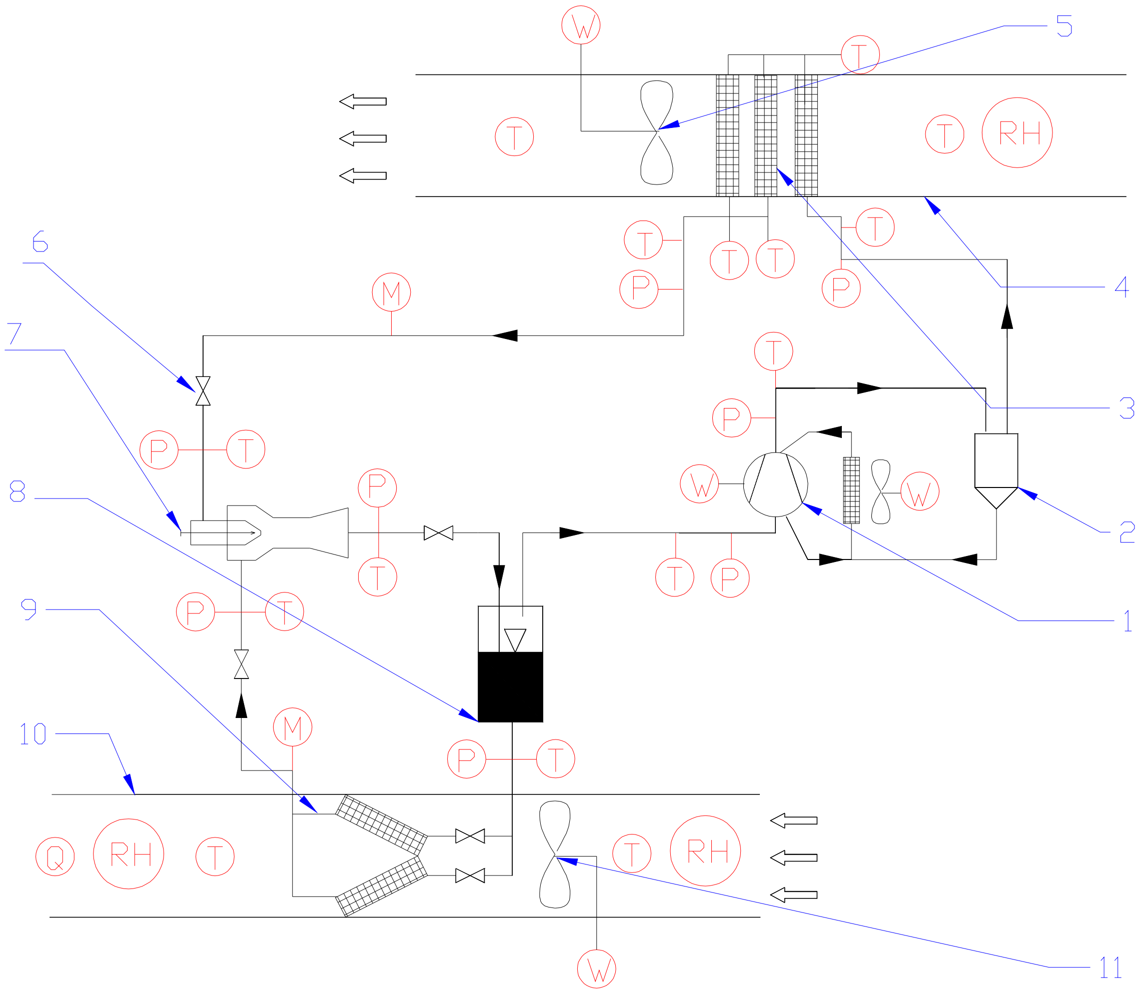

P: Pressure Transducer, T: Temperature Transducer, M: Mass Flow Meter,
W: Power, RH: Dew Point meter

Figure 5.16: Schematic of ejector expansion CO_2 ECU test setup

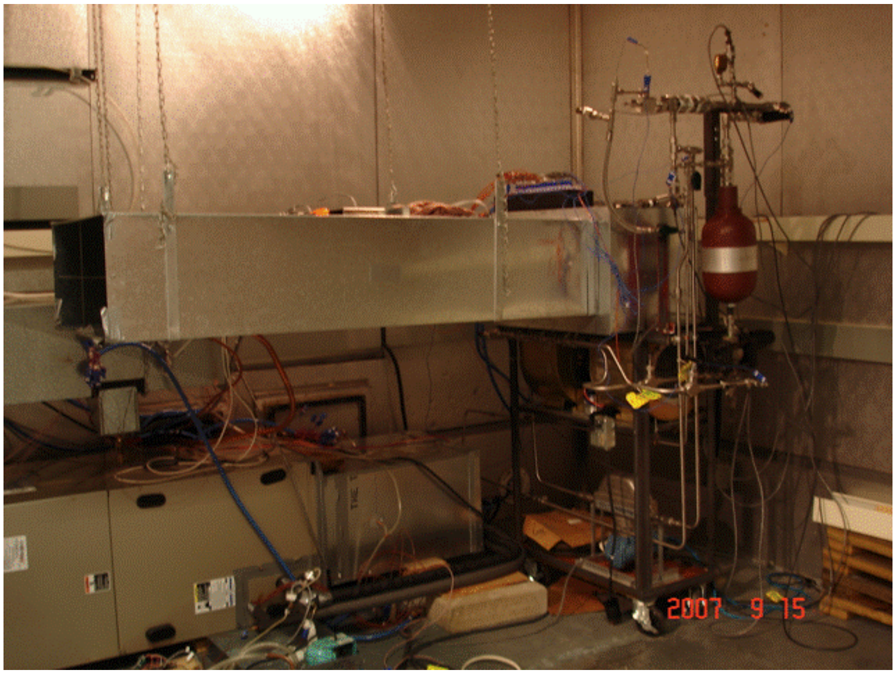

Figure 5.17: Indoor unit of ejector expansion CO_2 ECU test setup (modified)

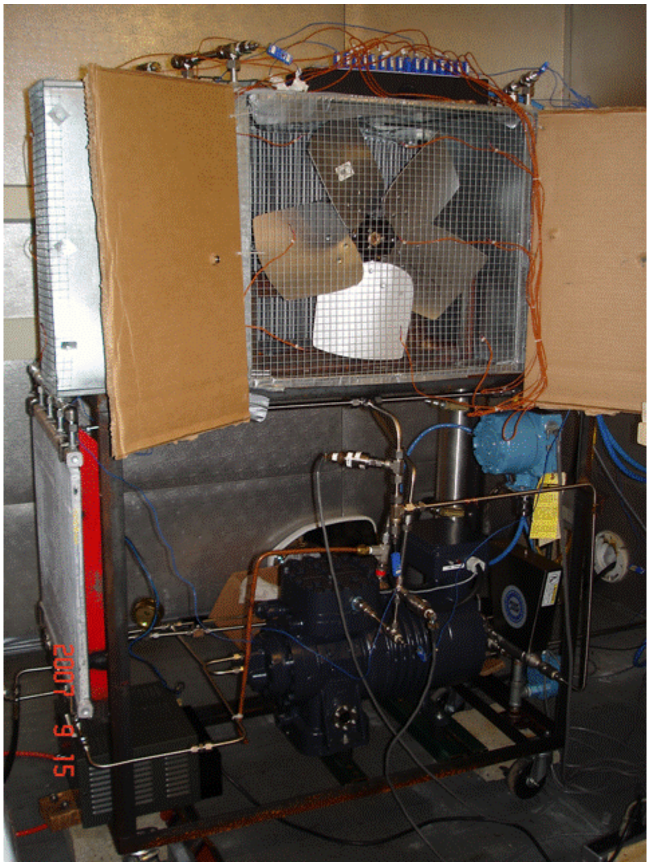

Figure 5.18: Outdoor unit of ejector expansion CO_2 ECU test setup (modified)

5.2.3. Ejector expansion CO_2 system test setup instrumentation

One pressure sensor and one thermocouple were added to the CO_2 based ECU test setup to measure the pressure and the temperature after the ejector outlet, respectively. Two high pressure switches (from ISAACS Company) were installed at the motive nozzle inlet and the diffuser exit to prevent any sudden pressure spikes in the ejector expansion device.

5.2.4. Ejector test data reduction

The test data recorded during the two-phase flow ejector tests are the CO_2 pressures and temperatures, and the mass flow rates at the inlet to the motive nozzle and the suction nozzle as well as the CO_2 pressure at the ejector outlet. The two-phase flow ejector model was used to determine the motive nozzle, suction nozzle and mixing section efficiencies based on the measured data. The overall flow chart to determine the internal ejector efficiencies is shown in Figure 5.19.

The details of how the motive and suction nozzle isentropic efficiencies and the mixing section efficiency are calculated using the two-phase flow ejector model as shown in Figures 5.20 to 5.23. The isentropic efficiency of the motive nozzle was determined by matching the measured motive nozzle mass flow rate to the motive nozzle mass flow rate predicted using the two-phase flow ejector model as shown in shown in Figures 5.20 and 5.21 for critical flow and non-critical flow, respectively. The isentropic efficiency of the suction nozzle was determined by matching the measured suction nozzle mass flow rate to the suction nozzle mass flow rate predicted using the two-phase flow ejector model as shown in Figure 5.22. The mixing section efficiency was determined by matching the measured ejector outlet pressure to the predicted ejector outlet pressure using the two-phase flow ejector model as shown in Figure 5.23.

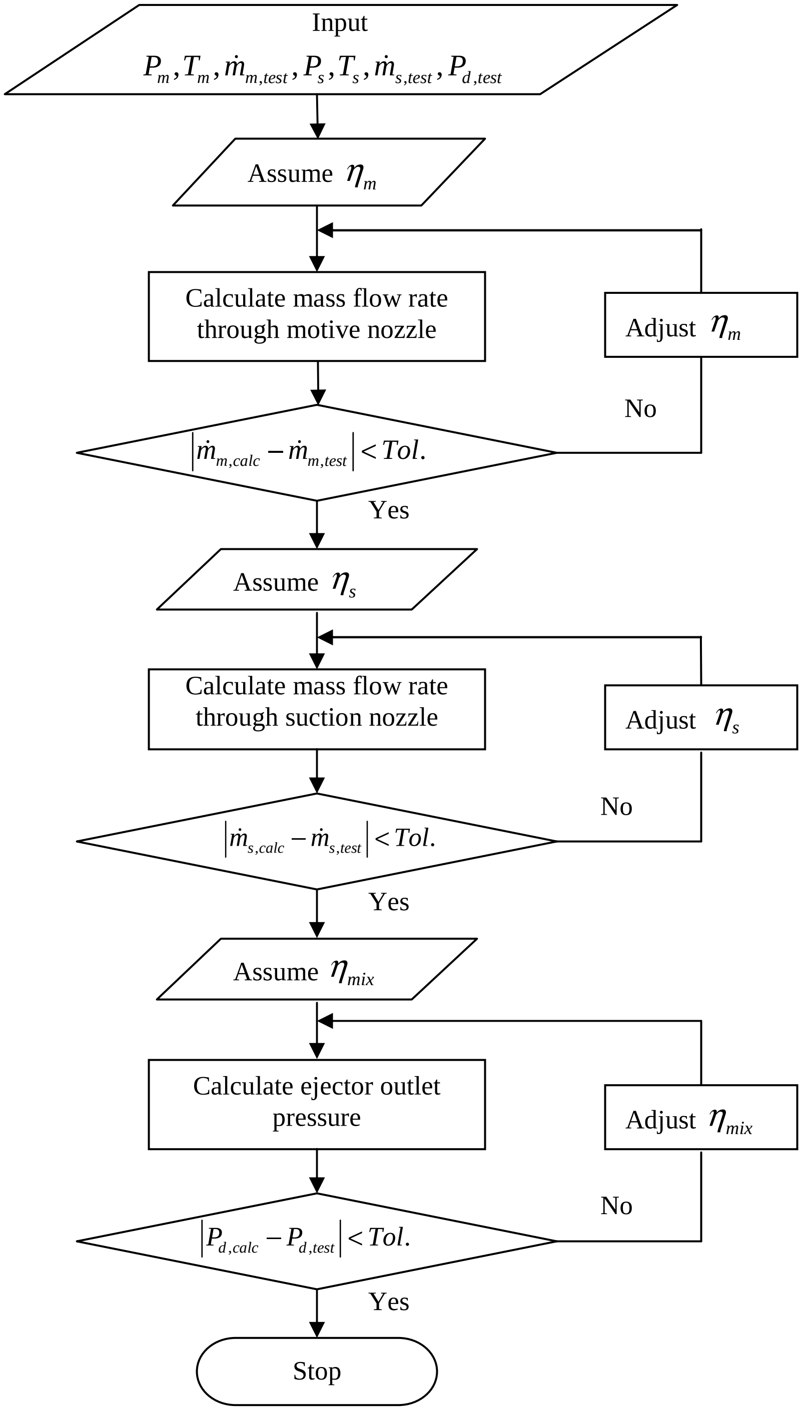

Figure 5.19: Flow chart to determine motive and suction nozzle isentropic efficiencies as well as mixing efficiency

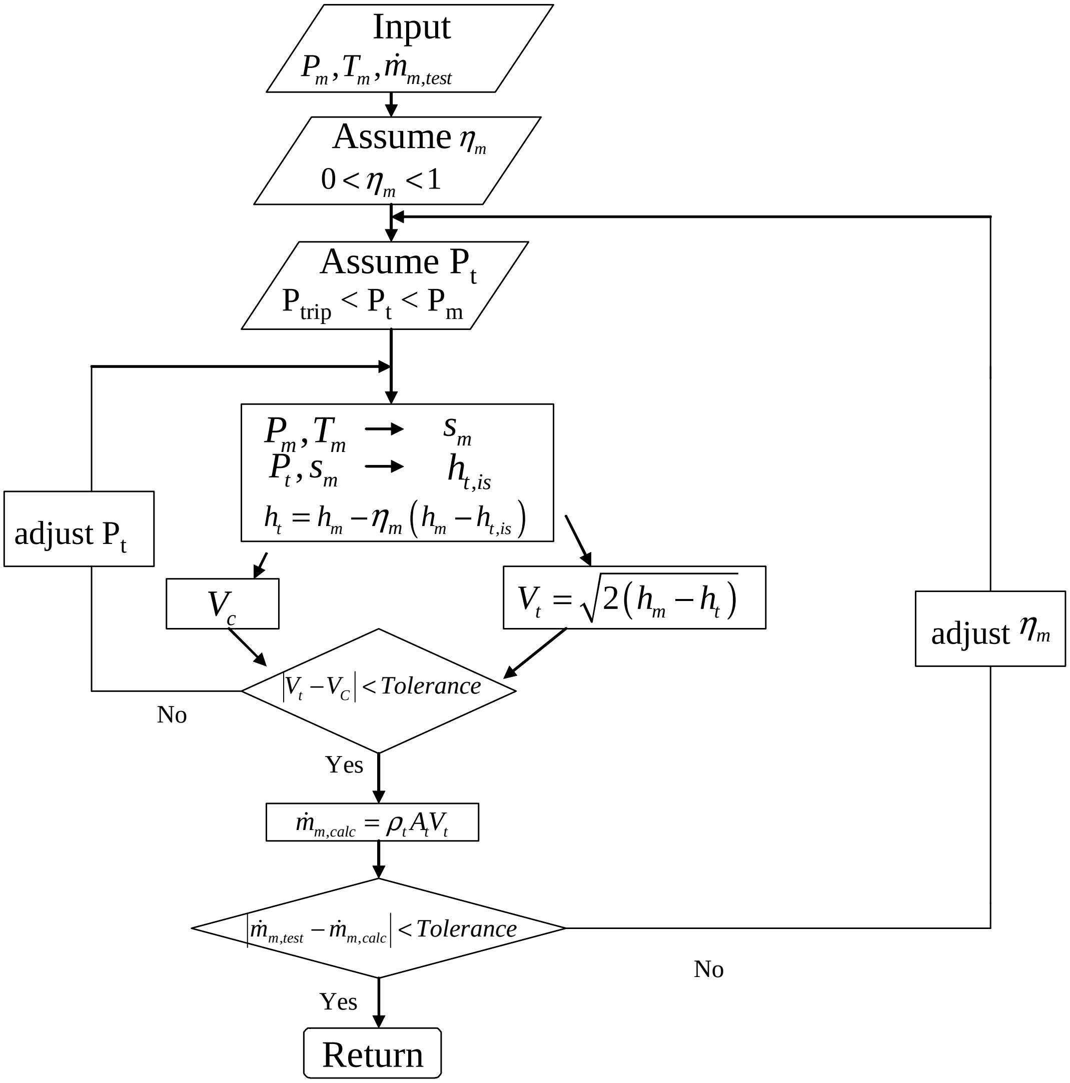

Figure 5.20: Flow chart to determine motive nozzle efficiency (critical flow)

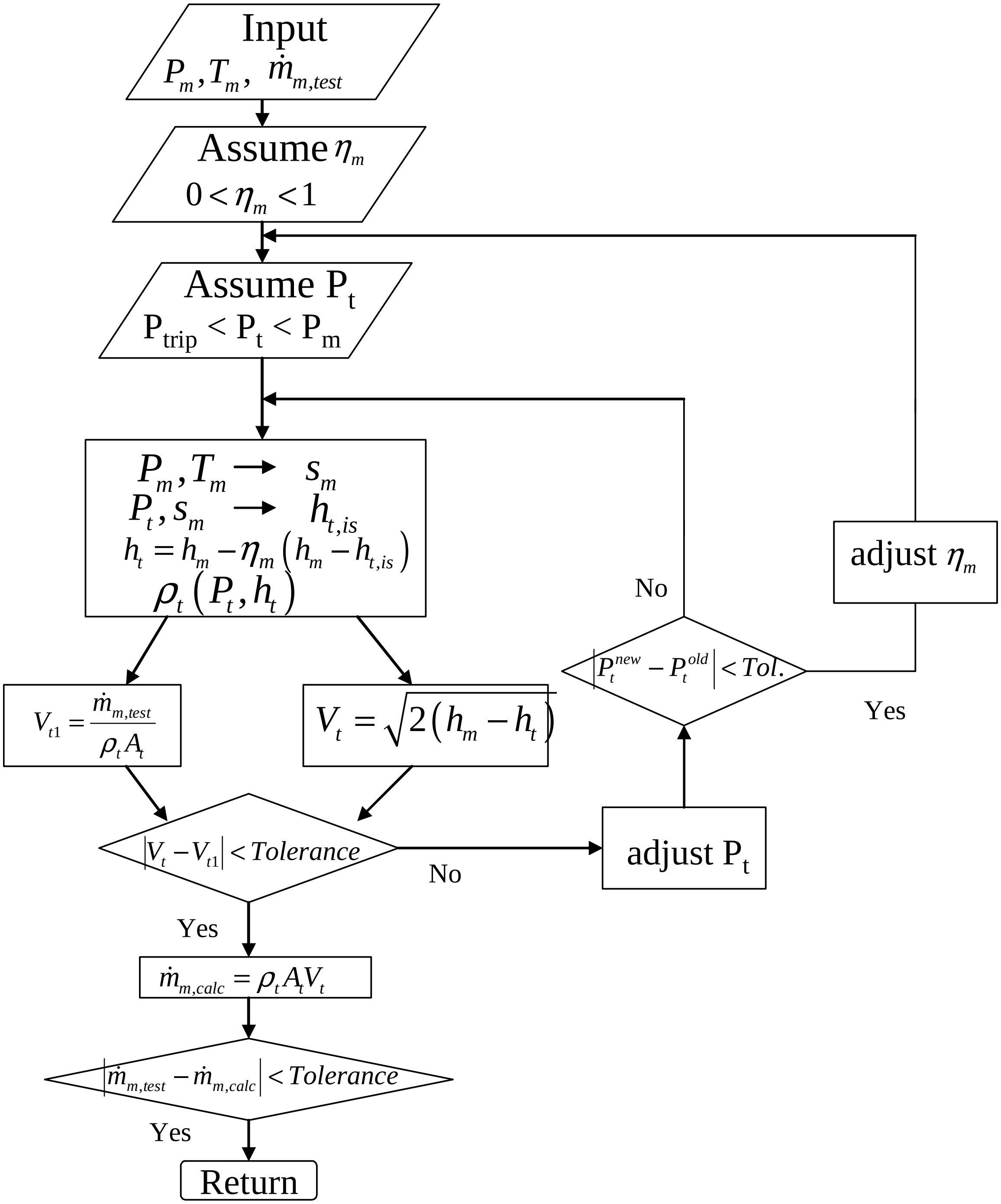

Figure 5.21: Flow chart to determine motive nozzle efficiency (non-critical flow)

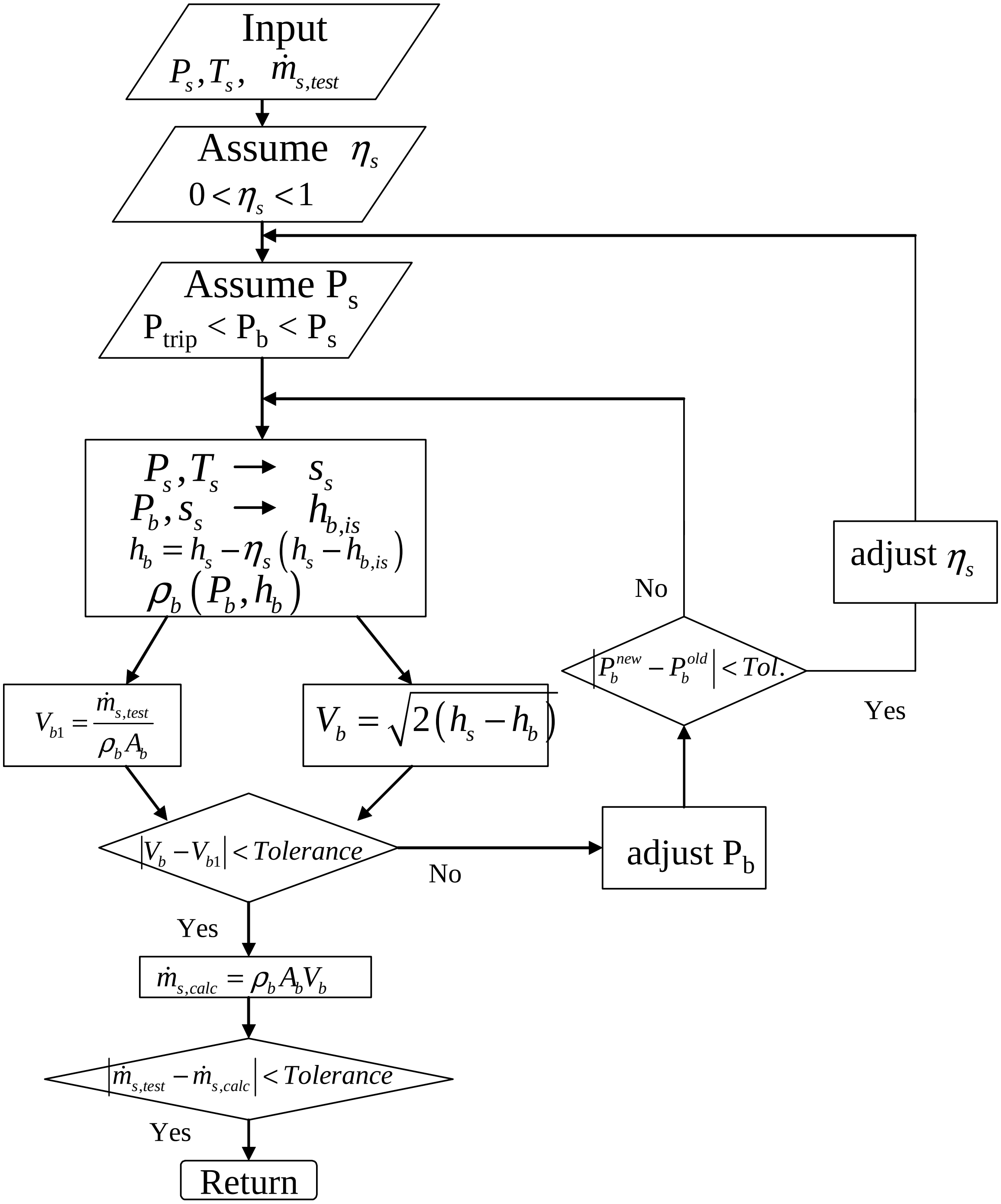

Figure 5.22: Flow chart to determine suction nozzle efficiency (non-critical flow)

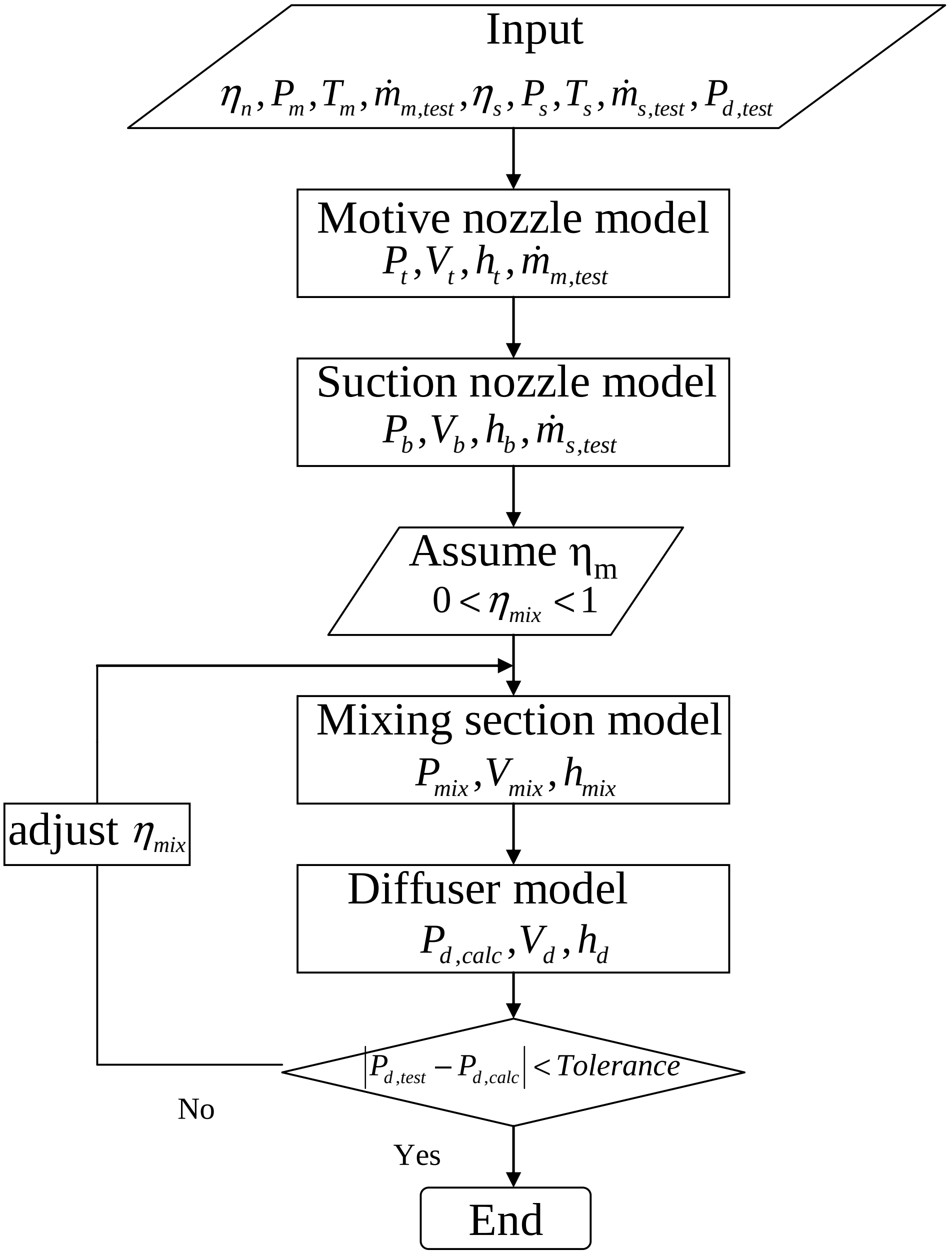

Figure 5.23: Flow chart to determine mixing efficiency

5.2.5. Ejector and ejector expansion ECU test uncertainty analysis

Table 5.3 presents the calculated efficiencies based on the measured values and the uncertainties that are associated with these efficiencies based on the uncertainties of the individual measurements. The uncertainties of the efficiencies were determined using a standard error analysis in EES (Klein 2004). It can be seen from Table 5.3 that the nozzle efficiencies and mixing section efficiency can be determined within ± 6% given the listed accuracy of the various measurement instrumentations. It can also be seen that the uncertainties associated with the motive nozzle inlet temperature of ±0.5 °C, L2 of ±0.2 mm, and motive nozzle and suction nozzle inlet pressures of ±0.019 MPa are the most significant contributions to the final uncertainties of the calculated motive nozzle isentropic efficiency η_m, motive nozzle isentropic efficiency η_s and mixing section efficiency η_{mix}, respectively. L2 is the distance from the motive nozzle exit to the mixing section inlet as shown in Figure 5.23.

Table 5.3: Uncertainty analysis of ejector components

Measured data	Value	Absolute uncertainty	η_m	η_s	η_{mix}
			Uncertainty Contributions		
L1 (mm)	54.03	0.2	0.01481%	0.00%	0.01472%
L2 (mm)	38.3	0.2	0.00%	97.64%	0.00%
P_m (MPa)	12.855	0.019	17.72%	0.00%	47.16%
P_s (MPa)	3.748	0.019	0.00%	0.8649%	47.15%
T_m (ºC)	50.88	0.5	69.33%	0.00%	3.279%
T_s (ºC)	21.63	0.5	0.00%	0.05455%	0.00%
$\dot{m}_m$ (kg/s)	0.18	0.0008	12.94%	0.00%	0.1062%
$\dot{m}_s$ (kg/s)	0.07	0.00035	0.00%	1.444%	1.607%
P_o (MPa)	4.499	0.019	0.00%	0.00%	0.6791%
Calculated Results			0.986	0.972	0.882
Absolute Uncertainty			0.01056	0.05734	0.02696
Relative Uncertainty			1.071%	5.9%	3.058%

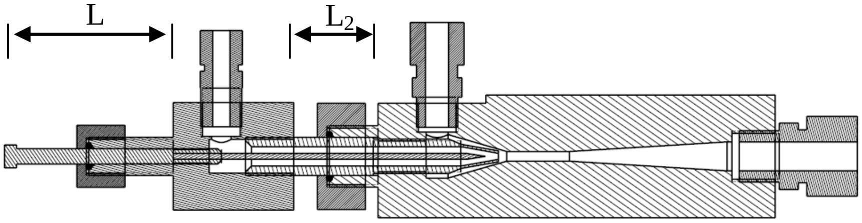

Figure 5.24: Schematic of ejector expansion device including length measurements

An uncertainty analysis was also conducted for the cooling capacity and COP calculations. Table 5.4 presents the results of the uncertainty analysis for the cooling capacity measured on the refrigerant side and the COP calculations. It can be seen that the refrigerant-side cooling capacity can be measured within ± 2.49% (3 σ) and the cooling COP within ± 2.64% (3 σ) using the refrigerant-side capacity. It can also be seen that the uncertainty associated with mass flow rate through the evaporator of ±0.00035 kg/s are the most significant contributions to the final uncertainty of the calculated cooling capacity and COP.

Table 5.4: Uncertainty analysis for the ejector cycle test

Measured data	Value	Absolute uncertainty	$\dot{Q}_{c,ref}$ (kW)	COP
			Uncertainty Contributions	
P_{diff} (MPa)	4.499	0.01897	10.01 %	9.09 %
$P_{e,o}$ (MPa)	3.829	0.01897	4.17 %	3.79 %
$T_{e,o}$ (°C)	22.34	0.5	22.65 %	20.57 %
$\dot{m}_{ref}$ (kg/s)	0.07	0.00035	63.17 %	57.38 %
$\dot{W}_{comp}$ (kW)	10.94	0.02188	0.00 %	9.18 %
Calculated Results			16.35	1.495
Absolute Uncertainty			0.1028	0.0099
Relative Uncertainty (1 σ)			0.63%	0.66%

5.3. Summary of ejector tests

Using the given accuracy of the various measurement instrumentations, both the refrigerant-side cooling COP and cooling capacity can be measured within ±5%. The motive nozzle and suction nozzle efficiencies and the mixing section efficiency can be determined within ±6%. In addition, both the refrigerant-side cooling COP and cooling capacity of the ejector expansion transcritical CO_2 air conditioning system can be determined within ±3%.

6. MODEL VALIDATION

The basic CO_2 transcritical air conditioning system simulation model and the ejector expansion transcritical air conditioning system simulation model were individually validated against the experimental data.

6.1. Basic transcritical CO_2 air conditioning system model validation

The predictions of the basic CO_2 transcritical air conditioning system model were validated using the CO_2 based bread board ECU test results.

6.1.1. CO_2 based bread board ECU tests results

The CO_2 based bread board ECU was tested according to the operation conditions specified in Table 6.1. The indoor room conditions were controlled at 80 ºF (26.7 ºC) dry bulb temperature and 50% relative humidity and the outdoor room dry bulb temperature was changed from 82 ºF (27.8 ºC) to 90 ºF (32.2 ºC), to 95 ºF (35 ºC), to 100 ºF (37.8 ºC), and to 105 ºF (40.6 ºC). At each set of indoor and outdoor room conditions, the high-side pressure was increased by closing the expansion valve to evaluate the effect of high-side pressure on system performance until the compressor discharge temperature was too high. The main test results are listed in Table 6.1. All experimental results can be found in Appendix E.

Table 6.1: Test results for basic CO_2 bread board ECU

Run No.	T_{id} (ºF)	Indoor Humidity (%)	T_{od} (ºF)	P_{dis} (MPa)	$T_{sup, comp}$ (ºC)	$T_{sup, eo}$ (ºC)	$\dot{W}_{comp}$ (kW)	$\dot{Q}_{c,ref}$ (kW)	cooling COP (-)
1	80	50	82	11.906	8.75	6.25	9.70	10.65	1.098
2	80	50	82	12.238	5.60	2.85	10.02	12.95	1.292
3	80	50	82	12.984	8.48	6.07	10.28	14.23	1.385
4	80	50	90	11.880	9.82	7.61	9.68	11.23	1.160
5	80	50	90	12.824	4.75	1.97	10.38	11.38	1.097
6	80	50	95	12.126	10.54	8.649	9.78	10.81	1.105
7	80	50	95	12.240	11.38	9.86	9.93	10.80	1.087
8	80	50	100	13.231	5.32	2.92	10.57	10.35	0.979
9	80	50	100	13.537	5.52	2.878	10.7	10.96	1.025
10	80	50	100	14.150	7.52	4.758	10.83	11.69	1.079
11	80	50	105	13.878	3.18	1.071	10.99	9.384	0.854
12	80	50	105	14.528	4.62	1.742	11.17	10.01	0.896

The compressor overall isentropic efficiencies and the volumetric efficiencies of the single-stage compressor are listed in Table 6.2. The overall isentropic efficiency is defined as:

$$\eta_{o,is} = \frac{\dot{m}\left(h_{is} - h_{suc}\right)}{\dot{W}_{comp}} \tag{7}$$

where $\dot{m}$ is the measured mass flow of the compressor, h_{is} is the enthalpy at the discharge pressure of that stage and at the same entropy as the one at the measured suction pressure and temperature of that stage, h_{suc} is the enthalpy at measured suction pressure and temperature, and $\dot{W}_{comp}$ is the electrical power consumption of that stage. The volumetric efficiency is calculated as follows:

$$\eta_{vol} = \frac{\dot{m} v_{suc}}{n V_{dis} / 60} \tag{8}$$

where v_{suc} is the specific volume at the suction pressure and temperature of each stage, n is the rotational speed of the compressor, and V_{dis} is the displacement volume of each stage.

Table 6.2: Overall isentropic efficiencies and volumetric efficiencies of single-stage CO_2 compressor

Run No.	$\eta_{o,is}$	η_{vol}
1	0.6087	0.7966
2	0.6029	0.7906
3	0.6101	0.7784
4	0.6084	0.7962
5	0.5908	0.7656
6	0.6059	0.7892
7	0.614	0.7952
8	0.6005	0.7686
9	0.6137	0.7786
10	0.6082	0.7532
11	0.5745	0.7279
12	0.5656	0.7009

To demonstrate the performance of the gas cooler during the tests of the CO_2 based bread board ECU, the measured state points of test run No. 3 are depicted in a carbon dioxide pressure-enthalpy diagram in Figure 6.1. It can be seen that at the gas cooler outlet temperature (state point 5) is above 40 ºC, even though the outdoor room air temperature during this test was only 27.8 ºC. It is obvious that the gas cooler of the bread board ECU does not have enough surface area to cool the CO_2 to a temperature close to the outdoor room air temperature.

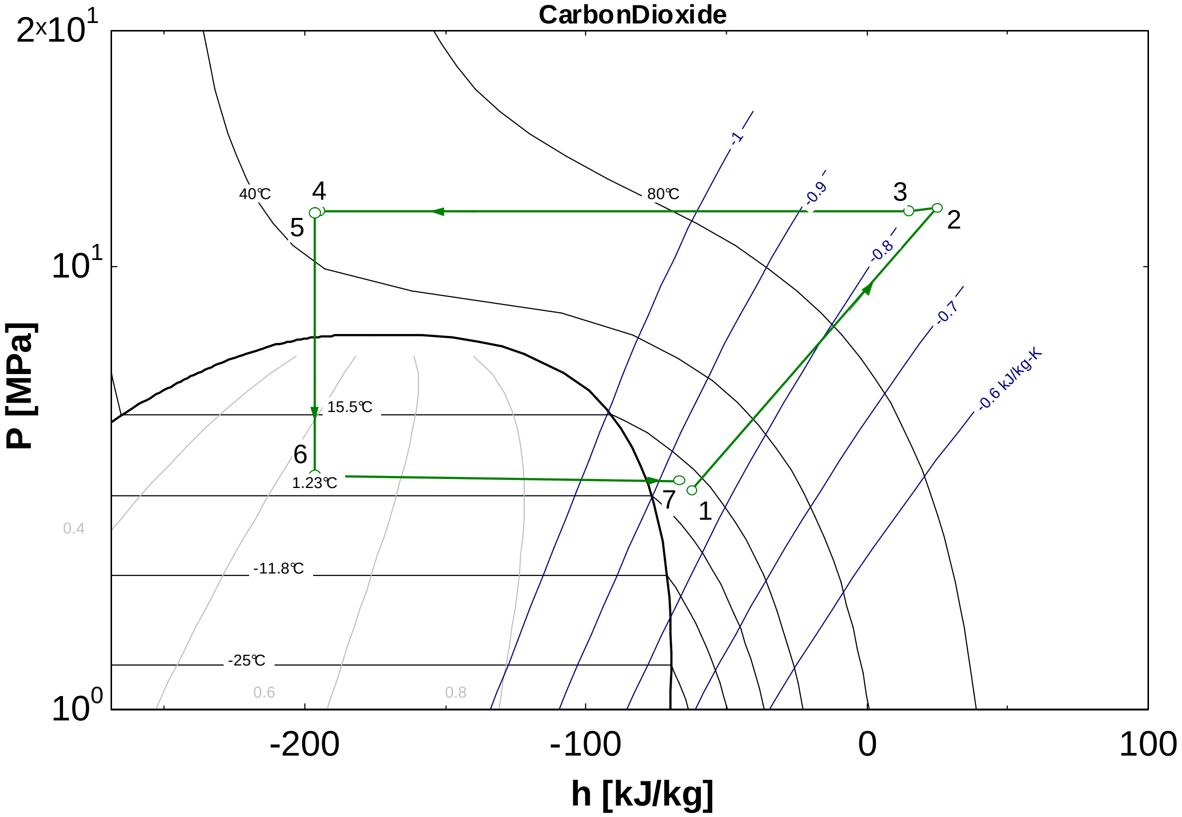

Figure 6.1: Measured state points of basic CO_2 bread board ECU in a pressure-enthalpy diagram (Test Run No. 3)

6.1.2. Model validation with CO_2 based bread board ECU test results

The test results of the basic CO_2 bread board ECU were used to validate predictions of the CO_2 air conditioning system simulation model. To validate the simulation model, the following parameters were used as the inputs to the simulation program:

- The measured compressor suction and discharge pressures.
- The measured air flow rate and air inlet temperature and humidity.
- The measured overall isentropic efficiency and volumetric efficiency of the compressors.

A comparison of the cooling COP and cooling capacity between the model predictions and the test results are shown in Figure 6.2 and Figure 6.3 respectively. It can be seen from Figure 6.2 and Figure 6.3 that the simulation model predicts the cooling COP and cooling capacity within ±10% of the measured data. It should be noted that the gas cooler air side heat transfer coefficient was adjusted with a tuning factor (0.35 to 0.7) during the simulation because the air flow path in the prototype gas cooler box is different to the standard cross flow pattern as required by the simulation program.

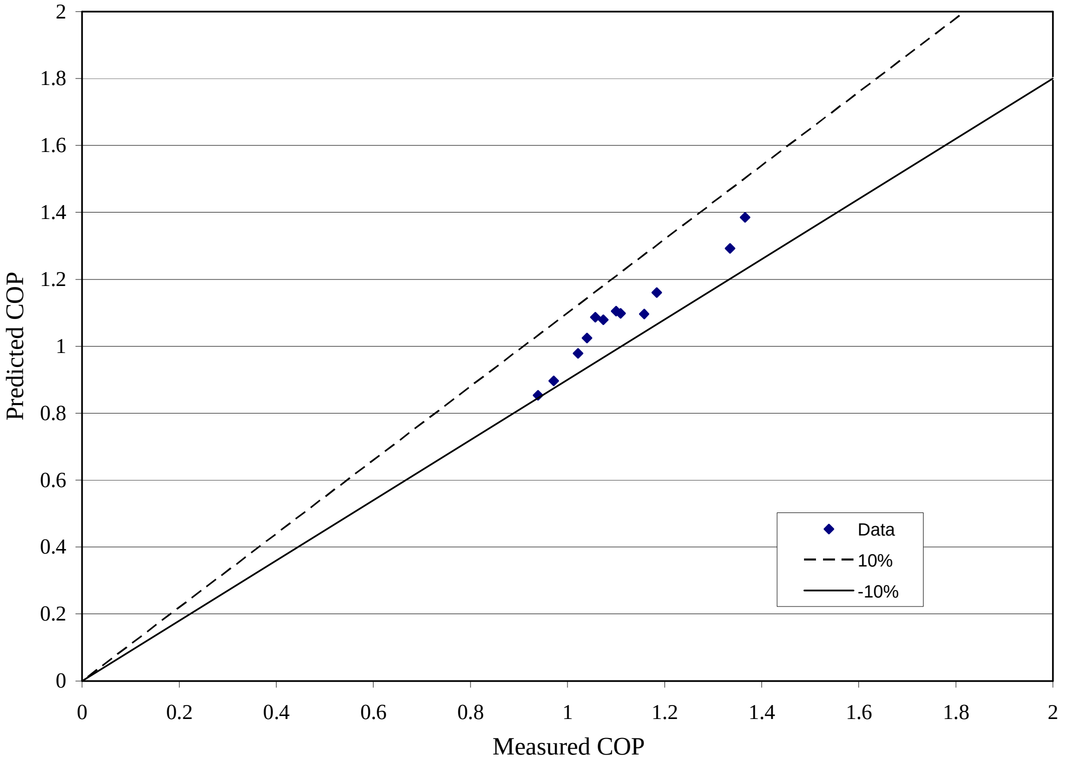

Figure 6.2: COP comparisons between simulation results and test results

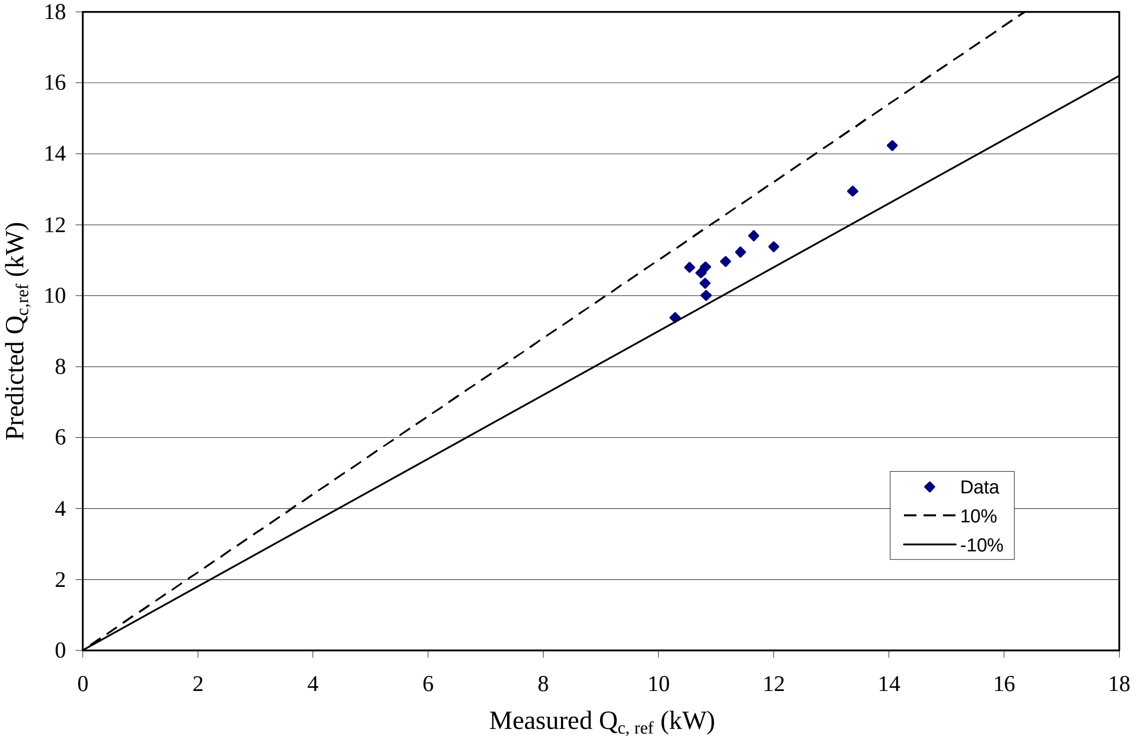

Figure 6.3: Cooling capacity comparisons between simulation results and test results

The statistical data of the deviations between the model predictions and the measured data for the basic transcritical CO_2 system is shown in Table 6.3. To further compare the simulation results and the test results, the measured and predicted state points of test run No. 3 are plotted in a pressure-enthalpy diagram of carbon dioxide for the single stage compression ECU as shown in Figure 6.4.

Table 6.3: Statistical data of deviation between the model predictions and the measured data for basic transcritical CO_2 system

Item	Mean Deviation	Standard Deviation	Maximum Deviation
COP (-)	3.11%	3.91%	7.4%
$\dot{Q}_{c,ref}$ (kW)	3.97%	3.71%	7.02%

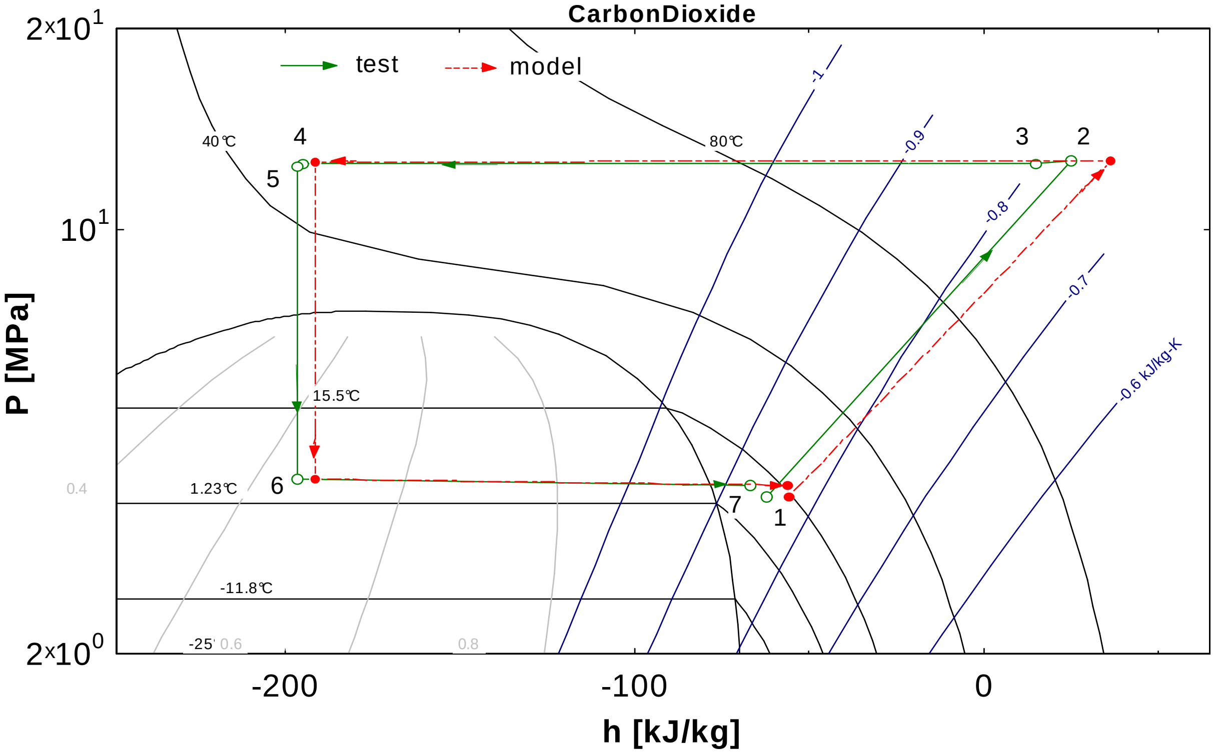

Figure 6.4: Measured and predicted state points of single-stage compression ECU (Test Run No. 3)

It can be seen from Figure 6.4 that the simulated cycle state points did not exactly match the measured state points. This is due to the fact that the pressure drop and heat transfer of all connection tubes between each component of the ECU are neglected during the simulation. In addition, the oil separator between the compressor outlet and the gas cooler inlet of the bread board ECU is not considered in the simulation. However, the deviations between the predicted state points and the measured state points did not significantly affect the predictions of the cooling capacity and cooling COP. This is because the effects of these deviations on the predictions of cooling capacity and cooling COP tend to cancel each other out. For example, based on the simulations, the predicted refrigerant enthalpy at the evaporator inlet is higher than the measured one. This leads to a higher predicted superheat at the evaporator outlet than the measured superheat. However, the simulated evaporator capacity still agrees with the measured evaporator capacity, since the capacity of the coil is mainly determined by the air side heat transfer. Even though the predicted refrigerant side parameters are not exactly the same as the measured ones, the model predicts a similar capacity as the measured capacity as long as air side parameters are kept the same.

It can also be seen from Figure 6.4 that the CO_2 gas cooler outlet temperature is approximately 46 ºC, which is significantly higher than the outdoor air temperature of 27.8 ºC. It indicates that the gas cooler of the bread board ECU is too small to cool the CO_2 to a temperature close to the outdoor air temperature.

6.2. Ejector expansion transcritical CO_2 air conditioning system model validation

The predictions of the ejector expansion transcritical air conditioning system model were validated using the ejector expansion CO_2 based ECU test results.

6.2.1. Ejector expansion CO_2 based ECU tests results

The ejector expansion CO_2 based ECU was tested according to the operation conditions specified in Appendix Table F.1. The indoor room conditions were controlled at 80 ºF (26.7 ºC) dry bulb temperature and 50% relative humidity and the outdoor room dry bulb temperature was changed from 82 ºF (27.8 ºC) to 95 ºF (35 ºC), to 100 ºF (37.8 ºC). In addition, test runs were conducted at an indoor temperature of 37ºF (2.8 ºC) with low indoor relative humidity of 5.39% to avoid frost formation and an outdoor temperature of 106ºF (41.1 ºC). At each set of indoor and outdoor room conditions, the high-side pressure was increased by adjusting the needle of the ejector to change the ejector throat area. Figure 6.5 presents the cooling COP of the CO_2 ejector expansion cycle as a function of the outdoor temperature. It can been seen from Figure 6.5 that generally the cooling COP of CO_2 ejector cycle decreases as the outdoor temperature increases. All experimental results of the ejector expansion CO2 system can be found in Appendix F.1.

6.2.2. Model validation with ejector expansion CO_2 based ECU test results

In order to validate the ejector expansion transcritical air conditioning system model, the isentropic efficiencies of the motive nozzle and suction nozzle as well as the mixing section efficiency were determined using the methods shown in Figures 5.19 to 5.23. Appendix Table F.2 lists the efficiencies determined by the measured parameters.

The ejector expansion CO_2 based ECU test results were used to validate the predictions by the ejector CO_2 air conditioning system simulation model. To validate the simulation model, the following parameters were used as the inputs to the simulation program:

- The measured compressor suction and discharge pressures.
- The measured air flow rate and air inlet temperature and humidity.

- The measured overall isentropic efficiency and volumetric efficiency of the compressors.
- The measured motive nozzle and suction nozzle isentropic efficiencies and the mixing section efficiency of the ejector.
- The ejector geometries (motive nozzle throat area, the diameter of mixing section and the diffuser outlet diameter).
- The CO_2 pressure at evaporator outlet.

The ejector-expansion CO_2 system was simulated with the same operating conditions and ejector geometries as those used during the 24 test runs. A comparison of the cooling COP and cooling capacity between the model predictions and the test results are shown in Figures 6.6 and 6.7 respectively. It can be seen from Figures 6.6 and 6.7 that the simulation model predicts the cooling COP within ±8% of the measured data and the cooling capacity within ±12% of the measured data. The statistical data of the deviations between the model predictions and the measured data for the ejector expansion transcritical CO_2 system is shown in Table 6.4.

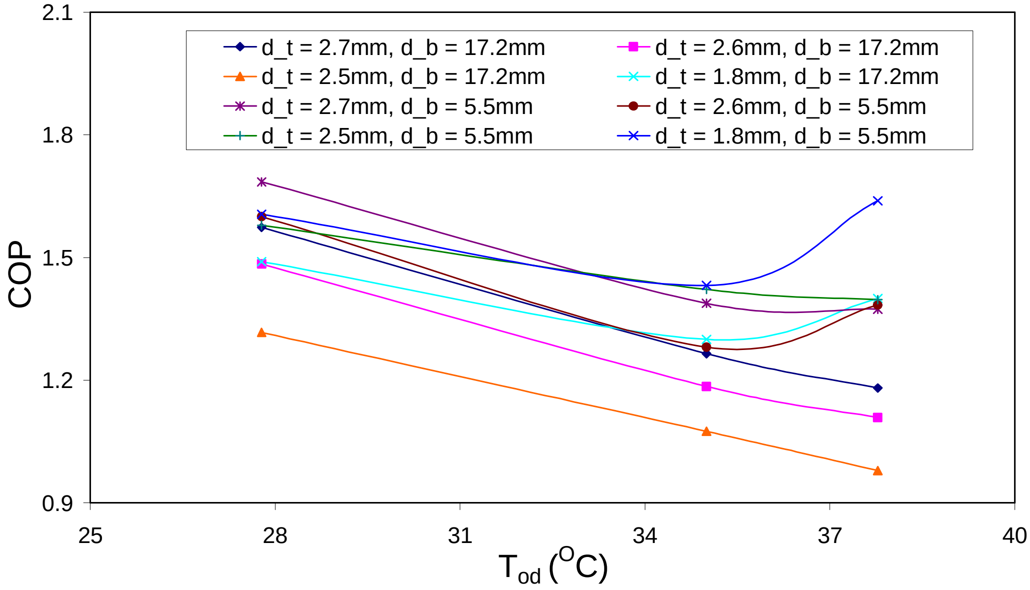

Figure 6.5: Cooling COP of CO_2 ejector expansion cycle versus outdoor temperature

Table 6.4: Statistical data of deviations between model predictions and measured data for ejector expansion transcritical CO_2 system

Item	Mean Deviation	Standard Deviation	Maximum Deviation
COP (-)	2.49%	3.14%	7.57%
$\dot{Q}_{c,ref}$ (kW)	3.32%	3.97%	11.23%

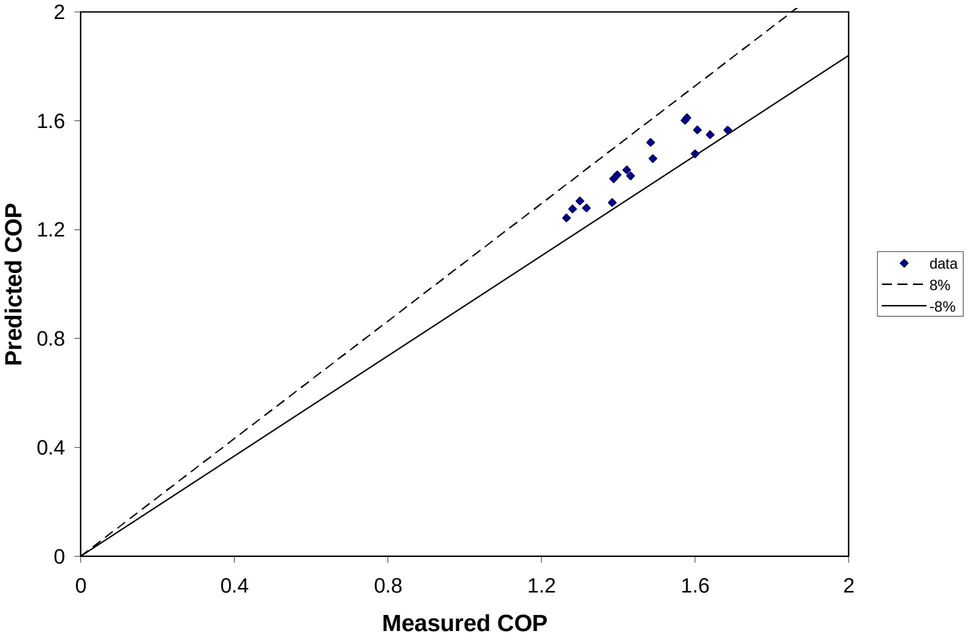

Figure 6.6: Predicted versus measured COP of CO_2 ejector cycle

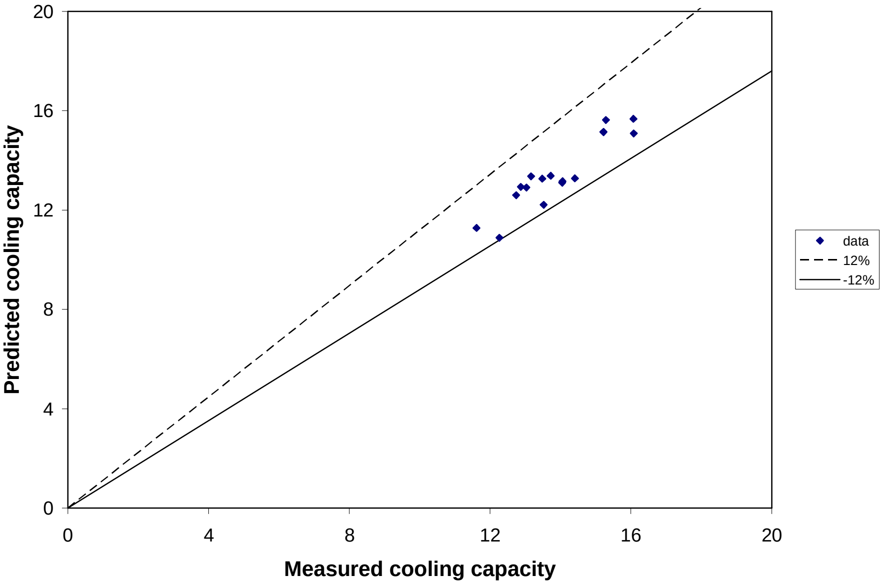

Figure 6.7: Predicted versus measured cooling capacity of CO_2 ejector cycle

To further compare the simulation results and the test results, the measured and predicted state points of test run No. 24 are plotted on a P-h diagram of carbon dioxide for the single stage compression ECU as shown in Figure 6.8. Table 6.5 lists the comparisons between the measured and predicted values of the COP, cooling capacity and compressor power consumption.

Table 6.5: Ejector expansion CO_2 cycle predicted results compared to test run No. 24 results

Test Run No. 24	COP	$\dot{Q}_{c,ref}$ (kW)	$\dot{W}_{comp}$ (kW)
Measurement	1.639	16.080	9.810
Predicted	1.549	15.086	9.738

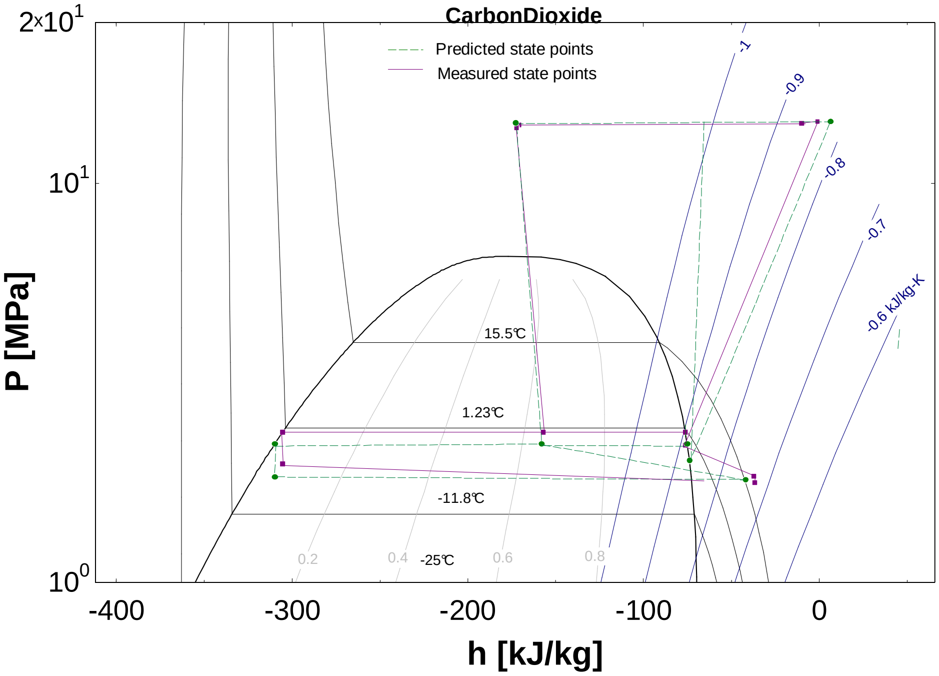

Figure 6.8: Measured and predicted state points of ejector expansion CO_2 transcritical ECU (Test run 24)

A comparison between the measured state points of the ejector expansion cycle (test run No. 3) and the predicted state points of the basic cycle is shown in Figure 6.9. It can be seen that the COP of the ejector cycle could be increased with a decrease of the pressure drop between the separator vapor outlet and the compressor inlet.

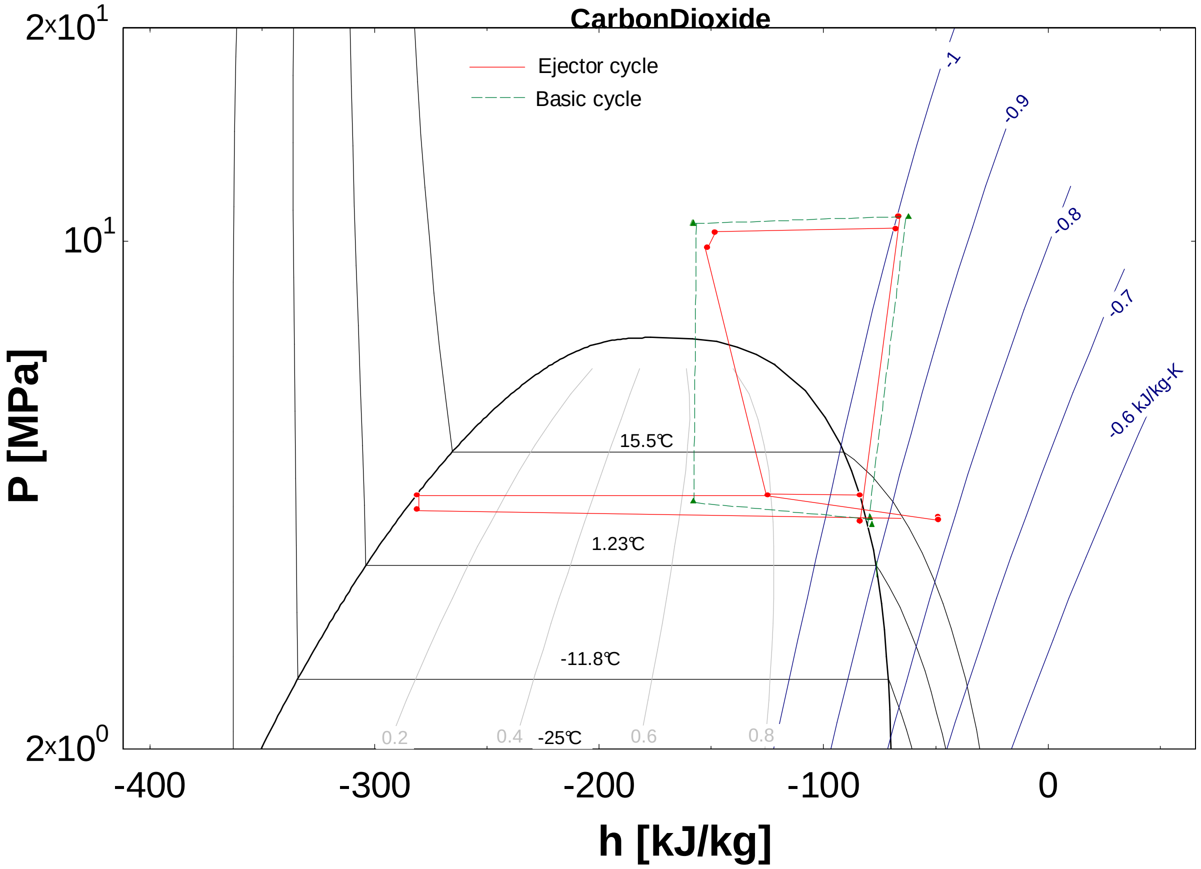

Figure 6.9: Comparison between measured state points of ejector cycle (test run No. 3) and predicted state points of basic cycle

6.4. Summary of validation

Experimental results were used to validate the existing transcritical CO_2 air conditioning system simulation model and the ejector expansion transcritical CO_2 air conditioning system simulation model. The transcritical CO_2 air conditioning system model predicts the cooling COP and cooling capacity with standard deviations of ±3.91% and ±3.71% of the measured results, respectively. The measured COP ranges from 0.854 to 1.385 at outdoor temperatures from 27.8 °C (82 °F) to 40.6 °C (106 °F) and an indoor temperature of 26.7 °C (80 °F). The ejector expansion transcritical CO_2 air conditioning system model predicts the cooling COP with a standard deviation of ±3.14% and the cooling capacity with a standard deviation of ±3.97% using the experimentally determined motive nozzle isentropic efficiency, suction nozzle isentropic efficiency, and mixing section efficiency. The measured COP ranges from 1.066 to 1.685 at outdoor temperatures from 27.8 °C (82 °F) to 37.8 °C (100 °F) and an indoor temperature of 26.7 °C (80 °F). Generally the cooling COP of CO_2 ejector cycle decreases as the outdoor temperature increases.

7. R410A EJECTOR EXPANSION SUBCRITICAL SYSTEM MODEL

R410A is one of the most widely used HFCs as a replacement of CFCs and HCFCs for air conditioning and refrigeration systems. R410A is a near-azeotropic mixture of R32 and R125 (fifty-fifty mass percent) and has a superior COP to CO_2 in cooling mode, especially on hot days. Table 7.1 lists the critical temperature and pressure of R410A and CO_2. R410A will benefit from the use of a two-phase ejector because it operates in the proximity of the critical point. However, few literature studies have been found to date that investigate the ejector expansion R410A sub-critical cycle.

Table 7.1: Comparison of the critical temperature and pressure between R410A and CO_2

	CO_2	R410A
Critical Temperature (°C)	31.05	72.0
Critical Pressure (bar)	73.865	47.7

7.1. Overview of ACMODEL

A detailed ejector expansion transcritical refrigeration system simulation model has been developed to predict the performance of ejector expansion air to air vapor compression systems with R410A as the refrigerant. The model is based on ACMODEL. ACMODEL is a very detailed simulation model to predict the performance of single stage heat pumps and air conditioning units. It was initially developed by Rossi (1995). Since then, the thermal systems research group at Ray W. Herrick Laboratories has been working on its further development to make it more accurate in performance predictions and more flexible for the user. ACMODEL is applicable for system simulation as well as for heat exchanger design. Currently it is able to model three refrigerants, namely R22, R410A and R407 but further refrigerants can be added. The major features, modeling approaches, and assumptions are:

- ACMODEL predicts the performance of single-stage vapor compression system using any arbitrary heat exchangers configuration. In addition, the latest version of ACMODEL can be used to analyze heat exchanger designs and optimize their geometry, materials, and heat transfer characteristics.
- ACMODEL is applicable for three different refrigerants, namely R22, R410A, and R407C using properties from REFPROP 7.0.
- ACMODEL can handle additional refrigerants using lookup tables and cubic spline interpolations.
- All model parameters and inputs are provided using batch files.
- ACMODEL has an extremely modular structure. The program code is separated into independent subroutines.
- ACMODEL has a robust equation solver. It uses Newton's method with damping to solve nonlinear equations. The structure of the component models is designed so that a large range of initial guesses can lead to reasonable outputs. Newton's method may have problems in cases of drastic derivatives. For vapor compression systems, when two-phase flow enters a fixed-area expansion device or a compressor, the refrigerant mass flow rate changes

significantly with the inlet quality. Special numerical techniques have been implemented in ACMODEL to deal with these cases.

- ACMODEL uses the ARI compressor map to predict mass flow rate and power consumption considering the suction density correction, as necessary.

ACMODEL has been extensively validated and successfully used in several projects. In particular, ACMODEL has been used extensively in ASHRAE 859-RP and ASHRAE 1173-RP, which were conducted by the PI. Within these projects, the model was verified with the experimental data of units ranging from 2.5-ton to 7.5-ton and using refrigerants R-22, R-410A, and R-407C. Several references can be found in literature for a detailed description of ACMODEL and of the experimental work (Shen et al. 2003, Harms et al. 2003, and Shen et al. 2004). The simulation model represents an advanced approach for a first order thermodynamic analysis of unitary heat pump systems.

7.2. R410A ejector subcritical model

The two-phase flow ejector model developed for the CO_2 transcritical cycle was modified to be incorporated into the subcritical R410A system model. In contrast to CO_2, R410A enters the motive nozzle of the ejector at sub-critical pressure and temperature and expands into the sub-critical two-phase region in the motive nozzle. It is assumed that the flow becomes critical at the exit. The iteration procedure for the simulation of the R410A motive nozzle is depicted in the flow chart in Figure 7.1. The suction nozzle flow model, mixing section flow model, and diffuser flow model for the subcritical R410A ejector in the ejector expansion vapor compression system are the same as the models used for the transcritical CO_2 ejector in the ejector expansion CO_2 system.

7.3. R410A ejector expansion vapor compression system model

A hermetically sealed reciprocating compressor model is used in the R410A ejector expansion vapor compression system model (ejector expansion ACMODEL). The flow chart in Figure 7.2 shows the system logic of ejector expansion ACMODEL.

The root search starts with four initial guesses of suction pressure P_1, discharge pressure P_2 and evaporator outlet pressure P_{10} and ejection ratio φ. The compressor model uses the guesses of P_1 and P_2 to calculate the refrigerant mass flow rate m_{comp}, power consumption, and exit enthalpy of the compressor h_2. Afterwards, the discharge line, the condenser, and the liquid line models are solved one by one, and the predicted degree of subcooling upstream of the expansion device $Tsub_{cal}$ is obtained. The predicted degree of subcooling is compared to a user-specified subcooling degree $Tsub_{speci}$ to get the first residual. With the guess of φ, the predicted suction stream mass flow rate φm_{comp} is calculated. The motive stream inlet pressure P_5, enthalpy h_5 and mass flow rate m_{comp} obtained from the liquid line model together with suction nozzle inlet pressure P_{10} and mass flow rate φm_{comp} are input into the ejector model. Then the separator model is solved. The predicted ejection ratio φ_{cal} obtained from separator model is compared to the guessed value φ to get the second residual.

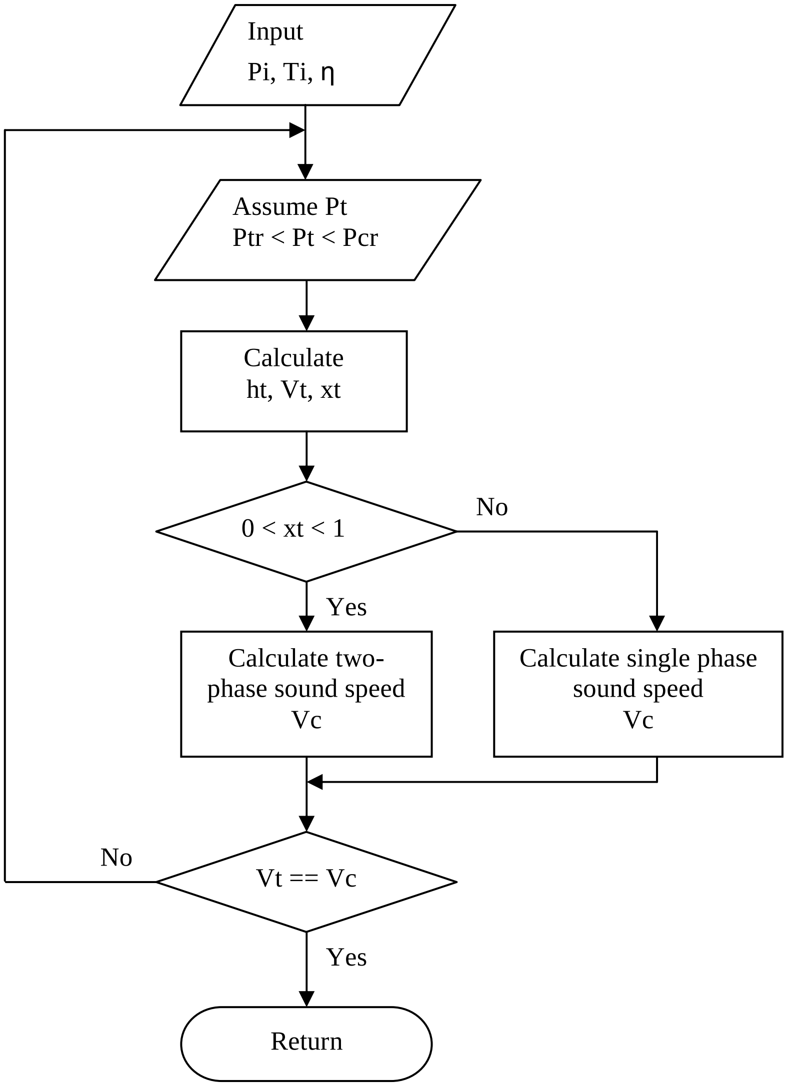

Figure 7. 1: Flow chart of motive nozzle simulation
(for subcritical ejector model)

Afterwards, the calculations continue in two directions. On the vapor side, by comparing the new evaporator exit enthalpy h_{8b} to the suction line model predicted evaporator exit enthalpy h_{8a}, the third residual is obtained. On the liquid side, with the evaporator entrance obtained from the separator liquid side as h_{11} and the evaporator exit pressure obtained from the suction line model as P_{10}, another evaporator exit enthalpy h_{10cal} is obtained from running the evaporator model. The predicted enthalpy of h_{10cal} is compared to a user specified enthalpy $h_{10speci}$ to get the forth residual. Eventually, there are four residuals, the residual between the predicted subcooling

$Tsub_{cal}$ and the specified subcooling $Tsub_{speci}$, the residual between the separator model predicted separator exit enthalpy h_{8b} and the suction line model predicted separator exit enthalpy h_{8a}, the residual between the evaporator model predicted evaporator exit enthalpy h_{10cal} and the specified evaporator exit enthalpy $h_{10speci}$, and the residual between the predicted ejection ratio φ_{cal} and the specified ejection ratio φ. Using the fourth residuals, the initial guess φ is updated until the residual is within the desired tolerance. Then using these first three residuals and Newton's method, the initial guesses are updated until the overall residual is within the desired tolerance.

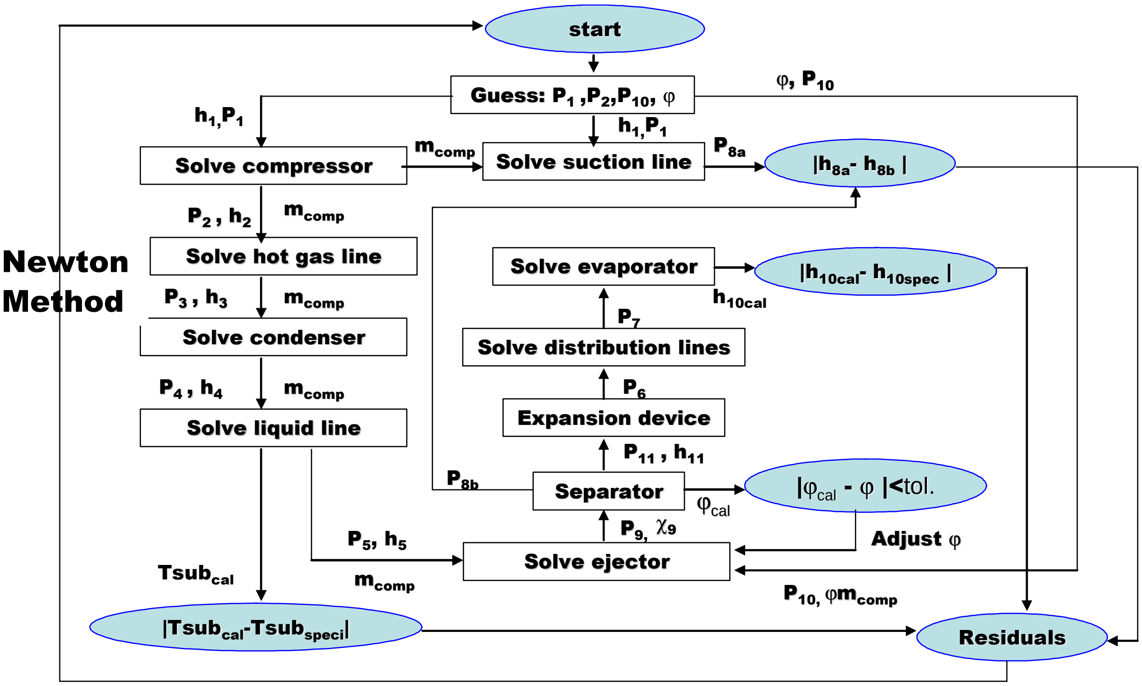

Figure 7.2: System logic of ejector expansion ACMODEL

7.4. R410A ejector modeling results

The effects of the ejector geometries on the ejector performance are shown in Figures 7.3 to 7.5. It can be seen from Figure 7.3 that the flow pressure and quality at diffuser outlet reach the maximum and minimum, respectively, at d_t of 1.8 mm, which mean that the ejector performance is optimal at this d_t value for the given operating conditions. Figure 7.4 shows that the flow pressure at the diffuser outlet first increases quickly with an increase of the mixing section diameter, and then increases slowly. The reversed behavior can be seen for the flow quality at the diffuser outlet. Figure 7.5 shows that the flow pressure at the diffuser outlet first increases quickly with an increase of the diffuser outlet diameter and then increases slowly. The reversed behavior can be seen for the flow quality at diffuser outlet. However, the flow pressure and the quality at diffuser outlet vary unnoticeably with an increase of diffuser outlet diameter.

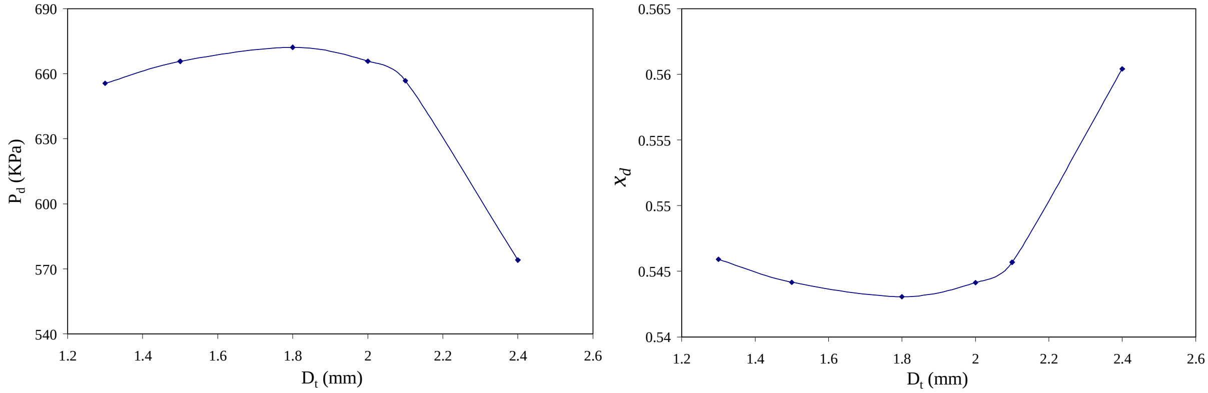

Figure 7.3: Ejector discharge pressure and quality versus motive nozzle throat diameter (P_m = 2220 kPa, T_m =50°C (122 °F), P_s = 598 kPa, T_s = -8.7°C (16.3 °F), D_{mix} = 6 mm, D_d = 1.5 mm)

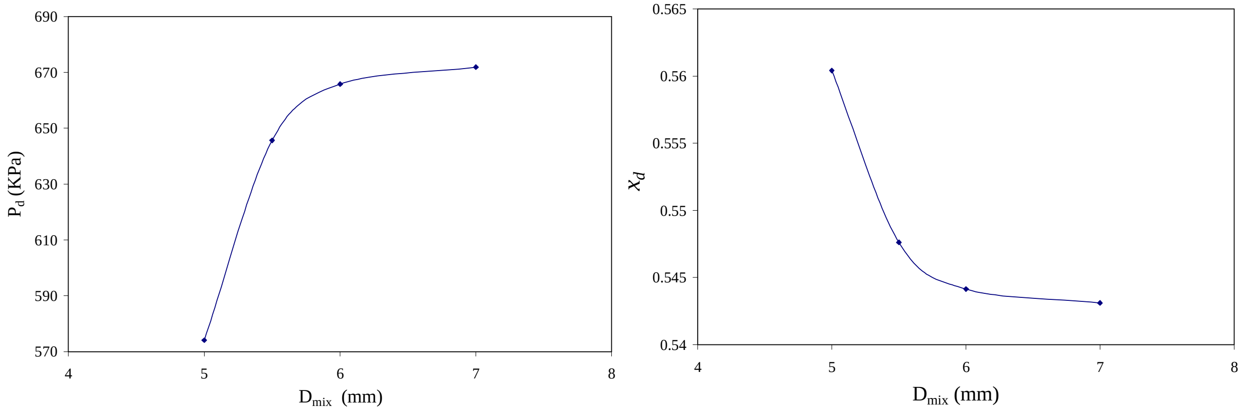

Figure 7.4: Ejector discharge pressure and quality versus mixing section diameter (P_m = 2220 kPa, T_m =50°C (122 °F), P_s = 598 kPa, T_s = -8.7°C (16.3 °F), D_t = 2 mm, D_d = 1.2 mm)

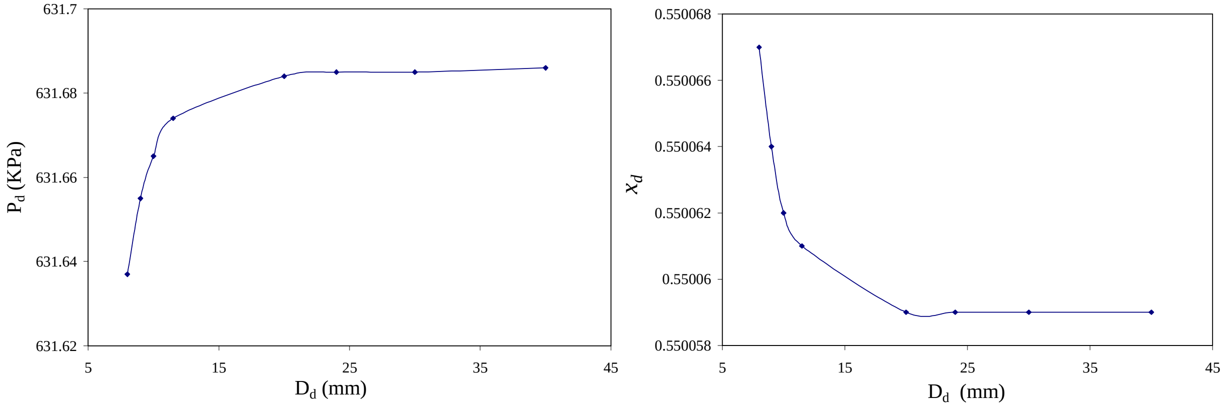

Figure 7.5: Ejector discharge pressure and quality versus diffuser exit diameter (P_m = 2220 kPa, T_m =50°C (122 °F), P_s = 598 kPa, T_s = -8.7°C (16.3 °F), D_t = 3 mm, D_{mix} = 8 mm)

7.5. R410A ejector cycle modeling results

The state points of basic vapor compression cycle and ejector-expansion vapor compression cycle are depicted in a pressure-enthaply diagram of R410A in Figure 7.6. The efficiencies of the motive nozzle, suction nozzle and mixing section are assumed to be 0.90, 0.80 and 0.80 respectively. Table 7.2 shows the heat exchanger specifications of the R410A gas cooler and evaporator models.

Table 7.2: Heat exchanger specifications of R410A gas cooler and evaporator models

Simulated CO_2 microchannel heat exchanger (Finned-tube)	gas cooler	evaporator
Total area air flows through entire coil (m^2)	1.0393	0.2962
Fin thickness (mm)	0.1143	0.1143
Fin height (mm)	0.201	0.201
Tube thickness (mm)	0.29972	0.31242
Tube inside diameter (mm)	6.93928	6.91896

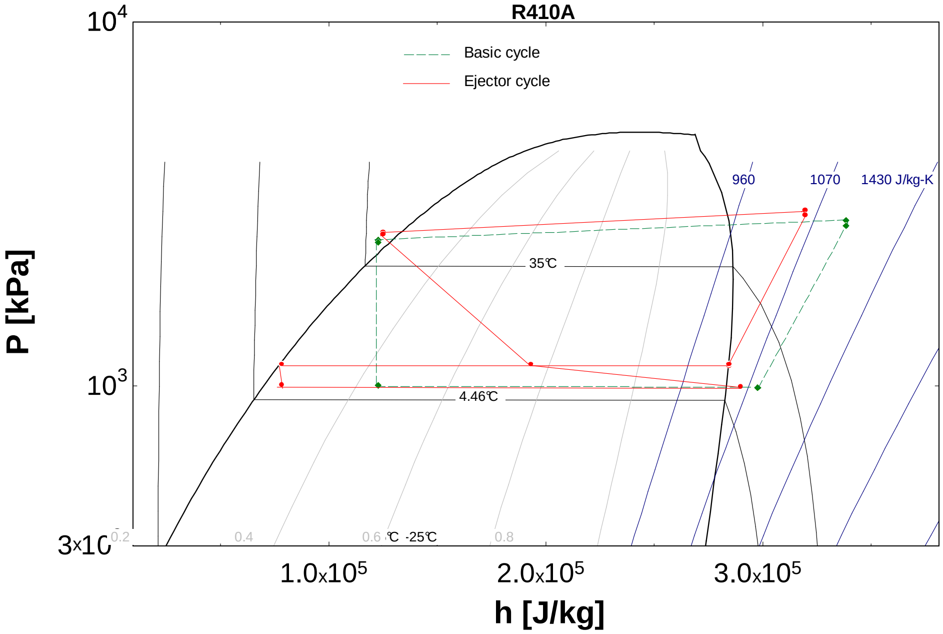

Figure 7.6: State points of R410A cycle based systems with and without ejector expansion (T_{id} = 26.7 °C (80 °F), T_{od} = 35 °C (95 °F) and P_{dis} = 11 MPa)

Figure 7.6 shows that when an ejector is used to replace the expansion valve in a R410A vapor compression cycle, the expansion work lost during the isenthalpic expansion will be recovered by the ejector to increase the evaporator outlet pressure to a higher pressure before the compressor. Due to the reduced pressure ratio across the compressor, the compression work will be reduced, which increases the COP of the system. The flow quality of the R410A at the evaporator inlet of the ejector cycle is lower than that of the basic cycle. Therefore, the cooling capacity of the ejector-expansion R410A cycle is higher than that of basic cycle at the same evaporation pressure, which also results in higher COP of the ejector cycle than that of the basic cycle as shown in Table 7.3. The COP and cooling capacity of the ejector expansion R410A based system are approximately 11.1% and 19.8% higher, respectively, than the ones of the basic R410A system.

Table 7.3: Comparison of cooling COP, cooling capacity, and compressor power between R410A basic cycle and ejector cycle (T_{id} = 26.7 °C (80 °F), RH_{id} = 50%, T_{od} = 35 °C (95 °F))

Type of cycle	COP [-]	$\dot{Q}_{eva,ref}$ [W]	Compressor Power [W]
Basic cycle (1’-2’-3’-4’-1’)	4.307	19385	4501
Ejector cycle (1-2-3-4-5-6-7-8):	4.786	23222	4852

8. PARAMETRIC STUDIES WITH SIMULATION MODELS

The validated ejector expansion transcritical CO_2 air conditioning system model was modified by adding the empirical equations of the ejector efficiencies and the compressor map into this model. This modified model was then used to investigate the COP and cooling capacity of the ejector cycle with different geometries under various operation conditions.

8.1. Empirical equations for the ejector efficiencies

In order to investigate the effects of the operation conditions and ejector geometries on the ejector efficiencies, the correlations of the ejector efficiencies as a function of pressure ratio, mass flow rate ratio, and throat diameter ratio were developed. Empirical equations (8.1) (8.2) and (8.3) express the motive nozzle efficiency η_m, the suction nozzle efficiency η_s and the mixing section efficiency η_{mix} as the functions of ejector geometry, pressure ratio and ejection ratio, respectively. The correlation for the motive nozzle efficiency is a function of the pressure ratio between the motive nozzle inlet and the suction nozzle inlet, as well as the diameter ratio between the ejector throat and the mixing section. The correlation for the suction nozzle efficiency is a function of the pressure ratio between the motive nozzle inlet and the suction nozzle inlet, as well as the ejection ratio. The correlation for the mixing section efficiency is a function of the ejection ratio and the diameter ratio between the ejector throat and the mixing section.

$$\begin{aligned}\eta_m &= -36.1367305 - 4.15962963\left(\frac{P_m}{P_s}\right) + 1.16131867\left(\frac{P_m}{P_s}\right)^2 - 0.106090279\left(\frac{P_m}{P_s}\right)^3 \\ &+212.320405\left(\frac{d_t}{d_{mix}}\right) - 355.359177\left(\frac{d_t}{d_{mix}}\right)^2 + 196.035242\left(\frac{d_t}{d_{mix}}\right)^3\end{aligned} \tag{8.1}$$

$$\begin{aligned}\eta_s &= -3173.171 + 934.102\left(\frac{P_m}{P_s}\right) - 314.4712\left(\frac{P_m}{P_s}\right)^2 + 79.52134\left(\frac{P_m}{P_s}\right)^3 - 12.22236\left(\frac{P_m}{P_s}\right)^4 \\ &+0.814459\left(\frac{P_m}{P_s}\right)^5 + 694222.1\varphi - 2956145\varphi^2 + 7950453\varphi^3 - 114327270\varphi^4 + 6689155\varphi^5 \\ &-649905.1Z + 2647000Z^2 - 6885025Z^3 + 9627161Z^4 - 5490126Z^5 \left(Z = \varphi\left(\frac{P_m}{P_s}\right)^{0.02}\right)\end{aligned} \tag{8.2}$$

$$\eta_{mix} = -6869.077 + 19308.18Z' - 18089.31Z'^2 + 5649.417Z'^3 \quad \left(Z' = \left(\frac{d_t}{d_{mix}}\right)^{0.1}(1+\varphi)^{0.35}\right) \tag{8.3}$$

The predicted ejector efficiencies were calculated using the above empirical equations and compared with the ejector efficiencies that were backed out from the test data using the ejector simulation model. The results of these comparisons are shown in Figures 8.1 to 8.3. The empirical equations can predict the ejector efficiencies within 5% standard error. The nozzle efficiencies and mixing section efficiency at values of 0.5 and below are low due to the effects of ejector geometries.

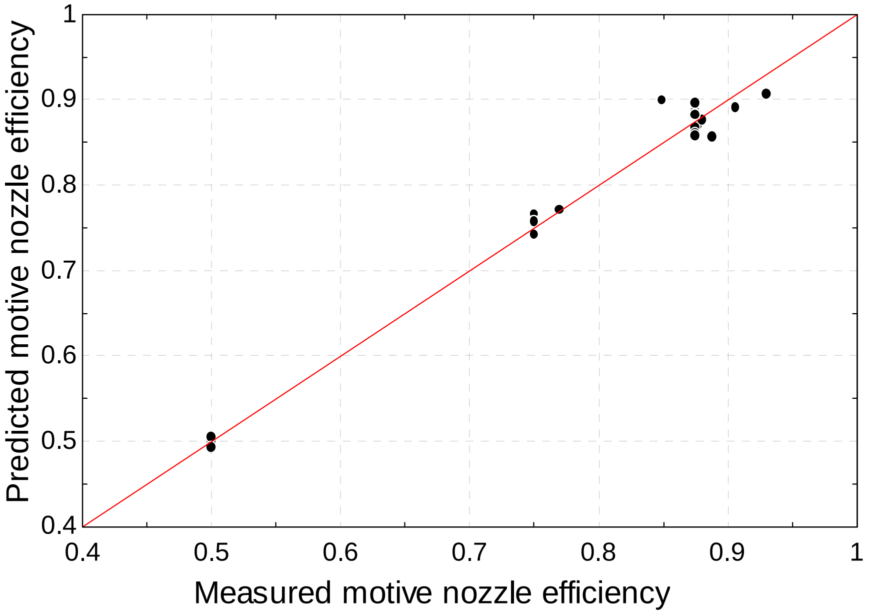

Figure 8.1: Predicted versus measured motive nozzle efficiency (R^2 = 98.95%)

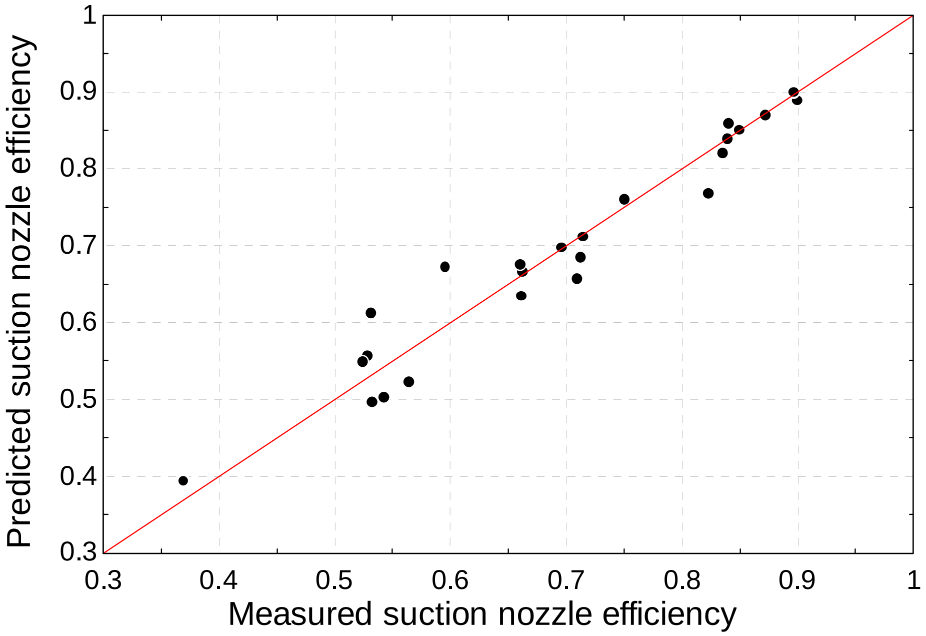

Figure 8.2: Predicted versus measured suction nozzle efficiency (R^2 = 93.79%)

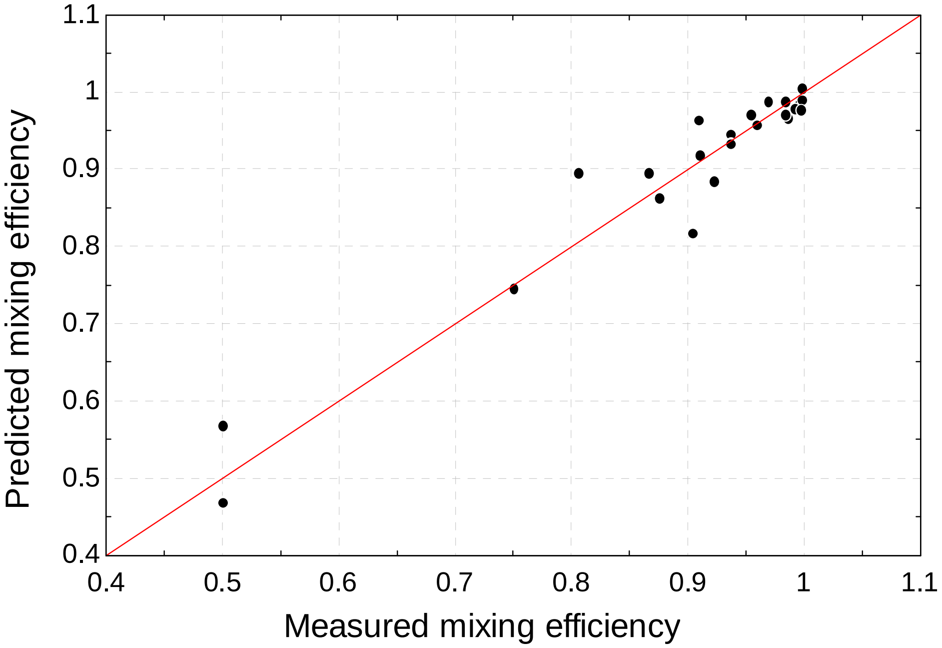

Figure 8.3: Predicted versus measured mixing efficiency ($R^2 = 93.52\%$)

8.2. Ejector expansion transcritical CO_2 system parametric study

The validated transcritical CO_2 air conditioning system simulation model were used to study the effects of the ejector geometries (throat diameter and mixing section diameter) on the performance of an ejector expansion transcritical CO_2 system. The assumed ejector efficiencies η_m, η_s and η_{mix} presented in Section 4.6 were replaced by the calculated η_m, η_s and η_{mix} using the empirical equations (8.1) (8.2) and (8.3), respectively.

Figures 8.4 and 8.5 show that the cooling COP and cooling capacity increase as the motive nozzle throat diameter D_t increases at T_{od} = 82 °F (27.8 °C), 90 °F (32.2 °C), 100 °F (37.8°C) at a mixing section diameter D_{mix} = 4 mm and a diffuser exit diameter D_d = 12 mm. The ejector cycle cannot operate at a nozzle throat diameter D_t larger than 2.9 mm because of the limitations of the motive nozzle efficiency at this assumed operation conditions. Figures 8.6 and 8.7 show that the cooling COP and cooling capacity reach maximum values at a mixing section diameter D_{mix} equal to 4.27 mm, 4.155 mm and 4.1 mm at outdoor temperatures of T_{od} = 82 °F (27.8 °C), 90 °F (32.2 °C), 100 °F (37.8 °C), respectively, at a nozzle throat diameter D_t = 2.6 mm and a diffuser exit diameter D_d = 12 mm.

The predicted ejector nozzle and mixing section efficiencies that were used in simulation results shown in Figures 8.4 and 8.5 are presented in Table 8.1. The predicted ejector nozzle and mixing section efficiencies that were used in simulation results shown in Figures 8.6 and 8.7 are presented in Table 8.2.

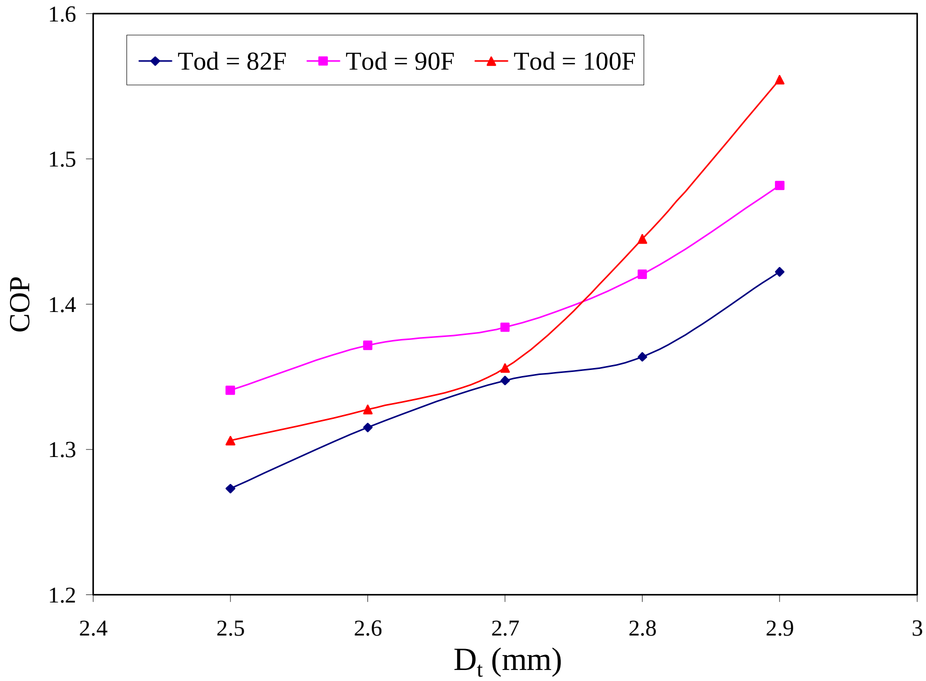

Figure 8.4: Cooling COP versus ejector throat diameter at different outdoor temperature (T_{id} = 80 °F (26.7 °C), P_{dis} = 8 MPa, D_{mix} = 4 mm, D_d = 12 mm)

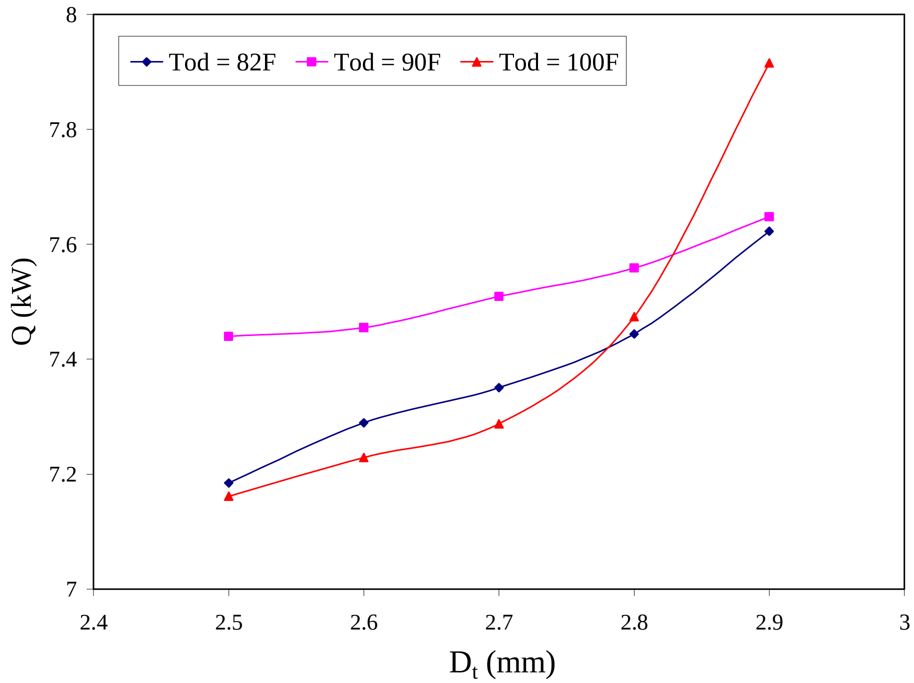

Figure 8.5: Cooling capacities versus ejector throat diameter at different outdoor temperature (T_{id} = 80 °F (26.7°C), P_{dis} = 8 MPa, D_{mix} = 4 mm, D_d = 12 mm)

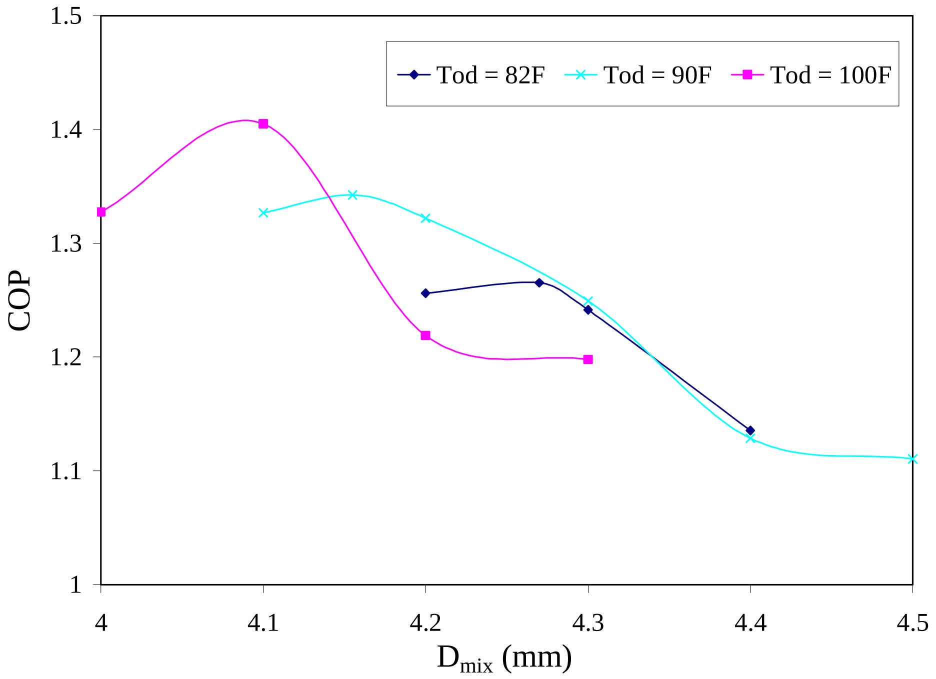

Figure 8.6: Cooling COP versus ejector mixing section diameter at different outdoor temperature (T_{id} = 80 °F (26.7 °C), P_{dis} = 8 MPa, D_t = 2.6 mm, D_d = 12 mm)

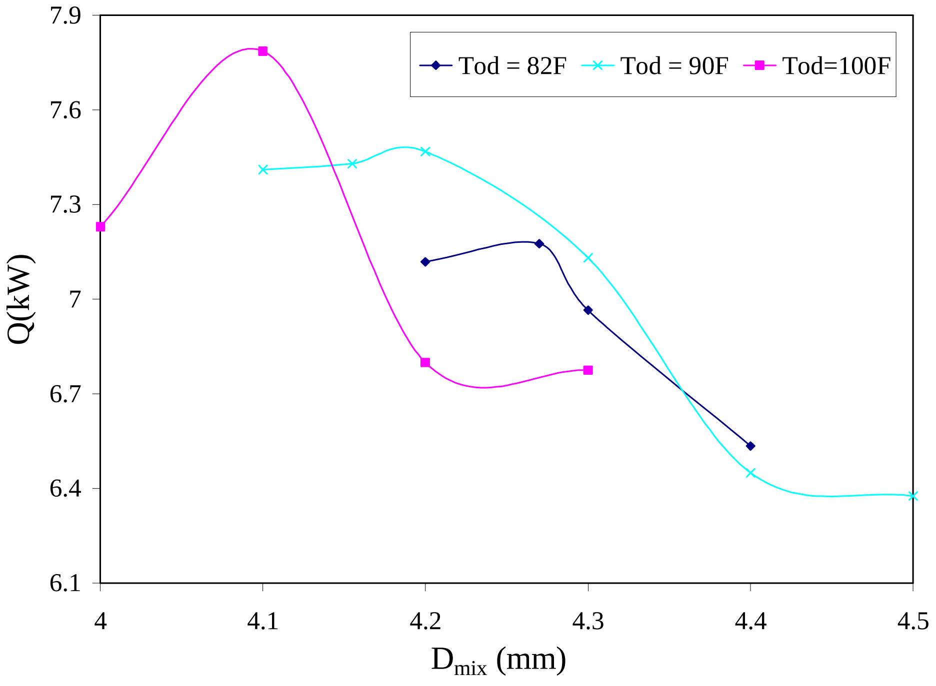

Figure 8.7: Cooling capacities versus ejector mixing section diameter at different outdoor temperature (T_{id} = 80 °F (26.7 °C), P_{dis} = 8 MPa, D_t = 2.6 mm, D_d = 12 mm)

Table 8.1: Ejector efficiencies for data points shown in Figures 8.4 and 8.5 calculated by using the ejector cycle model (T_{id} = 80 °F (26.7 °C), P_{dis} = 8 MPa, D_{mix} = 4 mm, D_d = 12 mm)

T_{od} (°F)	d_t (mm)	η_m	η_s	η_{mix}
82	2.5	0.961	0.561	0.768
82	2.6	0.920	0.569	0.828
82	2.7	0.910	0.584	0.860
82	2.8	0.956	0.584	0.902
82	2.9	0.984	0.582	0.931
90	2.5	0.965	0.563	0.768
90	2.6	0.923	0.576	0.819
90	2.7	0.915	0.584	0.856
90	2.8	0.961	0.575	0.889
90	2.9	0.987	0.551	0.918
100	2.5	0.966	0.584	0.720
100	2.6	0.925	0.579	0.779
100	2.7	0.918	0.555	0.826
100	2.8	0.964	0.516	0.868
100	2.9	0.994	0.510	0.910

Table 8.2: Ejector efficiencies for data points shown in Figures 8.6 and 8.7 calculated by using the ejector cycle model (T_{id} = 80 °F (26.7 °C), P_{dis} = 8 MPa, D_t = 2.6 mm, D_d = 12 mm)

T_{od} (°F)	D_m (mm)	η_m	η_s	η_{mix}
82	4.20	0.973	0.546	0.771
82	4.27	0.996	0.535	0.765
82	4.30	0.987	0.537	0.739
82	4.40	0.999	0.538	0.680
90	4.1	0.946	0.563	0.795
90	4.155	0.963	0.552	0.786
90	4.2	0.977	0.544	0.782
90	4.3	0.990	0.542	0.733
90	4.4	0.983	0.552	0.651
100	4.0	0.925	0.579	0.779
100	4.1	0.952	0.566	0.795
100	4.2	0.976	0.583	0.705
100	4.3	0.990	0.569	0.682

8.3. Performance comparison of transcritical CO_2 air conditioning system with and without ejector

A comparison of the cooling COP and cooling capacity between the test results of the ejector expansion transcritical CO_2 cycle and the model predictions of the basic cycle at the same external operating conditions are shown in Figure 8.8 and Figure 8.9, respectively. Considering that the gas cooler of the bread board ECU does not have enough surface area to cool the CO_2 to a temperature close to the outdoor room air temperature, the outdoor temperature of the CO_2 system was not set too high because the quality of the flow at the ejector exit increases as the temperature at the motive nozzle inlet increases as shown in Figure 3.13, which will cause less liquid flow through the evaporator. The ejector nozzle and mixing section efficiencies that were determined from the experiments for each test run of the ejector expansion transcritical CO_2 cycle are listed in Table F.2 in the Appendix.

It can be seen from Figures 8.8 and 8.9 that with an increase of the outdoor temperature, the cooling COP ratio and the cooling capacity ratio increase, which means that the ejector increases the CO_2 system performance more significantly at higher outdoor temperatures. The highest predicted improvements in cooling COP and cooling capacity were found to be 38.3% and 40.8%, respectively, at an outdoor temperature of 37.8 °C (100.0 °F), an indoor temperature of 26.7 °C (80.0 °F), and an indoor relative humidity of 50%. If the pressure drop between the separator gas outlet and compressor inlet is decreased, a further increase in cooling COP and cooling capacity can be obtained in the ejector expansion CO_2 system because of more compressor power saved. Figure 8.10 shows that a low ejection ratio is not desirable in the CO_2 system although a low ejection ratio is desirable for the performance of the ejector as a stand-alone device.

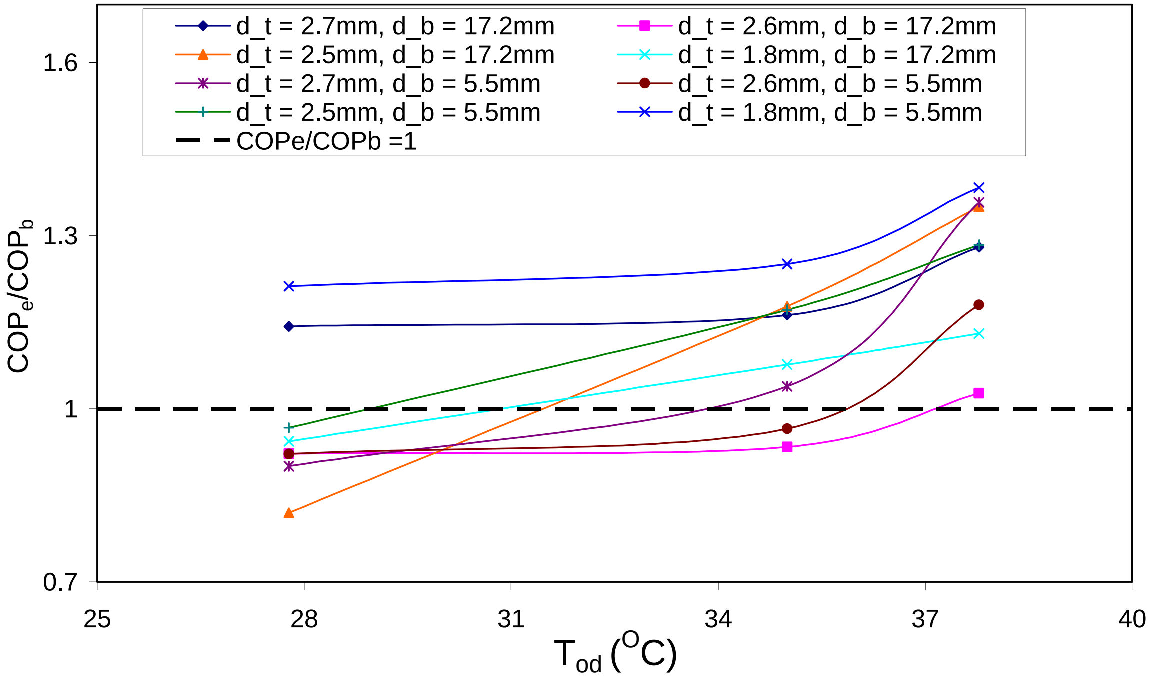

Figure 8.8: Cooling COP ratio between ejector cycle and basic cycle versus outdoor temperature

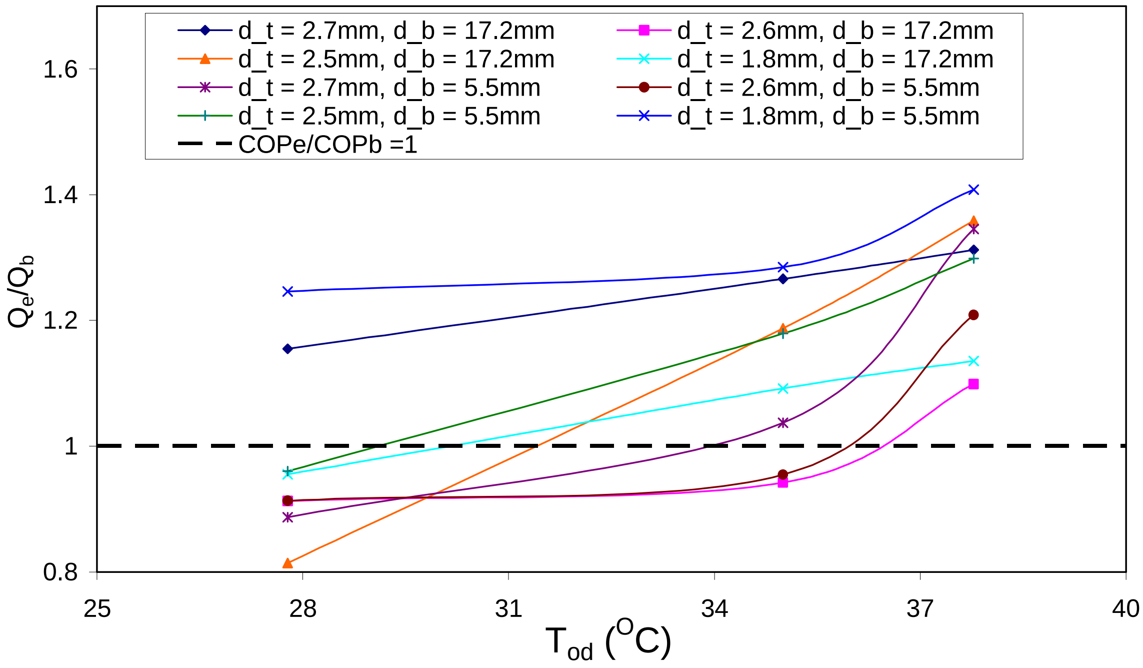

Figure 8.9: Cooling capacity ratio between ejector cycle and basic cycle versus outdoor temperature

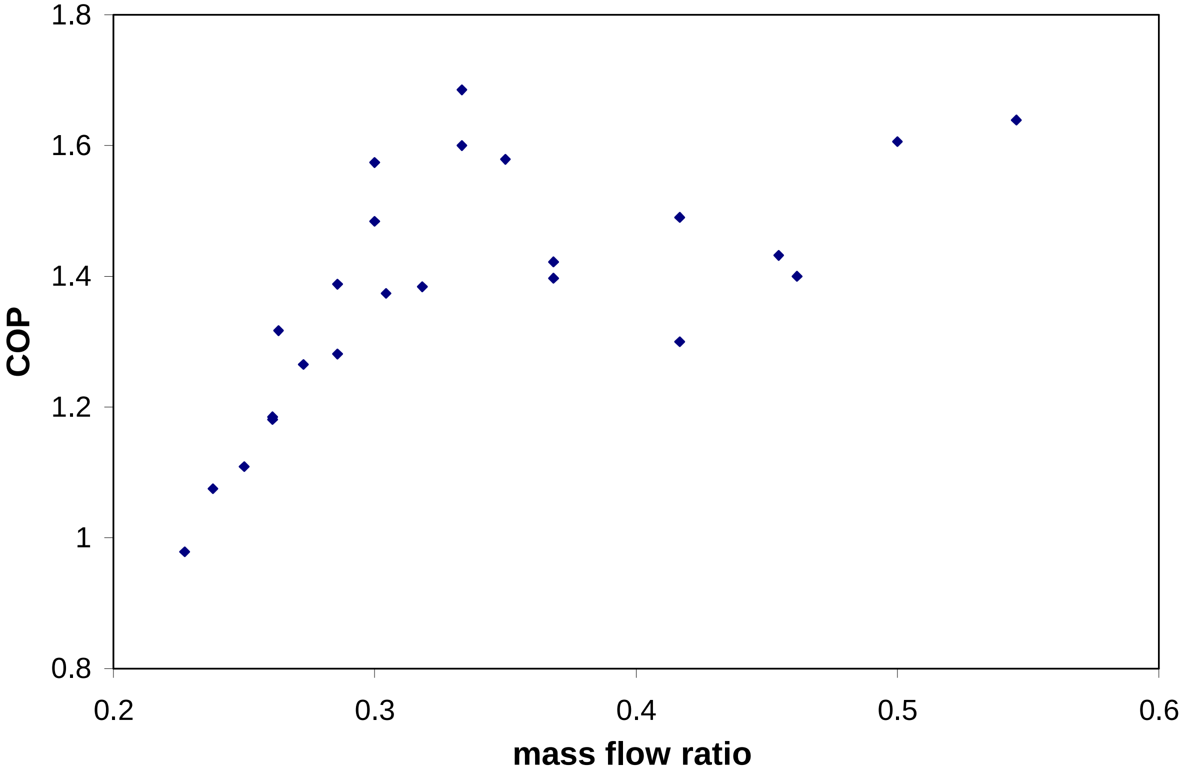

Figure 8.10: Cooling COP of CO_2 system versus mass flow ratio

8.4. Ejector expansion R410A vapor compression system parametric study

The cooling COP and cooling capacity of the R410A systems with and without an ejector expansion device as functions of the outdoor temperature are shown in Figures 8.8 and 8.9. It can be seen from these figures that the cooling COP and the cooling capacity of both systems decrease as the outdoor temperature increases. In addition, it can be seen from Table 8.3 that the increase in cooling COP and the cooling capacity of the ejector expansion R410A system compared to the basic R410A system can reach 17.9% and 20.8% respectively in the range of outdoor temperature from 27.9 °C (82.2 °F) to 50.9 °C (123.6 °F) with indoor temperature 26.9 °C (80.4 °F).

Table 8.3: Improvement in cooling COP and cooling capacity of R410A cycle with two-phase flow ejector (T_{id} = 26.9 °C (80.4 °F), RH_{id} = 50.8%; $\eta_m = 0.95$, $\eta_s = 0.85$, $\eta_{mix} = 0.90$; D_t = 5.8 mm, D_{mix} = 9.7 mm, D_d = 20.0 mm)

T_{od}	27.9°C	32.9°C	40.9°C	45.9°C	50.9°C
COP_e / COP_b	1.153	1.147	1.179	1.131	1.160
Q_e / Q_b	1.124	1.109	1.184	1.166	1.208

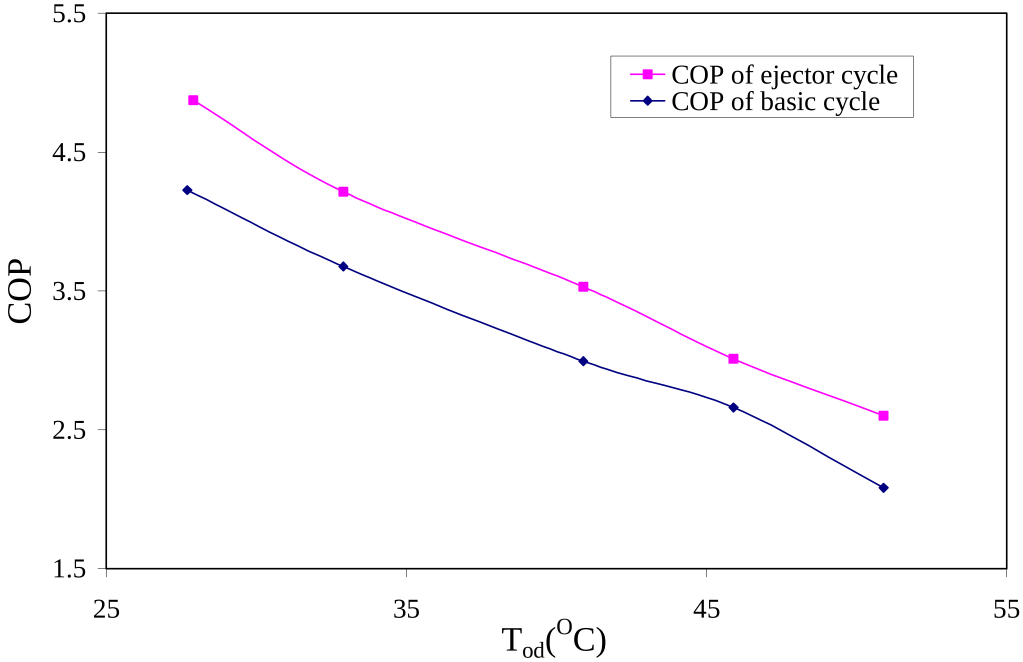

Figure 8.11: Cooling COP of R410A systems versus outdoor temperature (T_{id} = 26.9 °C; $\eta_m = 0.95$, $\eta_s = 0.85$, $\eta_{mix} = 0.90$; D_t = 5.8 mm, D_{mix} = 9.7 mm, D_d = 20.0 mm)

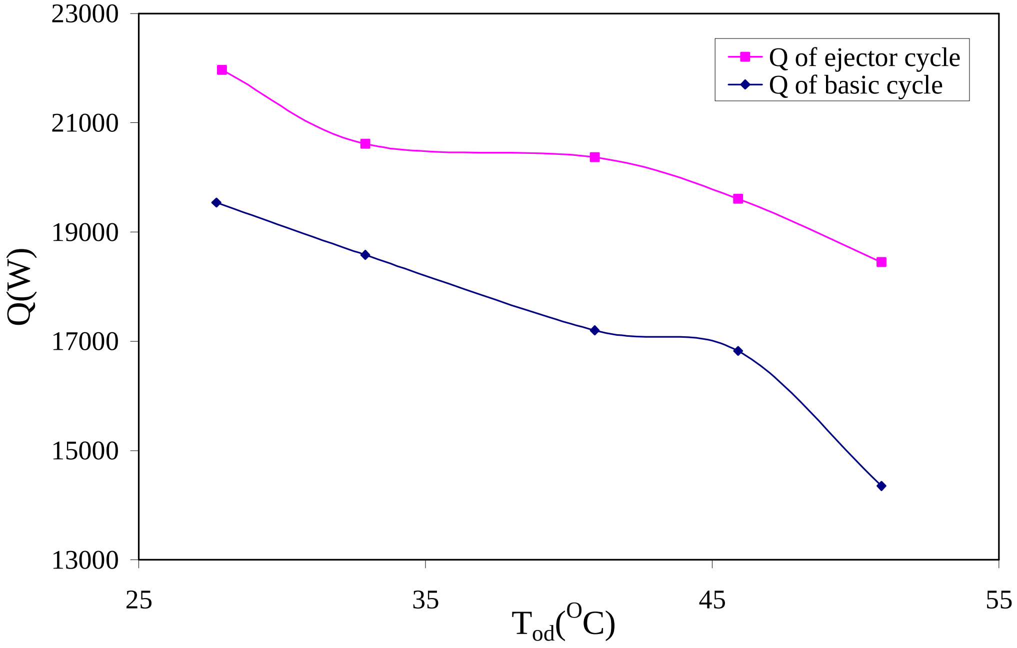

Figure 8.12: Cooling capacities of R410A systems versus outdoor temperature
(T_{id} = 26.9 °C; $\eta_m = 0.95$, $\eta_s = 0.85$, $\eta_{mix} = 0.90$; D_t = 5.8 mm, D_{mix} = 9.7 mm, D_d = 20.0 mm)

8.5 Discussion of simulation results

Empirical equations of the ejector efficiencies were developed using the experimental data. Based on the parametric studies shown in this chapter, it can be concluded that the cooling COP and the cooling capacity of the ejector expansion CO_2 air conditioning system vary with the variations of the throat diameter, the mixing section diameter and the outdoor temperature. A comparison of the cooling COP and cooling capacity between the ejector expansion cycle and the basic cycle showed that the ejector expansion device increases the performance of the CO_2 system more significantly as the outdoor temperature increases. The highest predicted improvements in cooling COP and cooling capacity were found to be 38.3% and 40.8%, respectively, at an outdoor temperature of 37.8 °C (100.0 °F), an indoor temperature of 26.7 °C (80.0 °F), and an indoor relative humidity of 50.0%. The cooling COP and cooling capacity of the ejector expansion R410A air conditioning system decrease with an increase of the outdoor temperature. An ejector expansion device improves the performance of the subcritical R410A air conditioning system significantly, especially at higher outdoor temperatures. The ejector expansion device increases the COP and cooling capacity of the subcritical R410A air conditioning system up to 17.9% and 20.8%, respectively, at an outdoor temperature of 40.9 °C (105.6 °F) and 50.9 °C (123.62 °F), an indoor temperature of 26.9 °C (80.4 °F), and an indoor relative humidity of 50.8%.

9. CONCLUSIONS AND RECOMENDATIONS

This study presented here included the following tasks: develop a two-phase flow ejector simulation model, develop an ejector expansion transcritical CO_2 system simulation model, validate the two-phase flow ejector simulation model with experimental results, validate the simulation model of the ejector expansion transcritical CO_2 system with experimental results, repeat the two-phase flow ejector model and system model development for R410A vapor compression systems and perform parametric studies with the ejector expansion transcritical CO_2 system and R410A vapor compression system simulation models.

A two-phase flow ejector simulation model was established, which consists of four sub-models for the motive nozzle flow, the suction nozzle flow, the mixing section flow, and the diffuser flow. The two-phase flow ejector model was incorporated into an existing transcritical CO_2 system simulation model and replaced the conventional expansion valve.

The existing transcritical CO_2 air conditioning system simulation model and the ejector expansion transcritical CO_2 system simulation model were validated using experimental results. Based on the given accuracy of the various measurement instrumentations, the refrigerant-side cooling capacity and cooling COP of the transcritical CO_2 air conditioning system can both be measured within ±5%. The motive nozzle and suction nozzle efficiencies and mixing section efficiency were determined within ±6%. In addition, both the refrigerant-side cooling capacity and cooling COP of the ejector expansion CO_2 system were determined within ±3%. The validations of the two models showed that the transcritical CO_2 air conditioning system model predicts the cooling COP and cooling capacity with standard deviations of ±3.91% and ±3.71% of the measured results, respectively. The ejector expansion transcritical CO_2 air conditioning system model predicts the cooling COP with a standard deviation of ±3.14% and cooling capacity with a standard deviation of ±3.97% using the experimentally determined motive nozzle isentropic efficiency, suction nozzle isentropic efficiency, and mixing section efficiency.

The ejector expansion sub-critical R410A vapor compression system simulation was developed by incorporating the modified two-phase flow ejector model into an existing R410A air conditioning system simulation model, called ACMODEL. The ejector expansion R410A system simulation model was exercised to predict the performance of an R410A air conditioning system with an ejector expansion device.

Empirical equations of the ejector efficiencies were developed using the experimental data. Based on the parametric studies, it was found that the cooling COP and the cooling capacity of the ejector expansion CO_2 air conditioning system vary with the variations of the throat diameter, the mixing section diameter and the outdoor temperature. A comparison of the cooling COP and cooling capacity between the ejector expansion cycle and the basic cycle showed that the ejector expansion device increases the performance of the CO_2 system more significantly as the outdoor temperature increases although generally the cooling COP of the ejector expansion CO_2 system deceases as the outdoor temperature increases. The highest predicted improvements in cooling COP and cooling capacity were found to be 38.3% and 40.8%, respectively, at an outdoor temperature of 37.8°C (100 °F), an indoor temperature of 26.7 °C (80.0 °F), and an indoor relative humidity of 50.0%.

The cooling COP and cooling capacity of the ejector expansion R410A air conditioning system decrease with an increase of the outdoor temperature. An ejector expansion device improves the performance of the subscritical R410A air conditioning system significantly, especially at higher outdoor temperatures. The ejector expansion device increases the COP and cooling capacity of the subcritical R410A air conditioning system by 17.9% and 18.4%, respectively, at an outdoor temperature of 40.9 °C (105.6 °F), an indoor temperature of 26.9 °C (80.4 °F), and an indoor relative humidity of 50.8%.

The COP improvement of the ejector expansion CO_2 system obtained in this study is greater than those found by other researchers, e.g., the COP of the basic CO_2 system improved by 7% in the study by Elbel and Hrnjak (2007) and by 20% in the study by Ozaki et al. (2004) using an ejector. One of the reasons is that optimal ejector geometries were adopted when the ejector was designed, such as the throat area, mixing section, diffuser diameter ratio and the distance from the motive nozzle exit to the mixing section constant area inlet. Another reason is the fact that the measured COP and cooling capacity of the ejector expansion system were compared with the modeling results of the basic system. There are some uncertainties associated with the modeling results. The model of the basic CO_2 system predicts the COP and cooling capacity within ±10% of the measured values. Finally, the experimental system chosen for the comparison is a military standard environmental control unit. The COP of the basic transcritical CO_2 system is poor, primarily due to very high approach temperatures between the gas cooler CO_2 outlet temperature and the air inlet temperature. The potential to improve the COP of this cycle by using an ejector is much greater than if the basic cycle would be optimized for this application.

The following recommendations are made for the future research regarding ejector expansion transcritical air conditioning systems:

- validate the two-phase flow ejector and the ejector expansion R410A air conditioning system simulation model using experimental results,
- develop empirical correlations for the R410A ejector efficiencies based on the experimental results, and
- develop a controllable ejector expansion device in which the throat area is adjustable by a needle as a function of the operation conditions and geometries to achieve optimum system performance.

REFERENCES

Adachi, Y., Kazuo, K., Masahiro, I., 1999, "Vapor Compression Type Refrigerator," *Japan Patent No. JP2000241033.*

Alexis, G.K., Rogdakis, E.D., 2003, "A Verification Study of Steam-Ejector Refrigeration Model," *Applied Thermal Engineering,* Vol. 23, pp. 29-36.

Attou, A., Seynhaeve, J.M., 1999, "Steady-State Critical Two-Phase Flashing Flow with Possible Multiple Choking Phenomenon, Part 1: Physical Modelling and Numerical Procedure," *Journal of Loss Prevention in the Process Industries,* Vol. 12, pp. 335-345.

Baek, J., Groll, E.A., Lawless, P., 2002, "Development of a Piston-Cylinder Expansion Device for the Transcritical Carbon Dioxide Cycle," *Proceedings of the International Refrigeration and Air Conditioning Conference at Purdue,* Purdue University, USA, pp. 457-466.

Bergander, M. J., 2006, "Refrigeration Cycle with Two-phase Condensing Ejector," *Proceeding of International Refrigeration and Air Conditioning Conference at Purdue*, Purdue University, USA, Paper No. R008.

Bouré, J.A., Fritte, A., Giot, M., Réocreux, M., 1976, "Highlights of Two-Phase Critical Flow: on the Links Between Maximum Flow Rates, Sonic Velocities, Propagation and Transfer Phenomena in Single and Two-Phase Flows," *International Journal of Multiphase Flow,* Vol. 13, pp. 1-22.

Braun, J.E., Klein, S.A., Mitchell, J.W., 1989, "Effectiveness Models for Cooling Towers and Cooling Coils," *ASHRAE Transactions*, Vol. 95, Part 2, pp. 164-174.

Braun, J.E., Groll, E.A., Klein, S.A., 1999, "Modeling and Design of Vapor Compression Systems Short Course," Ray W. Herrick Laboratories, Purdue University, West Lafayette, IN, Lecture 19, June 1-4.

Brown, J.S., Kim, Y., and Domanski, P.A., 2002, "Evaluation of Carbon Dioxide as R-22 Substitute for Residential Air-Conditioning," *ASHRAE Transactions,* Vol. 108, Part 2, pp. 954-964.

Chang, Y.J., Wang, C.C., Chang, W.J., 1994, "Heat Transfer and Flow Characteristics of Automotive Brazed Aluminum Heat Exchangers," *ASHRAE Transactions,* Vol. 100, pp. 643-652.

Chunnanond, K., Aphornratana, S., 2004, "Ejectors: Applications in Refrigeration Technology," *Renewable and Sustainable Energy Reviews,* Vol. 8, pp. 129-155.

Cizungu, K., Groll, M., Ling, Z.G., 2005, "Modelling and Optimization of Two-phase Ejectors for Cooling Systems," *Applied Thermal Engineering,* Vol. 25, pp. 1979-1994.

Cunningham, R.G., 1974, "Gas Compression with the Liquid Jet Pump," *Journal of Fluids Engineering,* Vol. 96, pp. 203-215.

Cunningham, R.G., Dopkin, R.J., 1974, “Jet Breakup and Mixing Throat Lengths for the Liquid Jet Gas Pump,” *Journal of Fluids Engineering,* Vol. 96, pp. 216-226.

Cunningham, R.G., 1995, “Liquid Jet Pumps for Two-Phase Flows,” *Journal of Fluids Engineering,* Vol. 117, pp.309-316.

Dabiri, A.E., Rice, C.K., 1981, “A Compressor simulation model with corrections for the level of suction gas superheat”, ASHARE Transactions, 87(2), pp. 771-780.

Deberne, N., Leone, J.F., Duque, A., Lallemand, A., 1999, “A Model for Calculation of Steam Injector Performance,” *International Journal of Multiphase Flow,* Vol. 25, pp. 841-855.

Deng, J., Jiang, P., Lu, T., Lu, W., 2007, “Particular Characteristics of Transcritical CO_2 Refrigeration Cycle with an Ejector,” *Applied Thermal Engineering*, Vol. 27, pp. 381-388.

Domanski, P. A., 1995, “Minimizing Throttling Losses in the Refrigeration Cycle,” *Proceedings of 19th International Congress of Refrigeration*, Vol. 1Vb, pp. 766-773.

Elbel, S.W., Hrnjak, P.S., 2004, “Effects of Internal Heat Exchanger on Performance of Transcritical CO_2 Systems with Ejector,” *Proceedings of 10th International Refrigeration and Air Conditioning Conference at Purdue,* Purdue University, USA, Paper No. R166.

Elbel S. and Hrnjak P., 2008, “experimental validation of a prototype ejector designed to reduce throttling losses encountered in transcritical R744 system operation”, *International Journal of Refrigeration,* vol. 31, pp. 411-422.

Elias, B. K., 2007, “Study and design of systems with improved energy efficiency operating with CO_2 as refrigerant,” Ph.D. Thesis, Ecole de Mines, Paris, France

Elliott, D.G., 1985, “Two-Phase Nozzle Flow Computation with Prescribed Shape,” *ASME Fluids Engineering Division FED,* Vol. 23, pp. 124-127.

Fischer, H.K., Rice, C.K., 1983, “The Oak Ridge Heat Pump Model: I. A Steady-State Computer Design Model for Air-to-Air Heat Pumps,” *Technical Report,* Oak Ridge National Laboratory.

Gay, N.H., 1931, “Refrigerating System,” *U.S. Patent No. 1836318.*

Ginzburg, YA. L., Idel′chik, I. YE., 1975, “Experimental Determination of Pressure Recovery Coefficients in Conical Diffusers at High Subsonic Velocities and Various Inlet Conditions,” *Fluid Mechanics – Soviet Research,* Vol. 4(3), pp. 59-67.

Harrell, G.S., Kornhauser, A.A., 1995, “Performance Tests of a Two Phase Ejector,” *Proceedings of the Intersociety Energy Conversion Engineering Conference*, Orlando, FL., Vol. 3, pp. 49-53.

Heidelck, R., Kruse, H., 2000, “Expansion Machines for Carbon Dioxide Based on Modified Reciprocating Machines,” *4th IIR-Gustav Lorentzen Conference on Natural Working Fluids at Purdue,* Purdue University, USA, pp. 455-462.

Henry, R.E., Fauske, H.K., 1971, "The Two-Phase Critical Flow of One-Component Mixtures in Nozzles, Orifices, and Short Tubes," *Journal of Heat Transfer,* Vol. 95, pp. 179-187.

Hesse, U., Tiedemann, T., 1999, "Klimaanlage für Kraftfahrzeuge," *German Patent No. DE19959439.*

Hesse, U., 2000, "Klimaanlage, insbesondere für Kraftfahrzeuge und Verfahren zum Betreiben einer Klimannlage, insbesondere für Kraftfahrzeuge," *German Patent No. DE10013191.*

Heyl, P., Kraus, W.E., and Quack, H., 1998, "Expander-Compressor for a More Efficient Use of CO_2 as Refrigerant," *Natural Working Fluids; IIR-Gustav Lorentzen Conference*, Oslo, Norway, pp. 240-248.

Huang, B.J., Chang, J.M., Wang, C.P., Petrenko, V.A., 1999, "A 1-D Analysis of Ejector Performance," *International Journal of Refrigeration,* Vol. 22, pp. 354-364.

Hubacher, B., Groll, E.A., 2002, "Measurement of Performance of Carbon Dioxide Compressors," *Final Report (ARTI Project 611-10070), Herrick Labs 2002-24, Report No. 0140-1.* Ray W. Herrick Laboratories, Purdue University, West Lafayette, IN.

Ishikawa, K., Nakamura, I, 1990, "Performance Chart and Optimum Geometries of Conical Diffusers with Uniform Inlet Flow and Tailpipe Discharge," *JSME International Journal*, Vol. 33(1), pp. 97-105.

Jeong, J., Saito, K., Kawai, S., Yoshikawa, C., Hattori, K., 2004, "Efficiency Enhancement of Vapor Compression Refrigerator Using Natural Working Fluids with Two-phase Flow Ejector," *Proceedings 6th IIR-Gustav Lorentzen Conference on Natural Working Fluids at Glasgow*, Glasgow, UK.

Kandlikar, S.G., 1990, "A General Correlation for Saturated Two-Phase Flow Boiling Heat Transfer Inside Horizontal and Vertical Tubes," *Journal of Heat Transfer,* Vol. 112, pp. 219-228.

Katto, Y., 1968, "Dynamics of Compressible Saturated Two-Phase Flow (Critical Flow)," *Bulletin of Japanese Society of Mechanical Engineers,* Vol. 11, pp. 1135.

Katto, Y., 1969, "Dynamics of Compressible Saturated Two-Phase Flow (Critical Flow-Sequel, and Flow in a Pipe)," *Bulletin of Japanese Society of Mechanical Engineers,* Vol. 12, pp. 1417.

Keenan, J. H., Neumann, E. P., 1942, "A Simple Air Ejector", *Journal of Applied Mechanics*, Vol. 64, pp. A75-A84.

Keenan, J. H., Neumann, E. P., Lustwerk, F., 1950, "An Investigation of Ejector Design by Analysis and Experiment", *Journal of Applied Mechanics*, Vol. 17, pp. 299-809.

Kemper, G.A., Harper, G.F., Brown, G.A., 1966, "Multiple Phase Ejector Refrigeration System," *U.S. Patent No. 3277660.*

Kim, M.H., Pettersen, J., Bullard, C.W., 2004, “Fundamental Process and System Design Issues in CO_2 Vapor Compression Systems,” *Progress in Energy and Combustion Science*, Vol. 30, pp.119-174.

Klein, S.A., 2004, “Engineering Equation Solver,” *F-Chart Software.*

Kornhauser, A.A., 1990, “The Use of an Ejector as a Refrigerant Expander,” *Proceedings of the 1990 USNC/IIR – Purdue Refrigeration Conference*, Purdue University, USA, pp. 10-19.

Ksayer, E. B., Clodic, D., 2006, “Enhancement of CO_2 Refrigeration Cycle Using an Ejector: 1D analysis,” *Proceeding of International Refrigeration and Air Conditioning Conference at Purdue*, Purdue University, USA, Paper No. R058.

Kuraeva, I. V., Protopopov, V.S., 1974, “Mean Friction Coefficients for Turbulent Flow of a Liquid at a Supercritical Pressure in Horizontal Circular Tubes,” *High Temperature*, Vol. 12, No. 1, pp. 194-196.

Lear, W.E., Sherif, S.A., Steadham, J.M., 2000, “Design Considerations of Jet Pumps with Supersonic Two-Phase Flow and Shocks for Refrigeration and Thermal Management Applications,” *International Journal of Energy Research*, Vol. 24, pp. 1373-1389.

Lear, W.E., Parker, G.M., Sherif, S.A., 2002, “Analysis of Two-Phase Ejectors with Fabri Choking,” *Journal of Mechanical Engineering Science*, Vol. 216, Part C, pp. 607-621.

Li, D., Baek, J.S., Groll, E.A., Lawless, P.B., 2000, “Thermodynamic Analysis of Vortex Tube and Work Output Expansion Devices for The Transcritical Carbon Dioxide Cycle,” *4th IIR-Gustav Lorentzen Conference on Natural Working Fluids at Purdue*, Purdue University, USA, pp. 433-440.

Li, D., Groll, E.A., 2005, “Transcritical CO_2 Refrigeration Cycle with Ejector-Expansion Device,” *International Journal of Refrigeration*, vol. 28, pp. 766-773.

Liu, J.P., Chen, J.P., Chen, Z.J., 2002, “Thermodynamic Analysis on Trans-Critical R744 Vapor-Compression/Ejection Hybrid Refrigeration Cycle,” *Proc. 5th IIR-Gustav Lorentzen Conference on Natural Working Fluids at Guangzhou*, Guangzhou, China, pp. 184-188.

Maurer, T., Zinn, T., 1999, “Untersuchung von Entspannungsmaschinen mit Mechanischer Leistungsauskopplung für die Transkritische CO_2-Kältemaschine,” *DKV-Tagungsbericht*, Vol. 26, pp. 264-277.

McQuiston, F.C., 1978, “Correlaiton of Heat, Mass and Momentum Transport Correlations for Plate-Fin-Tube Heat Transfer Surface with Staggered Tubes,” *ASHRAE Transactions*, Vol. 84, No. 1, pp. 294-309.

Menegay, P., 1991, “Experimental Investigation of an Ejector as a Refrigerant Expansion Engine,” *M.S. Thesis*, Virginia Polytechnic Institute and State University, Blacksburg, VA.

Menegay, P., Kornhauser, A.A., 1994, “Ejector Expansion Refrigeration Cycle with Underexpanded Motive Nozzle,” *Proceedings of the Intersociety Energy Conversion Engineering Conference*, Monterey, CA., Vol. 2, pp. 915-920.

Menegay, P., Kornhauser, A.A., 1995, “Development of A Semi-Parabolic Two-Fluid Model for Two-Phase Ejectors,” *Proceedings of the Intersociety Energy Conversion Engineering Conference,* Orlando, FL., Vol. 3, pp. 7-12.

Menegay, P., Kornhauser, A.A., 1996, “Improvements to the Ejector Expansion Refrigeration Cycle,” *Proceedings of the Intersociety Energy Conversion Engineering Conference*, Washington DC., Vol. 2, pp. 702-706.

Munday, J.T., Bagster, D.F., 1977, “A New Ejector Theory Applied to Steam Jet Refrigeration,” *Industrial Engineering Chemical Process Research and Development,* Vol. 16, pp. 442-449.

Neve, R.S., 1988, “The Performance and Modeling of Liquid Jet Gas Pumps,” *International Journal of Heat and Fluid Flow,* Vol. 9, pp. 156-164.

Neve, R.S., 1991, “Diffuser Performance in Two-Phase Jet Pumps,” *International Journal of Multiphase Flow,* Vol. 17, pp. 267-272.

Newton, A.B., 1972a, “Capacity Control for Multiple-Phase Ejector Refrigeration Systems,” *U.S. Patent No. 3670519.*

Newton, A.B., 1972b, “Controls for Multiple-Phase Ejector Refrigeration Systems,” *U.S. Patent No. 3701264.*

Nickl. J., Will, G., Kraus, W., Quack, H., 2002, “Design Considerations for a Second Generation CO_2-expander,” *5th IIR-Gustav Lorentzen Conference on Natural Working Fluids at Guangzhou,* Guangzhou, China, pp. 189-196.

Ochi, J., Ayukawa, K., Kawahara, G., 1996, “Application of Three-Layer Model Analysis to Single-Component Two-Phase Critical Flow through a Converging Nozzle,” *International Journal of JSME,* Vol. 39, Series B, pp. 80-85.

Ortiz, T. M., Li, D., E. A. Groll, 2003, “Evaluation of the Performance Potential of CO_2 as a Refrigerant in Air-To-Air Air Conditioners and Heat Pumps: System Modeling and Analysis”, *Ray W. Herrick Labs Research Report HL 2003-20,* Purdue University, West Lafayette, IN, USA.

Owen, I., Abdul-Ghani, A., Amini, A.M., 1992, “Diffusing A Homogenized Two-Phase Flow,” *International Journal of Multiphase Flow,* Vol. 18, pp. 531-540.

Ozaki, Y., Takeuchi, H., Hirata, 2004, “Regeneration of Expansion Energy by Ejector in CO_2 Cycle,” *Proceedings 6th IIR-Gustav Lorentzen Conference on Natural Working Fluids at Glasgow*, Glasgow, UK.

Parker, G.M., Lear, W.E., 2001, "On an Optimum Geometry of a Two-Phase Ejector," *Proceedings of IECEC'01 36th Intersociety Energy Conversion Engineering Conference,* Savannah, Georgia, pp. 1187-1194

Petrov, N.E., Popov, V.N., 1985, "Heat Transfer and Resistance of Carbon Dioxide Being Cooled in The Supercritical Region," *Thermal Engineering,* Vol. 32, No. 3, pp. 131-134.

Petterson, J., Rieberer, R., Munkejord, S.T., 2000, "Heat Transfer and Pressure Drop for Flow of Supercritical and Subcritical CO_2 in Microchannel Tubes," *SINTEF Energy Research Technical Report,* TR A5127.

Rao, N.S., Kremer, H., 1993, "A General Method of Designing Gas and Gas-Liquid Injectors Using Laws of Turbulent Jet Mixing," *Chemical Engineering Technology,* Vol. 16, pp. 94-101.

Robinson, D.M., and Groll, E.A., 1998, "Efficiencies of Transcritical CO_2 Cycles With and Without an Expansion Turbine," *International Journal of Refrigeration*, Vol. 21, pp. 577-589.

Robinson, D.M., 2000, "Modeling of Carbon Dioxide Based Air-To-Air Air Conditioners," *Ph.D. Dissertation,* Purdue University, West Lafayette, IN, USA.

Rogdakis, E.D., Alexis, G.K., 2000, "Design and Parametric Investigation of an Ejector in an Air-Conditioning System," *Applied Thermal Engineering,* Vol. 20, pp. 213-226.

Romstedt, P., Werner, W., 1986, "Numerical Analysis of Critical Two-Phase Flow in a Convergent-Divergent Nozzle," *Nuclear Science and Engineering,* Vol. 92, pp. 71-83.

Rusly, E., Aye, L., Charters, W.W.S, Ooi, A., 2005, "CFD Analysis of Ejector in a Combined Ejector Cooling System," *International Journal of Refrigeration*, Vol. 28, pp. 1092-1101.

Selvaraju, A., Mani, A., 2006, "Experimental Investigation on R134a Vapour Ejector Refrigeration System," *International Journal of Refrigeration,* Vol. 29, pp. 1160-1166.

Stosic, N., Smith, I., Kovacevic, A., 2002, "A Twin Screw Combined Compressor and Expander for CO_2 Refrigeration Systems," *Proceedings of the International Compressor Engineering Conference at Purdue,* Purdue University, USA., pp. 703-710.

Sun, D.W. 1995, "Recent Developments in the Design Theories and Applications of Ejectors — a Review," *Journal of Institute of Energy,* Vol. 68, pp. 65-79.

Wadle, M., 1988, "Theoretical and Numerical Examination of a Two-Phase Flow in a Diverging Nozzle," *Nuclear Science and Engineering,* Vol. 100, pp.89-104.

Wang, C.C., Lin, Y.T., Lee, C.J., 2000, "Heat and Momentum Transfer for Compact Louvered Fin-and-Tube Heat Exchangers in Wet Conditions," *International Journal of Heat and Mass Transfer,* Vol. 43, pp. 3443-3452.

Westphalen, D., Dieckmann, J., 2004, “Scroll Expander for Carbon Dioxide Air Conditioning Cycles,” *Proceedings of 10th International Refrigeration and Air Conditioning Conference at Purdue*, Purdue University, USA, Paper No. R023.

Witte, J.H., 1969, “Mixing Shocks in Two-Phase Flow,” *Journal of Fluid Mechanics*, Vol. 36, Part 4, pp. 639-655.

Yin, J.M., Bullard, C.W., Hrnjak, P.S., 2001, “R-774 Gas Cooler Model Development and Validation,” *International Journal of Refrigeration*, Vol. 24, pp. 692-701.

Young, J.B., Guha, A., 1991, “Normal Shock-Wave Structure in Two-Phase Vapour-Droplet Flows,” *Journal of Fluid Mechanics*, Vol. 228, pp. 243-274.

Yu, J., Li, Y. 2006, “A Theoretical Study of a Novel Regenerative Ejector Refrigeration Cycle,” *International Journal of Refrigeration*, in press.

APPENDICES

Appendix A: Compressor model for transcritical CO_2 air conditioning system

The following assumptions for the compressor model are made:

- The compressor operates at steady state.
- The changes in kinetic and potential energy are neglected.
- The compressor mechanical efficiency is constant.
- The motor efficiency is constant.
- The pressure losses in the suction and discharge lines are neglected.
- The fraction of heat loss through the compressor shell is constant.
- The compressor overall isentropic efficiency and volumetric efficiency are functions of the compressor pressure ratio.

A.1. Governing equations of the compressor model

Using the above assumptions, the hermetic compressor model consists of following governing equations.

The definition of the volumetric efficiency is given as:

$$\eta_{vol} = \frac{\dot{m}}{\dot{m}_{th}} = \frac{\dot{m}}{n\left(\frac{V_{dis}}{v_{suc}}\right)} \tag{A.1}$$

where $\dot{m}$ is the mass flow rate of the refrigerant through compressor, n is the compressor speed, V_{dis} is the displacement volume of compressor, and v_{suc} is the specific volume of the refrigerant at the suction port.

The overall isentropic efficiency of a hermetic compressor is defined as:

$$\eta_{total} = \frac{\dot{m}(h_{isen} - h_{suc})}{\dot{W}_{comp}} \tag{A.2}$$

where h_{isen} is the discharge enthalpy assuming an isentropic compression process from the suction port state point to the given discharge pressure. h_{suc} is the enthalpy of the refrigerant at the suction port and $\dot{W}_{comp}$ is the total power input to the compressor.

The compressor motor efficiency is defined as:

$$\eta_{motor} = \frac{\dot{W}_{shaft}}{\dot{W}_{comp}} \tag{A.3}$$

where $\dot{W}_{shaft}$ is the mechanical power output from the motor shaft.

The compressor mechanical efficiency is defined as:

$$\eta_{mech} = \frac{\dot{W}_{refrig}}{\dot{W}_{shaft}} = \frac{\dot{m}(h_{dis} - h_{suc})}{\dot{W}_{shaft}} \tag{A.4}$$

where $\dot{W}_{refrig}$ is the compression power done by the compressor on the refrigerant and h_{dis} is the enthalpy of the refrigerant at the discharge port.

The difference between $\dot{W}_{comp}$ and $\dot{W}_{refrig}$ is converted into the heat, which is transferred to the refrigerant inside the compressor. It can be calculated as:

$$\dot{Q}_{refrig} = (1-\eta_{mech}\eta_{motor})\dot{W}_{comp} \tag{A.5}$$

According to Fischer and Rice (1983), part of the heat that is transferred to the refrigerant will be lost through the compressor shell to the environment and can be expressed as:

$$\dot{Q}_{shell} = 0.9\dot{Q}_{refrig} \tag{A.6}$$

When the compressed refrigerant flows from the discharge port to the compressor shell outlet, there will be heat transfer from the discharge line to the refrigerant in the suction chamber. Fischer and Rice (1983) correlated the rate of this heat loss to the power input to the compressor as indicated in Equation (A.7):

$$\dot{Q}_{loss} = 0.03\dot{W}_{comp} \tag{A.7}$$

Thus, the energy balance of the refrigerant between the discharge port and compressor shell outlet becomes:

$$\dot{Q}_{loss} = \dot{m}(h_{dis} - h_{out}) \tag{A.8}$$

where h_{out} is the enthalpy of refrigerant at the compressor outlet.

The energy balance of the refrigerant between the compressor inlet and the suction port can be written as follows:

$$\dot{m}(h_{suc} - h_{in}) = \dot{Q}_{loss} + \dot{Q}_{refrig} - \dot{Q}_{shell} \tag{A.9}$$

where h_{in} is the enthalpy of the refrigerant at the compressor inlet.

A.2. Computation sequence of the compressor model

The compressor simulation model requires the following input parameters:

- Compressor running speed and displacement volume
- Compressor inlet pressure and temperature, i.e., superheat
- Compressor outlet pressure
- Compressor mechanical efficiency and motor efficiency
- Compressor total efficiency and volumetric efficiency values or correlations

The outputs of the compressor simulation model are the mass flow rate of refrigerant through the compressor, the power input to the compressor, the outlet temperature of the refrigerant, and the heat loss to the environment. The calculation sequence based on the governing equations listed above is as follows:

1) It is assumed that the temperature and pressure of the refrigerant at the suction port are the same as the one at the compressor inlet.

2) The mass flow rate, $\dot{m}$, and compressor power input, $\dot{W}_{comp}$, are calculated using Equations (A.1) and (A.2).
3) The heat transfer rates, $\dot{Q}_{refrig}$, $\dot{Q}_{shell}$ and $\dot{Q}_{loss}$ are calculated using Equations (A.5), (A.6) and (A.7)
4) The suction port state point is updated based on Equation (A.9).
5) Steps 2), 3) and 4) are repeated until the iteration on the suction port state point converges.
6) The discharge port state point is determined based on Equations (A.3) and (A.4).
7) The compressor outlet state point is determined based on Equation (A.8).

Appendix B: Gas cooler model for transcritical CO_2 air conditioning system

The following assumptions are made for the gas cooler model:

- The gas cooler operates at steady state.
- The air flow velocity is uniform across the face area.
- The refrigerant distribution is uniform for each micro-channel in the same flow path.
- Fin edges are adiabatic.
- Both tube and fin have constant density and thermal conductivity.
- The heat transfer and pressure drop calculation are decoupled over a single finite segment of a multi-port-extruded tube.
- Constant heat transfer coefficients and friction factors are assumed for each single finite segment of a multi-port-extruded tube.
- The changes in potential energy are neglected.

B.1. Governing equations of gas cooler model

The governing equations of the gas cooler model are listed in the following.

Both the air-side heat transfer coefficients and air-side friction factors are calculated using the correlations proposed by Chang et al. (1994) as shown below:

$$j_H = 0.291\,\mathrm{Re}_{Lp}^{-0.589}\,\varepsilon^{0.438} \tag{B.1}$$

$$f = 0.805\,\mathrm{Re}_{Lp}^{-0.514}\left(\frac{p_f}{L_p}\right)^{-0.72}\left(\frac{H_f}{L_p}\right)^{-1.22}\left(\frac{L_l}{L_p}\right)^{1.97} \tag{B.2}$$

where j_H is the Colburn j-factor and ε is the heat exchanger fining factor suggested by McQuiston (1978).

The correlations given in Equations (B.1) and (B.2) are recommended for the following Reynolds numbers and fining factors:

$$100 < Re_{Lp} < 700$$
$$7 < \varepsilon < 12$$

Two different correlations are used to calculate the refrigerant side heat transfer coefficient based on the value of mass flux inside the micro-channel. In case that the mass flux is above 350 kg/m^{2}s, the modified Gnielinski correlation developed by Petterson et al. (2000) is used to calculate the refrigerant side heat transfer coefficient:

$$Nu = Nu_m\left(\frac{\mathrm{Pr}}{\mathrm{Pr}_w}\right)^{0.11} \tag{B.3}$$

where

$$Nu_m = \frac{\frac{f}{8}(\mathrm{Re}-1000)\,\mathrm{Pr}}{1+12.7\sqrt{\frac{f}{8}}\left(\mathrm{Pr}^{\frac{2}{3}}-1\right)}\left[1+\left(\frac{d}{l}\right)^{\frac{2}{3}}\right] \tag{B.4}$$

and

$$f = \left\{ -1.8 \log \left[\frac{6.9}{\mathrm{Re}} + \left(\frac{1}{3.7} \frac{\varepsilon}{d} \right)^{1.11} \right] \right\}^{-2} \tag{B.5}$$

In case that the mass flux is lower than 350 kg/m^{2}s, the correlation developed by Petrov and Popov (1985) is used to calculate the refrigerant side heat transfer coefficient:

$$Nu_w = Nu_{w,ppk} \left(1 - \frac{M q''_w}{G} \right) \left(\frac{\bar{c}_p}{c_{p,w}} \right)^n \tag{B.6}$$

where

$$n = \begin{cases} 0.66 - K \left(\frac{q''_w}{G} \right) & \text{if } \frac{\bar{c}_p}{c_{p,w}} \le 1.0 \\ 0.9 - K \left(\frac{q''_w}{G} \right) & \text{if } \frac{\bar{c}_p}{c_{p,w}} > 1.0 \end{cases} \tag{B.7}$$

and where M = 0.001 kg/J, and K = 0.00041 kg/J. $\bar{c}_p$ is defined as:

$$\bar{c}_p = \frac{h_b - h_w}{T_b - T_w} \tag{B.8}$$

$Nu_{w,ppk}$ in Equation (B.6) represents the Nusselt number determined by the Petukhov-Popov-Kirilov correlation with the thermophysical and transport properties evaluated at the inside tube wall temperature. The Petukhov-Popov-Kirilov correlation is used to calculate the circumferentially averaged local Nusselt number for in-tube cooling of a single phase flow where the thermophysical properties are either constant or weakly varying. It can be expressed as:

$$Nu_{ppk} = \frac{\frac{f_o}{8} \mathrm{Re} \, \mathrm{Pr}}{12.7 \sqrt{\frac{f_o}{8}} \left(\mathrm{Pr}^{\frac{2}{3}} - 1 \right) + 1.07} \tag{B.9}$$

where the friction factor, f_o, is determined by the Filonenko correlation:

$$f_o = \left(0.79 \ln(\mathrm{Re}) - 1.64 \right)^{-2} \tag{B.10}$$

The refrigerant side friction factor is calculated by the correlation developed by Kuraeva and Protopopov (1974) as follows:

$$f = \begin{cases} f_o \left(\frac{\mu_w}{\mu_b} \right)^{0.22} & \text{if } \frac{Gr}{\mathrm{Re}} < 5 \times 10^{-4} \\ 2.15 f_o \left(\frac{\mu_w}{\mu_b} \right)^{0.22} \left(\frac{Gr}{\mathrm{Re}} \right)^{0.1} & \text{if } 5 \times 10^{-4} \le \frac{Gr}{\mathrm{Re}} \le 3 \times 10^{-1} \end{cases} \tag{B.11}$$

where f_o is determined by Equation (B.10).

The heat transfer rate based on the overall heat transfer coefficient is determined by the effectiveness-NTU method:

$$\dot{Q} = \varepsilon c_{\min}\left(T_{refrig,i} - T_{air,i}\right) \tag{B.12}$$

where c_{min} is the smaller one of $\dot{m}_{refrig} c_{p,refrig}$ and $\dot{m}_{air} c_{p,air}$, while the larger one between those two is defined as c_{max}.

The heat exchanger effectiveness, ε, is given by

$$\varepsilon = 1 - \exp\left[\left(\frac{1}{C_r}\right) NTU^{0.22}\left\{\exp\left[-C_r NTU^{0.78}\right] - 1\right\}\right] \tag{B.13}$$

for heat transfer between two unmixed fluids in cross flow configuration, or by

$$\varepsilon = \frac{1 - \exp\left[-NTU\left(1 - C_r\right)\right]}{1 - C_r \exp\left[-NTU\left(1 - C_r\right)\right]} \tag{B.14}$$

for heat transfer between two unmixed fluids in counter flow configuration. C_r and NTU are defined as follows:

$$C_r = \frac{c_{\min}}{c_{\max}} \tag{B.15}$$

$$NTU = \frac{UA}{c_{\min}} \tag{B.16}$$

The overall conductance UA is given by:

$$UA = \frac{1}{\dfrac{1}{h_{air}\eta_o A_{air}} + \dfrac{\ln\left(r_o / r_i\right)}{2\pi L k_w} + \dfrac{1}{h_{refrig} A_{refrig}}} \tag{B.17}$$

where

$$\eta_o = 1 - \frac{A_{fin}}{A_{air}}\left(1 - \eta_{fin}\right) \tag{B.18}$$

$$\eta_{fin} = \frac{\tanh\left(m L_{fin}\right)}{m L_{fin}} \tag{B.19}$$

$$m = \sqrt{\frac{2 h_{air}}{k_{air} t_{fin}}} \tag{B.20}$$

The heat transfer rate can also be determined from the refrigerant side conductance and the temperature difference between the inside wall and the refrigerant using the following equation:

$$\dot{Q}_{refrig} = \left(UA\right)_{refrig}\left(T_{refrig} - T_{iw}\right) \tag{B.21}$$

where

$$\left(UA\right)_{refrig} = h_{refrig} A_{refrig} \tag{B.22}$$

The pressure drop associated with the contraction when the refrigerant flows from the distribution header into a micro-channel inside a multi-port-extruded tube is calculated as:

$$\Delta p_c = \frac{1}{2} K_c \rho V^2 \tag{B.23}$$

The pressure drop of a refrigerant flowing inside a multi-port-extruded tube is caused by two effects: friction and density change of the refrigerant. For each finite segment along the micro-channel of a multi-port-extruded tube, the pressure drop associated with the frictional loss is calculated by:

$$\Delta p_f = f \frac{L}{2D} \rho V^2 \tag{B.24}$$

The pressure drop due to the refrigerant density change is calculated by:

$$\Delta p_a = G^2 \left(\frac{1}{\rho_o} - \frac{1}{\rho_i} \right) \tag{B.25}$$

The pressure drop associated with the expansion when the refrigerant flows from a micro-channel inside a multi-port-extruded tube into the collection header is calculated by:

$$\Delta p_e = \frac{1}{2} K_e \rho V^2 \tag{B.26}$$

The air side pressure drop is calculated similarly to the refrigerant side pressure drop. The pressure drop associated with the entrance loss when the air first flows into the heat exchanger slab is calculated by:

$$\Delta p_{en,air} = K_{en} \frac{G_{air}^2}{2\rho_{air}} \tag{B.27}$$

The pressure drop associated with the exit loss when the air flows out of the heat exchanger slab is calculated by:

$$\Delta p_{ex,air} = K_{ex} \frac{G_{air}^2}{2\rho_{air}} \tag{B.28}$$

The pressure drop associated with the frictional loss when the air flows among the fins of one segment of the heat exchanger slab is calculated by:

$$\Delta p_{f,air} = f_{air} \frac{\Delta W}{2d_{eqv}} \frac{G_{air}^2}{\rho_{air}} \tag{B.29}$$

where d_{eqv} is defined as:

$$d_{eqv} = \frac{4\sigma V_{seg}}{A_{seg}} \tag{B.30}$$

and V_{seg} is the total volume occupied by one segment of the coil, A_{seg} is the total air contact area of one segment of the slab. The fraction of free space volume for one segment of the slab, σ, is calculated by:

$$\sigma = \frac{1 - \frac{t_{fin}}{p_{fin}}}{1 + \frac{h_{tube}}{h_{fin}}} \tag{B.31}$$

The pressure drop due to the air density change for one segment of the slab is calculated by:

$$\Delta p_{air,a} = G_{air}^{2}\left(\frac{1}{\rho_{air,o}} - \frac{1}{\rho_{air,i}}\right) \tag{B.32}$$

B.2. Computation sequence of the gas cooler model

The gas cooler simulation model requires the following input parameters:

- Refrigerant mass flow rate, inlet temperature and pressure (outputs of the compressor model)
- Air inlet temperature and volume flow rate
- Geometric parameters
- Flow circuits configuration
- Thermal conductivity of tube and fin material
- Head loss coefficients
- Number of segments for each MPE tubes

The outputs of the gas cooler simulation model are the refrigerant and air-side pressure drop, the heat transfer rate, and the refrigerant and air-side outlet state points. The calculation sequence based on the governing equations listed above is as follows:

The refrigerant side pressure drop in the distribution header is calculated. The inlet state points for the segments of the multi-port-extruded tubes at the start of the refrigerant flow path are determined.

The refrigerant and air inlet state points for each segment of the multi-port-extruded tubes of a heat exchanger slab are determined if that is possible or otherwise assumed.

The heat transfer rate and refrigerant and air-side pressure drop are calculated for each segment. The refrigerant and air-side outlet state points are determined for each segment.

Step 2) and 3) are repeated until the iteration for all assumed values converges.

The refrigerant side pressure drop in the collection header is calculated. The outlet state points of the refrigerant and the air, and the total heat transfer rate of the slab is determined.

For each segment of the multi-port-extruded tube when both the refrigerant and air inlet states are known, the calculation of the heat transfer rate and the refrigerant and air-side pressure drop is executed in the following sequence:

1) An inner wall temperature is assumed for the segment at a value between the inlet refrigerant temperature and inlet air temperature.
2) The refrigerant-side heat transfer coefficient is calculated and the heat transfer rate is estimated using Equation (B.21).

3) The outer wall temperature is determined based on the estimated heat transfer rate and the assumed inner wall temperature.
4) The air-side heat transfer coefficient is calculated. The heat exchanger effectiveness ε and NTU is determined using Equations (B.13) to (B.20).
5) A new value for the heat transfer rate is calculated using Equation (B.12).
6) If the values of the heat transfer rate based on Equation (B.12) and based on Equation (B.21) do not agree with each other, the inner wall temperature is updated and the sequence starts again at step 2). Steps 2) to 6) are repeated until the iteration on the heat transfer rate converges.
7) The refrigerant and air-side outlet temperatures and the heat transfer rate of the segment are calculated.
8) The refrigerant and air-side pressure drops are calculated.

The calculation sequence of multiple heat exchanger slabs that make up one gas cooler is arranged based on the refrigerant side interconnection and the air side flow configuration. The total heat transfer rate of the gas cooler is equal to the summation of the heat transfer rates of all slabs. The total refrigerant side pressure drop can be determined based on the pressure drops for each slab and the refrigerant side interconnection of these slabs. The total air side pressure drop can also be determined from the air side pressure drop of each slab and the air flow configuration of the gas cooler. Finally, the overall refrigerant and air-side outlet state points can be determined for the gas cooler.

Appendix C: Evaporator model for transcritical CO_2 air conditioning system

The following assumptions are made for the evaporator model:

- The evaporator operates at steady state.
- The air flow velocity is uniform across the face area.
- The refrigerant distribution is uniform for each micro-channel in the same flow path.
- The fin edges are adiabatic.
- Both the tube and fin have constant density and thermal conductivity.
- The heat transfer and pressure drop calculation can be decoupled for each single finite segment of multi-port-extruded tubes.
- Constant heat transfer coefficients and friction factors are assumed for each single finite segment of the multi-port-extruded tubes.
- Each finite segment of the multi-port-extruded tubes is either dry or wet for the whole segment air side surface.
- CO_2 is either a two-phase mixture or a single-phase vapor inside each single finite segment of multi-port-extruded tubes.
- Frost build up is not considered.
- The changes in potential energy are neglected.

C.1. Governing equations of evaporator model

The governing equations of the evaporator model can be listed as indicted below. Some of the governing equations are the same as for the ones of the gas cooler model. The important additional equations are for the wet-surface analysis on the air side and the two-phase flow analysis on the refrigerant side.

The air-side heat transfer coefficients for both dry segments and wet segments are determined by using the same Chang et al. (1994) correlation (Equation (B.1)) as used in the gas cooler model. The air-side friction factors for a dry surface are calculated using the accompanying Chang et al. (1994) correlation (Equation (B.2)). The air-side friction factors for a wet surface are calculated using the Wang et al (2000) correlation:

$$f = 2.814\,\mathrm{Re}_{D_c}^{f_1}\left(\frac{F_p}{D_c}\right)^{f_2}\left(\frac{P_l}{D_c}\right)^{f_3}\left(\frac{P_l}{P_t}+0.091\right)^{f_4}\left(\frac{L_p}{F_p}\right)^{1.958} N^{0.04674} \qquad \text{(C.1)}$$

where

$$f_1 = 1.223 - 2.857\left(\frac{F_p}{D_c}\right)^{0.71}\left(\frac{P_l}{P_t}\right)^{-0.05} \qquad \text{(C.2)}$$

$$f_2 = 0.8079\ln\left(\mathrm{Re}_{D_c}\right) \qquad \text{(C.3)}$$

$$f_3 = 0.8932\ln\left(\mathrm{Re}_{D_c}\right) \qquad \text{(C.4)}$$

$$f_4 = -0.999\ln\left(\frac{2\Gamma}{\mu_f}\right) \qquad \text{(C.5)}$$

The single-phase refrigerant-side heat transfer coefficients are calculated using the modified Gnielinski correlation (Equation (B.3)) developed by Petterson et al. (2000). The single-phase refrigerant-side friction factors are calculated using the Churchill correlation (Yin et al., 2001) as shown below:

$$f = 8\left\{\left(\frac{8}{\text{Re}}\right)^{12} + \left[\left(2.457\ln\left(\frac{1}{\left(\frac{7}{\text{Re}}\right)^{0.9} + 0.27e}\right)\right)^{16} + \left(\frac{37530}{\text{Re}}\right)^{16}\right]^{-\frac{3}{2}}\right\}^{\frac{1}{12}} \tag{C.6}$$

The two-phase refrigerant-side heat transfer coefficients are calculated using the Kandlikar correlation (Kandlikar, 1990) as recommended by Pettersen et al. (2000):

$$h = h_l\left[c_1 Co^{c_2}\left(25Fr'\right)^{c_5} + c_3 Bo^{c_4} F_f\right] \tag{C.7}$$

where h_l is calculated using the Dittus-Boelter correlation:

$$h_l = 0.023\,\text{Re}_l^{0.8}\,\text{Pr}_l^{0.4}\frac{k_l}{d} \tag{C.8}$$

Table C.1 lists the constants applicable to Equation (C.7) for carbon dioxide as reported by Pettersen et al. (2000).

Table C.1: Kandlikar Correlation Constants for Carbon Dioxide.

Constant	Convective Boiling	Nucleate Boiling
F_{fl}	1.0	1.0
c_1	1.1360	0.6683
c_2	-0.9	-0.2
c_3	667.2	1058.0
c_4	0.7	0.7
c_5 (vertical tubes: any Fr, horizontal tubes: Fr > 0.4)	0	0
c_5 (horizontal tubes: Fr ≤ 0.4)	0.3	0.3

The two-phase refrigerant-side friction factors are calculated using the Churchill correlation (Equation (C.6)) in which the Reynolds number is evaluated using a homogeneous two-phase density and viscosity as given below:

$$\frac{1}{\rho} = \frac{x}{\rho_v} + \frac{1-x}{\rho_l} \tag{C.9}$$

$$\mu = x\mu_v + (1-x)\mu_l \tag{C.10}$$

For a dry surface, the overall heat transfer of a single finite segment of the multi-port-extruded tubes in the evaporator is calculated almost in the same way as it is calculated in the gas cooler with the following differences.

The heat exchanger effectiveness of a single finite segment containing two-phase refrigerant is:

$$\varepsilon = 1 - \exp(-NTU) \tag{C.11}$$

The dry segment heat transfer rate calculated using the effectiveness-NTU method is:

$$\dot{Q} = \varepsilon c_{\min}\left(T_{air,in} - T_{refrig,in}\right) \tag{C.12}$$

If the outer wall temperature of a finite segment is below the dew point temperature of the inlet air to this segment, the segment is assumed to be all wet. For a wet surface heat transfer calculation, the method developed by Braun et al. (1989, 1999) is used and can be summarized as follows.

The overall effective fin efficiency is defined as:

$$\eta_o^* = 1 - \frac{A_{fin}}{A_{air}}\left(1 - \eta_{fin}^*\right) \tag{C.13}$$

where

$$\eta_{fin}^* = \frac{\tanh\left(m^* L_{fin}\right)}{m^* L_{fin}} \tag{C.14}$$

$$m^* = \sqrt{\frac{2h_{air}c_{p,s}}{kt_f c_p}} \tag{C.15}$$

and where $c_{p,s}$ is the effective specific heat of saturated air evaluated at a given temperature.

The effective number of transfer units is defined as:

$$NTU^* = \frac{(UA)^*}{\dot{m}_{air}} \tag{C.16}$$

where

$$(UA)^* = \frac{1}{\dfrac{c_{p,air}}{h_{air}\eta_o^* A_{air}} + \dfrac{\ln\left(r_o/r_i\right)}{2\pi L k_w} + \dfrac{c_{p,s}}{h_{ref}A_{ref}}} \tag{C.17}$$

The total heat transfer rate based on the effectiveness is given by:

$$\dot{Q}_{NTU} = \dot{m}_{air}\varepsilon^*\left(h_{air,in} - h_{sat,T_{ow}}\right) \tag{C.18}$$

where

$$\varepsilon^* = 1 - \exp\left(-NTU^*\right) \tag{C.19}$$

$$h_{sat,T_{ow}} = h_{air}\left(T_{ow}, \omega_{sat}\right) \tag{C.20}$$

The air outlet temperature is given by:

$$T_{air,out} = T_{ow} - \left(T_{ow} - T_{air,in}\right)\exp\left(-NTU_o\right) \tag{C.21}$$

where

$$NTU_o = \frac{\eta_o h_{air} A_{air}}{\dot{m}_{air} c_{p,air}} \tag{C.22}$$

The sensible heat transfer rate can be calculated as:

$$\dot{Q}_{sens} = \dot{m}_{air} c_{p,air} \left(T_{air,in} - T_{air,out}\right) \tag{C.23}$$

The latent heat transfer rate can be obtained as:

$$\dot{Q}_{lat} = \dot{Q}_{NTU} - \dot{Q}_{sens} \tag{C.24}$$

The air outlet humidity ratio can be obtained as:

$$\omega_{out} = \omega_{in} - \frac{\dot{Q}_{lat}}{\dot{m}_{air} h_{fg,water}} \tag{C.25}$$

The pressure drop and fan power calculations in the evaporator are performed in the same way as the ones for the gas cooler.

C.2. The computation sequence for evaporator segments

The evaporator simulation model requires the following input parameters:

- Refrigerant mass flow rate, inlet quality and pressure
- Air inlet temperature, humidity and volume flow rate
- Geometric parameters
- Flow circuits configuration
- Thermal conductivity of tubes and fins material
- Head loss coefficients
- Number of segments for each MPE tubes

The outputs of the evaporator simulation model are the refrigerant and air side pressure drops, the heat transfer rate, and the refrigerant and air-side outlet state points. The computation of the evaporator model is executed the same way as the one of the gas cooler model with the exception of the calculation of each finite segment of the multi-port-extruded tubes. The computation of each finite segment of the multi-port-extruded tubes of the evaporator model is carried out in the following sequence:

1) An inner wall temperature for this segment at a value between the inlet refrigerant temperature and inlet air temperature is assumed.
2) The refrigerant-side heat transfer coefficient is calculated and the heat transfer rate is estimated using Equation (B.21). Whether to use a single-phase heat transfer coefficient or a two-phase heat transfer coefficient is determined by the inlet refrigerant quality.
3) The outer wall temperature is determined based on the estimated heat transfer rate and the assumed inner wall temperature.

4) If the outer wall temperature is below the dew point of the inlet air, a wet analysis of the segment is performed to obtain a new value for the heat transfer rate using Equation (C.18).
5) If the outer wall temperature is above the dew point of the inlet air, a dry analysis of the segment is performed to obtain a new value for the heat transfer rate using Equation (B.12).
6) If the value of heat transfer rate based on Equation (B.12) or based on Equation (C.18) does not agree with the one based on Equation (B.21), the inner wall temperature is updated and the sequence starts again at step 2). Steps 2) to 6) are repeated until the iteration on the heat transfer rate converges.
7) The refrigerant and air-side outlet temperatures and the heat transfer rate of the segment are calculated.
8) The refrigerant and air-side pressure drops are calculated.

Appendix D: Separator model for ejector expansion transcritical CO_2 air conditioning system

A schematic of the separator is shown in Figure D.

The assumptions used in the separator model are listed below:

- The separator operates at steady state.
- The heat losses from the separator to the environment are neglected.
- The kinetic and potential energy changes are neglected.
- The refrigerant mixture inside the separator reaches phase equilibrium.
- The quality of vapor leaves for the compressor inlet equals one.
- The liquid refrigerant leaves for the evaporator is saturated liquid.

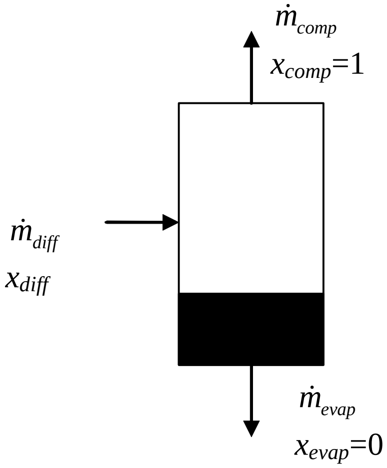

Figure D: schematic of separator model.

The governing equations of the separator model are listed next.

The conservation of mass across the separator results in the following equation:

$$\dot{m}_{diff} = \dot{m}_{comp} + \dot{m}_{evap} \tag{D.1}$$

In addition, the following mass balance is established:

$$\dot{m}_{diff} x_{diff} = \dot{m}_{comp} \tag{D.2}$$

The evaporator mass flow rate is the same as the suction stream mass flow rate and can be correlated using the motive stream mass flow rate $\dot{m}_{nozzle}$ and the definition of ejection ratio φ:

$$\dot{m}_{evap} = \varphi \dot{m}_{nozzle} \tag{D.3}$$

Thus, the ejection ratio and the ejector outlet CO_2 quality must satisfy:

$$(1+\varphi) x_{diff} = 1 \tag{D.4}$$

Appendix E: Experimental data for transcritical CO_2 air conditioning system

Table E.1: Data for CO_2 bread board ECU

Basic cycle	1	2	3	4	5	6	7	8
P_{atm} (kPa)	100.35	99.88	99.88	99.91	99.64	99.58	99.42	99.42
T_{id} (ºC)	26.7	26.7	26.7	26.7	26.7	26.7	26.7	26.7
RH_{id} (%)	50.0	50.0	50.0	50.0	50.0	50.0	50.0	50.0
T_{od} (ºC)	27.8	27.8	27.8	32.2	32.2	35.0	35.0	37.8
$T_{air,eo}$ (ºC)	16.60	17.13	17.09	17.42	16.69	16.43	17.59	16.33
T_{dew} (ºC)	9.22	11.93	11.62	9.97	12.53	11.76	12.01	12.58
$\dot{V}_{eva,air}$ (m^3/s)	0.987	1.062	1.062	1.062	1.062	1.056	1.072	1.056
$T_{air,go}$ (ºC)	50.77	51.03	51.89	54.10	56.50	57.11	58.71	61.01
$P_{comp,i}$ (bar)	36.13	38.11	36.79	36.49	38.83	36.76	37.28	38.93
$T_{comp,i}$ (ºC)	10.12	9.02	10.54	11.57	8.89	12.57	13.95	9.56
$P_{comp,o}$ (bar)	119.06	122.38	129.84	118.80	128.24	121.26	122.40	132.31
$T_{comp,o}$ (ºC)	122.7	119.75	132.2	125.52	123.48	128.5	129.69	128.5
$P_{gc,i}$ (bar)	117.26	120.70	128.34	117.49	126.90	119.51	121.24	130.32
$T_{gc,i}$ (ºC)	115.79	113.85	124.90	118.97	117.86	121.95	123.06	122.74
$P_{gc,o}$ (bar)	117.16	120.25	128.23	117.07	126.43	119.37	120.91	130.31
$T_{gc,o}$ (ºC)	50.97	47.99	45.87	50.22	51.97	51.44	52.91	54.81
$P_{exv,i}$(bar)	115.57	118.56	126.92	115.52	124.61	117.96	119.29	128.56
$T_{exv,i}$(ºC)	50.09	47.23	45.24	49.48	51.20	51.30	52.10	54.86
$P_{eva,i}$ (bar)	38.18	40.28	38.91	38.69	40.97	39.79	39.45	41.93
$P_{eva,o}$ (bar)	37.84	39.81	38.40	38.15	40.53	38.47	38.92	40.73
$T_{eva,o}$ (ºC)	9.39	7.96	9.78	11.07	7.79	12.43	14.09	8.93
$\dot{m}_{gc}$ (kg/s)	0.11	0.12	0.11	0.11	0.12	0.11	0.11	0.12
$\dot{m}_{eva}$ (kg/s)	0.11	0.12	0.11	0.11	0.12	0.11	0.11	0.12
$\dot{W}_{comp}$ (kW)	9.70	10.02	10.28	9.68	10.38	9.78	9.93	10.57
$\dot{W}_{fan,gc}$ (kW)	1.23	1.17	1.18	1.17	1.15	1.14	1.14	1.13
$\dot{W}_{fan,eva}$ (kW)	1.15	1.18	1.18	1.19	1.18	1.18	1.19	1.18
$\dot{Q}_{eva,ref}$ (kW)	10.65	12.95	14.23	11.23	11.38	10.81	10.8	10.35
COP	1.098	1.292	1.385	1.160	1.097	1.105	1.087	0.979

Table E.1: Data for CO_2 bread board ECU (continued)

Basic cycle	9	10	11	12
P_{atm} (kPa)	99.42	99.42	99.42	99.42
T_{id} (ºC)	26.7	26.7	26.7	26.7
RH_{id} (%)	50.0	50.0	50.0	50.0
T_{od} (ºC)	37.8	37.8	40.6	40.6
$T_{air,eo}$ (ºC)	16.25	16.35	16.53	16.29
T_{dew} (ºC)	12.35	11.41	13.09	12.4
$\dot{V}_{eva,air}$ (m^3/s)	1.054	1.064	1.060	1.060
$T_{air,go}$ (ºC)	61.35	61.89	64.02	64.65
$P_{comp,i}$ (bar)	38.58	37.54	39.84	38.82
$T_{comp,i}$ (ºC)	9.41	10.36	8.32	8.75
$P_{comp,o}$ (bar)	135.37	141.50	138.78	145.28
$T_{comp,o}$ (ºC)	131.9	141.3	130.0	139.0
$P_{gc,i}$ (bar)	133.5	139.8	136.7	143.4
$T_{gc,i}$ (ºC)	125.8	134.2	124.5	132.6
$P_{gc,o}$ (bar)	133.5	140	136.7	143.6
$T_{gc,o}$ (ºC)	54.52	53.31	57.43	56.45
$P_{exv,i}$(bar)	131.9	138.6	134.9	142.1
$T_{exv,i}$(ºC)	54.37	53.15	57.25	56.27
$P_{eva,i}$ (bar)	41.27	40.05	42.56	41.38
$P_{eva,o}$ (bar)	38.58	37.54	39.84	38.82
$T_{eva,o}$ (ºC)	8.5	9.19	7.99	7.52
$\dot{m}_{gc}$ (g/s)	0.12	0.11	0.12	0.11
$\dot{m}_{eva}$ (g/s)	0.12	0.11	0.12	0.12
$\dot{W}_{comp}$ (kW)	10.7	10.83	10.99	11.17
$\dot{W}_{fan,gc}$ (kW)	1.12	1.10	1.09	1.10
$\dot{W}_{fan,eva}$ (kW)	1.18	1.18	1.17	1.18
$\dot{Q}_{eva,ref}$ (kW)	10.96	11.69	9.384	10.01
COP	1.025	1.079	0.854	0.896

Appendix F: Experimental data for ejector expansion transcritical CO_2 air conditioning system

Table F.1: Data for ejector expansion CO_2 bread board ECU
(the values for d_t are measured values)

Ejector cycle	1	2	3	4	5	6	7	8
P_{atm} (kPa)	99.87	99.87	99.87	101.32	101.41	100.29	99.84	98.38
T_{id} (ºC)	26.7	26.7	26.7	26.7	26.7	26.7	26.7	26.7
RH_{id} (%)	50.0	50.0	50.0	50.0	50.0	50.0	50.0	50.0
T_{od} (ºC)	27.8	27.8	27.8	27.8	27.8	27.8	27.8	27.8
d_b (mm)	17.2	17.2	17.2	17.2	5.5	5.5	5.5	5.5
d_t (mm)	2.7	2.6	2.5	1.8	2.7	2.6	2.5	1.8
$T_{air,eo}$ (ºC)	21.14	20.97	21.44	20.18	21.28	21.03	19.78	20.68
T_{dew} (ºC)	13.93	13.58	13.32	13.23	11.21	12.50	12.60	13.74
$\dot{V}_{eva,air}$ (m^3/s)	1.129	1.129	1.121	1.048	1.137	1.121	1.107	1.093
$T_{air,go}$ (ºC)	43.01	43.86	43.54	46.20	42.72	44.41	45.64	51.31
$P_{comp,i}$ (bar)	42.79	43.5	41.39	32.69	41.53	41.29	42.81	34.71
$T_{comp,i}$ (ºC)	7.82	8.47	6.37	-3.46	6.49	6.1	7.74	-1.12
$P_{comp,o}$ (bar)	103.2	107.1	108.2	119.6	98.75	105	122.2	131.6
$T_{comp,o}$ (ºC)	70.4	71.05	70.46	95.12	73.6	76.12	75.32	108.7
$P_{gc,i}$ (bar)	98.69	102.63	104.02	117.97	95.76	102.30	120.25	130.66
$T_{gc,i}$ (ºC)	67.01	67.74	67.46	90.48	69.76	72.57	72.51	103.4
$P_{gc,o}$ (bar)	96.74	100.78	102.77	117.50	92.66	99.53	117.18	129.45
$T_{gc,o}$ (ºC)	42.89	44.56	47.52	43.19	41.3	44.52	47.58	47.71
$P_{dif,o}$(bar)	46.62	47.44	44.94	34.63	45.12	44.77	46.55	36.73
$P_{eva,i}$ (bar)	43.18	43.76	42.99	32.9	40.9	40.36	41.39	31.75
$P_{eva,o}$ (bar)	42.19	42.86	41.99	31.07	39.68	39.15	40.36	31.11
$T_{eva,o}$ (ºC)	23.86	22.01	25.37	21.7	24.58	23.51	17.1	24.89
$\dot{m}_{gc}$ (g/s)	0.2	0.2	0.19	0.12	0.18	0.18	0.2	0.12
$\dot{m}_{eva}$ (g/s)	0.06	0.06	0.05	0.05	0.06	0.06	0.07	0.06
$\dot{W}_{comp}$ (kW)	8.59	8.87	8.81	9.05	8.34	8.79	9.68	10.01
$\dot{W}_{fan,gc}$ (kW)	1.2	1.2	1.19	1.19	1.2	1.18	1.2	1.13
$\dot{W}_{fan,eva}$ (kW)	1.5	1.56	1.56	1.52	1.42	1.4	1.29	1.17
$\dot{Q}_{eva,ref}$ (kW)	13.52	13.16	11.61	13.48	14.05	14.06	15.29	16.07
COP	1.574	1.484	1.317	1.490	1.685	1.600	1.579	1.606

Table F.1: Data for ejector expansion CO_2 bread board ECU (continued)

Ejector cycle	9	10	11	12	13	14	15	16
P_{atm} (kPa)	99.87	99.87	99.87	101.32	101.44	100.29	100.03	100.31
T_{id} (ºC)	26.7	26.7	26.7	26.7	26.7	26.7	26.7	26.7
RH_{id} (%)	50.0	50.0	50.0	50.0	50.0	50.0	50.0	50.0
T_{od} (ºC)	35.0	35.0	35.0	35.0	35.0	35.0	35.0	35.0
d_b (mm)	17.2	17.2	17.2	17.2	5.5	5.5	5.5	5.5
d_t (mm)	2.7	2.6	2.5	1.8	2.7	2.6	2.5	1.8
$T_{air,eo}$ (ºC)	22.06	22.02	21.54	19.84	22.31	21.65	20.52	20.30
T_{dew} (ºC)	13.36	13.19	13.88	13.38	12.71	13.31	13.11	12.09
$\dot{V}_{eva,air}$ (m^3/s)	1.145	1.145	1.131	1.033	1.56	1.137	1.123	1.068
$T_{air,go}$ (ºC)	49.91	50.66	51.02	54.16	49.79	51.73	54.14	53.23
$P_{comp,i}$ (bar)	47	47.76	45.13	34.75	45.36	45.51	44.34	32.87
$T_{comp,i}$ (ºC)	11.87	12.46	10.09	-1.01	10.31	10.25	9.33	-3.25
$P_{comp,o}$ (bar)	116.5	120.6	120.2	130.7	111.6	118.6	129.1	125.3
$T_{comp,o}$ (ºC)	74.15	75.05	78.12	108.5	76.08	80.51	88.8	112.5
$P_{gc,i}$ (bar)	111.36	115.44	115.46	129.25	107.94	115.44	126.90	124.24
$T_{gc,i}$ (ºC)	71.1	72.13	75.11	103.2	72.78	77.41	85.56	106.5
$P_{gc,o}$ (bar)	108.98	113.25	114.01	128.63	104.50	112.21	123.93	123.44
$T_{gc,o}$ (ºC)	49.08	50.38	51.08	49.86	47.91	51.06	54.09	49.57
$P_{dif,o}$(bar)	51.38	52.25	49.07	36.71	49.48	49.5	48.13	34.62
$P_{eva,i}$ (bar)	47.42	48.16	46.76	34.16	44.46	44.34	41.99	29.72
$P_{eva,o}$ (bar)	46.7	47.45	45.97	32.38	43.5	43.4	41.04	29.03
$T_{eva,o}$ (ºC)	23	21.19	23.98	17.8	24.5	21.36	19.74	23.4
$\dot{m}_{gc}$ (g/s)	0.22	0.23	0.21	0.12	0.21	0.21	0.19	0.11
$\dot{m}_{eva}$ (g/s)	0.06	0.06	0.05	0.05	0.06	0.06	0.07	0.05
$\dot{W}_{comp}$ (kW)	9.69	9.99	9.91	9.9	9.39	9.95	10.7	9.58
$\dot{W}_{fan,gc}$ (kW)	1.18	1.18	1.18	1.16	1.18	1.16	1.16	1.14
$\dot{W}_{fan,eva}$ (kW)	1.53	1.39	1.42	1.5	1.52	1.53	1.47	1.14
$\dot{Q}_{eva,ref}$ (kW)	12.26	11.84	10.65	12.87	13.03	12.74	15.22	13.72
COP	1.265	1.185	1.075	1.300	1.388	1.281	1.422	1.432

Table F.1: Data for ejector expansion CO_2 bread board ECU (continued)

Ejector cycle	17	18	19	20	21	22	23	24
P_{atm} (kPa)	99.87	99.87	99.87	101.32	101.32	100.29	100.03	100.31
T_{id} (°C)	26.7	26.7	26.7	26.7	26.7	26.7	26.7	26.7
RH_{id} (%)	50.0	50.0	50.0	50.0	50.0	50.0	50.0	50.0
T_{od} (°C)	37.8	37.8	37.8	37.8	37.8	37.8	37.8	37.8
d_b (mm)	17.2	17.2	17.2	17.2	5.5	5.5	5.5	5.5
d_t (mm)	2.7	2.6	2.5	1.8	2.7	2.6	2.5	1.8
$T_{air,eo}$ (°C)	22.62	22.44	21.88	20.30	22.69	22.21	20.75	20.47
T_{dew} (°C)	13.41	13.23	13.33	13.45	11.65	13.57	12.82	13.85
$\dot{V}_{eva,air}$ (m^3/s)	1.150	1.150	1.137	1.123	1.166	1.145	1.117	1.087
$T_{air,go}$ (°C)	52.65	53.34	53.95	57.97	53.07	54.22	57.05	56.11
$P_{comp,i}$ (bar)	48.37	48.99	46.84	36.97	48.56	47.08	44.88	33.53
$T_{comp,i}$ (°C)	13.12	13.56	11.68	1.49	13.15	11.71	9.71	-2.37
$P_{comp,o}$ (bar)	120.8	124.9	125.8	141	121.1	124.5	130.3	129.5
$T_{comp,o}$ (°C)	76.68	77.5	80.91	112.9	77.72	81.6	92.01	115.2
$P_{gc,i}$ (bar)	115.42	119.44	120.73	138.36	116.90	121.14	127.98	128.43
$T_{gc,i}$ (°C)	73.69	74.64	78.01	107.9	74.67	78.57	88.72	109.3
$P_{gc,o}$ (bar)	51.29	52.57	53.64	53.12	51.55	53.48	56.05	51.95
$T_{gc,o}$ (°C)	51.29	52.57	53.64	53.12	51.55	53.48	56.05	51.95
$P_{dif,o}$(bar)	52.9	53.58	50.92	39.03	53.11	51.29	48.45	35.38
$P_{eva,i}$ (bar)	48.77	49.29	48.43	35.86	47.65	45.73	42.03	31.04
$P_{eva,o}$ (bar)	48.09	48.63	47.76	34.15	46.85	44.9	40.98	29.46
$T_{eva,o}$ (°C)	23.7	21.85	23.57	18.01	23	21.73	20.13	20.16
$\dot{m}_{gc}$ (g/s)	0.23	0.24	0.22	0.13	0.23	0.22	0.19	0.11
$\dot{m}_{eva}$ (g/s)	0.06	0.06	0.05	0.06	0.07	0.07	0.07	0.06
$\dot{W}_{comp}$ (kW)	10.11	10.43	10.44	10.67	10.18	10.41	10.89	9.81
$\dot{W}_{fan,gc}$ (kW)	1.17	1.17	1.16	1.14	1.18	1.16	1.15	1.12
$\dot{W}_{fan,eva}$ (kW)	1.44	1.32	1.59	1.44	1.6	1.7	1.59	1.13
$\dot{Q}_{eva,ref}$ (kW)	11.94	11.57	10.22	14.94	13.98	14.41	15.22	16.08
COP	1.181	1.109	0.979	1.400	1.374	1.384	1.397	1.639

Table F.1: Data for ejector expansion CO_2 bread board ECU (continued)

Ejector cycle	25	26	27	28	29
P_{atm} (kPa)	99.72	99.72	99.72	99.72	99.72
T_{id} (ºC)	2.8	2.8	2.8	2.8	2.8
RH $_{id}$ (%)	5.39	5.39	5.39	5.39	5.39
T_{od} (ºC)	41.1	41.1	41.1	41.1	41.1
d_b (mm)	10.0	10.0	10.0	10.0	10.0
d_t (mm)	1.8	20.	2.5	2.6	2.7
$T_{air,eo}$ (ºC)	-2.91	-1.52	1.12	2.56	3.06
T_{dew} (ºC)	-2.68	-2.45	-2.36	-2.38	-2.37
$\dot{V}_{eva,air}$ (m^3/s)	1.076	1.093	1.113	1.123	1.127
$T_{air,go}$ (ºC)	56.57	56.55	53.19	51.06	50.29
$P_{comp,i}$ (bar)	30.87	35.03	38.35	40.42	41.68
$T_{comp,i}$ (ºC)	-5.46	-0.41	3.3	5.54	6.81
$P_{comp,o}$ (bar)	137.1	128.7	113.5	106.5	104.9
$T_{comp,o}$ (ºC)	122	98.19	79.14	71.1	68.31
$P_{gc,i}$ (bar)	135.65	115.10	101.01	94.80	93.36
$T_{gc,i}$ (ºC)	114.7	94.44	76.54	68.45	65.52
$P_{gc,o}$ (bar)	135.90	126.43	109.65	101.24	98.86
$T_{gc,o}$ (ºC)	48.91	53.74	53	50.92	50.09
$P_{dif,o}$(bar)	32.72	37.91	42.25	44.96	46.63
$P_{eva,i}$ (bar)	28.68	30.54	35.38	38.11	39.34
$P_{eva,o}$ (bar)	28.09	30.03	35.24	38.05	39.3
$T_{eva,o}$ (ºC)	-9.11	-6.7	-0.59	2.54	3.83
$\dot{m}_{gc}$ (g/s)	0.0917	0.1272	0.1594	0.1795	0.1897
$\dot{m}_{eva}$ (g/s)	0.0526	0.0603	0.0463	0.0555	0.0593
$\dot{W}_{comp}$ (kW)	9.65	9.84	9.19	8.76	8.64
$\dot{W}_{fan,gc}$ (kW)	1.18	1.19	1.18	1.2	1.21
$\dot{W}_{fan,eva}$ (kW)	1.49	1.52	1.5	1.51	1.48
$\dot{Q}_{eva,ref}$ (kW)	12.63	13.61	9.804	11.27	11.75
COP	1.309	1.383	1.067	1.287	1.36

Table F.2: Two-phase flow ejector data to determine motive and suction nozzle efficiencies and mixing efficiency (the values for d_t are measured values)

Run No.	d_b (mm)	d_t (mm)	P_m (bar)	T_m (°C)	$\dot{m}_m$ (g/s)	P_s (bar)	T_s (°C)	$\dot{m}_s$ (g/s)	P_d (bar)	η_m (-)	η_s (-)	η_{mix} (-)
1	17.2	2.7	91.14	42.89	200.0	41.68	23.49	60.0	46.62	0.930	0.750	0.987
2	17.2	2.6	95.12	44.56	200.0	42.32	21.67	60.0	47.44	0.877	0.709	0.960
3	17.2	2.5	98.08	44.92	190.0	41.60	25.07	50.0	44.94	0.906	0.531	0.751
4	17.2	1.8	116.01	43.19	120.0	30.54	21.58	50.0	34.63	0.500	0.899	0.867
5	5.5	2.7	87.45	41.30	180.0	39.07	24.08	60.0	45.12	0.880	0.696	0.997
6	5.5	2.6	94.94	44.52	180.0	38.51	23.06	60.0	44.77	0.770	0.712	0.997
7	5.5	2.5	112.73	47.58	200.0	39.65	16.78	70.0	46.55	0.750	0.849	0.993
8	5.5	1.8	127.86	47.02	120.0	30.32	24.09	60.0	36.73	0.500	0.872	0.999
9	17.2	2.7	101.64	49.08	220.0	46.24	22.59	60.0	51.38	0.849	0.564	0.911
10	17.2	2.6	105.81	50.38	230.0	46.97	20.72	60.0	52.25	0.875	0.528	0.876
11	17.2	2.5	108.10	51.08	210.0	45.6	23.72	50.0	49.07	0.875	0.823	0.501
12	17.2	1.8	126.93	49.86	120.0	31.76	17.74	50.0	36.71	0.500	0.662	0.807
13	5.5	2.7	97.76	47.91	210.0	42.97	24.04	60.0	49.48	0.888	0.542	0.938
14	5.5	2.6	106.15	51.06	210.0	42.81	20.95	60.0	49.5	0.750	0.532	0.938
15	5.5	2.5	119.18	54.09	190.0	40.28	19.33	70.0	48.13	0.750	0.835	0.970
16	5.5	1.8	122.07	48.96	110.0	28.28	22.84	50.0	34.62	0.500	0.714	0.910
17	17.2	2.7	105.00	51.29	230.0	47.65	23.31	60.0	52.90	0.875	0.524	0.923
18	17.2	2.6	109.18	52.57	240.0	48.18	21.41	60.0	53.58	0.875	0.661	0.905
19	17.2	2.5	112.73	53.64	220.0	47.40	23.32	50.0	50.92	0.875	0.369	0.501
20	17.2	1.8	136.74	53.12	130.0	33.48	17.76	60.0	39.03	0.500	0.896	0.955
21	5.5	2.7	105.27	51.55	230.0	46.33	22.62	70.0	53.11	0.875	0.595	0.985
22	5.5	2.6	111.05	53.48	220.0	44.34	21.28	70.0	51.29	0.750	0.660	0.998
23	5.5	2.5	120.43	56.05	190.0	40.23	19.60	70.0	48.45	0.750	0.840	0.985
24	5.5	1.8	126.26	51.25	110.0	28.67	19.79	60.0	35.38	0.500	0.839	0.999
25	10	1.8	134.86	48.00	91.7	27.68	-10.25	52.6	32.72	0.500	0.828	0.703
26	10	2.0	124.44	52.63	127.2	29.41	-7.84	60.3	37.91	0.500	0.513	0.718
27	10	2.5	105.98	50.96	159.4	34.56	-1.4	46.3	42.25	0.677	0.519	0.711
28	10	2.6	95.94	47.65	179.5	37.46	1.86	55.5	44.96	0.795	0.691	0.759
29	10	2.7	92.59	46.1	189.7	38.72	3.16	59.3	46.63	0.881	0.766	0.779

Appendix G: Comparisons of the state points of R410A based systems with and without ejector expansion

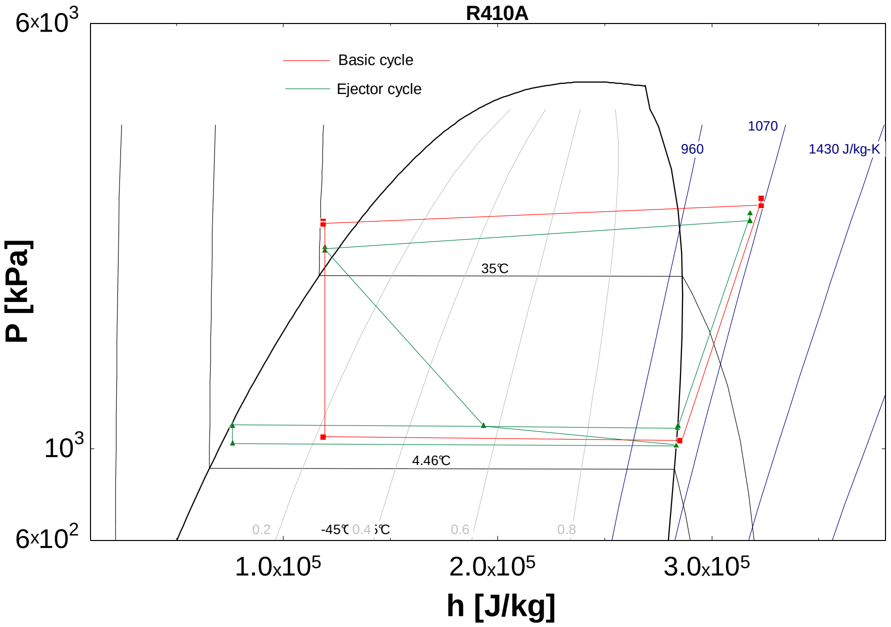

Appendix G1: State points of R410A cycle based systems with and without ejector expansion (T_{od} = 27.9°C(82.2°F), T_{id} = 26.9°C(80.4°F), RH_{id} = 50.8%)

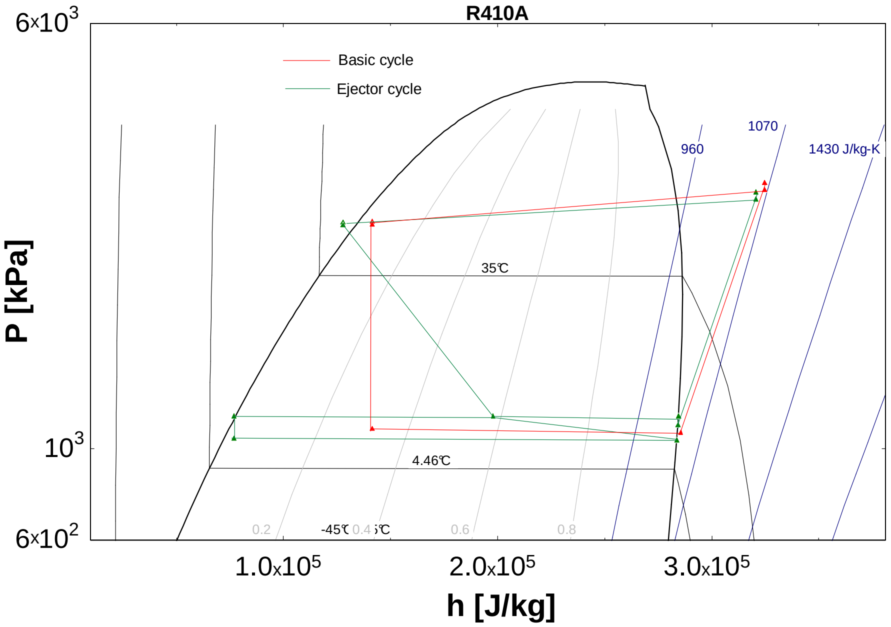

Appendix G2: State points of R410A cycle based systems with and without ejector expansion (T_{od} = 32.9°C(91.2°F), T_{id} = 26.9°C(80.4°F), RH_{id} = 50.8%)

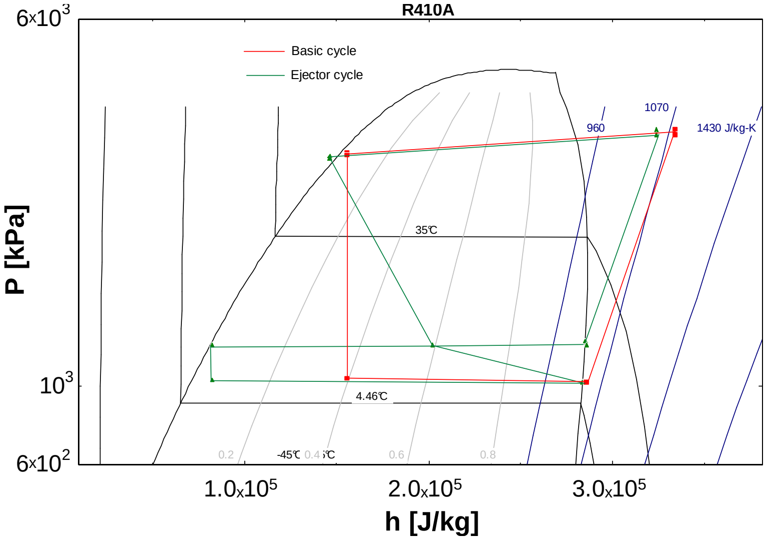

Appendix G3: State points of R410A cycle based systems with and without ejector expansion (T_{od} = 40.9°C (105.6 °F), T_{id} = 26.9°C (80.4 °F), RH_{id} = 50.8%)

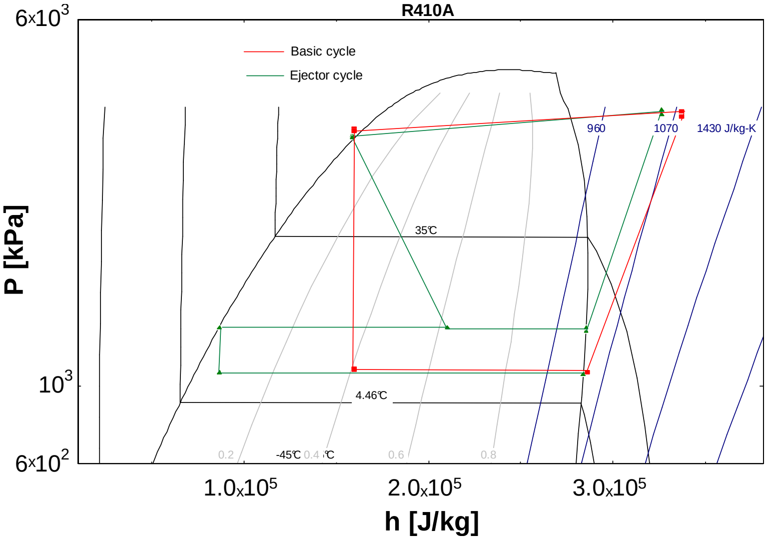

Appendix G4: State points of R410A cycle based systems with and without ejector expansion (T_{od} = 45.9°C (114.6 °F, T_{id} = 26.9°C (80.4 °F), RH_{id} = 50.1%)

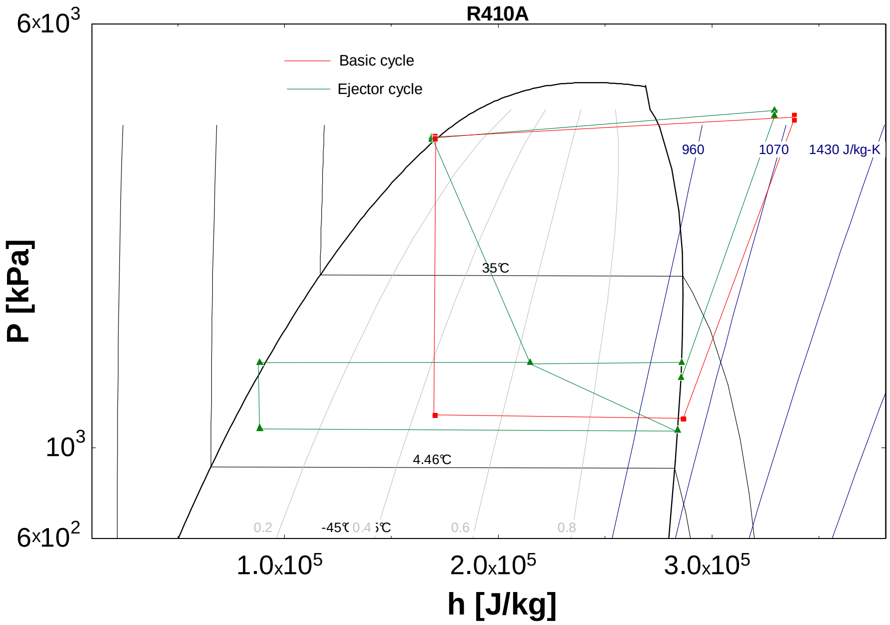

Appendix G5: State points of R410A cycle based systems with and without ejector expansion (T_{od} = 50.9°C (123.6 °F), T_{id} = 26.9°C (80.4 °F), RH_{id} = 50.1%)